INFORMATION TO USERS

This manuscript has been reproduced from the microfilm master. UMI films the text directly from the original or copy submitted. Thus, some thesis and dissertation copies are in typewriter face, while others may be from any type of computer printer.

The quality of this reproduction is dependent upon the quality of the copy submitted. Broken or indistinct print, colored or poor quality illustrations and photographs, print bleedthrough, substandard margins, and improper alignment can adversely affect reproduction.

In the unlikely event that the author did not send UMI a complete manuscript and there are missing pages, these will be noted. Also, if unauthorized copyright material had to be removed, a note will indicate the deletion.

Oversize materials (e.g., maps, drawings, charts) are reproduced by sectioning the original, beginning at the upper left-hand corner and continuing from left to right in equal sections with small overlaps.

Photographs included in the original manuscript have been reproduced xerographically in this copy. Higher quality 6" x 9" black and white photographic prints are available for any photographs or illustrations appearing in this copy for an additional charge. Contact UMI directly to order.

ProQuest Information and Learning
300 North Zeeb Road, Ann Arbor, MI 48106-1346 USA
800-521-0600

UMI®

The Hydrolysis of Phosphates in Ras Bound Nucleotides and Model Systems --- An FTIR Study

by

Hu Cheng

A dissertation submitted to the Graduate Faculty in Physics in partial fulfillment of the requirements for the degree of Doctor of Philosophy. The City University of New York

2001

Bell & Howell Information and Learning Company
300 North Zeeb Road
P.O. Box 1346
Ann Arbor, MI 48106-1346

This manuscript has been read and accepted for the Graduate Faculty in Physics in the satisfaction of the dissertation requirement for the degree of Doctor of Philosophy.

5/17/01
Date

Chair of Examining Committee

5/30/01
Date

Executive Officer

R. Birke

J. Gersten

M. Gunner

T. Leyh

Supervisory Committee

THE CITY UNIVERSITY OF NEW YORK

Abstract

The Hydrolysis of Phosphates in Ras Bound Nucleotides and Model Systems --- An FTIR Study

by

Hu Cheng

Advisor: Professor Robert H. Callender

The hydrolysis of dianionic phosphate monoesters is studied using FTIR and Raman spectroscopy. We have measured the frequencies of both symmetric and antisymmetric vibrational modes for the phosphate in various monoesters. The bond length of the bridging P-O bond is computed using an empirical formula. The relationship between bond length and the pK_a of the leaving group is investigated. We also measured the symmetric and antisymmetric frequencies of the phosphate modes in PNPP and PP in various DMSO/water mixtures. The hydrolysis rate is measured in parallel to explore the correlation with the bond length.

We have developed the isotope edited IR difference spectroscopy to measure the antisymmetric vibrational modes of phosphates in GTP and GDP bound to Ras. Structural information is obtained from their vibrational frequencies. It turns out that when GTP•Mg and GDP•Mg move from solution into the active site of Ras, the non-bridging O••P••O angle of the γ-phosphate of GTP is opened by 2.7°; yet, the angular freedom of the γ-phosphate is comparable to that in solution. In contrast, the motion of the γ-phosphate of GTP is highly restricted, suggesting that it positions the γ-phosphate for nucleophilic attack. The β,γ-bridging O-P bond of bound GTP is weakened, being lengthened by 0.005 Å in the active site, corresponding to a bond order decrease of 0.012

valence units (v.u.). With the study of phosphate monoesters, the observed binding change is consistent with a Ras-mediated hydrolysis mechanism that parallels that for solution hydrolysis.

The pK_a of γ-phosphate is predicted to be about 2.9 if it acts as a general base in the hydrolysis of GTP in Ras. Our work investigated this mechanism by studying the pH dependence of Ras•GTP•Mg and Ras•GDP•Mg from their vibrational spectra. The results show that the γ-phosphate is not protonated at pH > 3.3. GTP remains bound to Ras at pH as low as 2.0. A titration study of the Amide I band shows that Ras•GTP•Mg and Ras•GMP•Mg undergoes conformation changes that appear to be two-state reversible transition in the pH range of 5.4-2.6 and a non-reversible transition in the pH range of 2.6-1.7.

ACKNOWLEDGEMENTS

I would like to express my sincere gratitude to Professor Robert H. Callender for his guidance and supervision during the course of this thesis work. He is very insightful and profound, giving me a lot of great ideas and inspiration.

I would like to thank Dr. Hua Deng for many constructive suggestions and detailed instructions. He shared so much of his knowledge with me. His extensive experiences are part of the source of the outcome of my research.

I am greatly indebted to Dr. Ruel Desamero for many valuable advices and suggestions. I really appreciate the happiness of our cooperation. He helps me in all aspects of my research work.

I owe a great deal to Professor Thomas Leyh and Dr. Sean Sukal. They synthesized the key compounds and purified the protein of my experiments. They also proposed many ideas in designing the experiments. Besides, I benefited a lot from the discussion with them.

My special gratitude goes to Dr. Miriam Gulotta for very careful proof-reading and improving the English of the thesis; I am grateful to Dr. Hong Deng and Dr. Edward for their generous help. I also thank Professor Danier Herschlag and Ms. Ivana Danilo Nikolic for synthesizing the chemicals and valuable discussions.

Table of Contents

List of Tables

List of Figures

Abbreviations

GTP	guanosine triphosphate
GDP	guanosine diphosphate
DMSO	dimethyl sulfoxide
PNPP	*para*-nitrophenyl phosphate
PP	Phenyl phosphate
(β-$^{18}O_3$)GDP	guanosine 5' diphosphate with ^{18}O labeled on the three oxygen atoms of the terminal phosphate.
(γ-$^{18}O_3$)GTP	guanosine 5' triphosphate with ^{18}O labeled on the three oxygen atoms of the terminal phosphate
DTT	dithioerythritol
Tris	tris(hydroxymethyl)aminoethane
FTIR	Fourier transformed Infrared
FSD	Fourier self-deconvolution
PNPA	*p*-nitrophenyl acetate
EDTA	(ethelenedinitrilo)-tetracetic aicd
vu	valence unit

CHAPTER I

INTRODUCTION

1.1 Phosphoryl Transfer Reaction

Phosphoryl transfer is an important biological reaction: the PO_3 group is transferred between two anions (equation 1.1). The chemistry of phosphoryl transfer from phosphate esters is essential and ubiquitous in biological systems. For instance, energy is released upon the hydrolysis of ATP, signal transduction is controlled by the recycling between GTP and GDP bound to G proteins, glycolysis and gluconeogenesis are regulated by interconverting glucose-1-P and glucose-6-P catalyzed by the enzyme phospho-glucomutase, etc. It seems that there might be many different ways in which the enzymes catalyze the hydrolysis reaction. In the past decades, much work has been done to understand the mechanisms of these reactions in solution and to get insights into what is going on for the enzyme-catalyzed phosphoryl transfer (see e.g. Admiraal, 1995; Cleland, 1995; Maegley, 1996).

$$ROH + R'OPO_3^{2-} \longleftrightarrow R'O^- + ROPO_3^{2-} + H^+ \qquad (1.1)$$

Chemists have long discovered that the hydrolysis of dianions of monoester phosphates is a dissociative reaction (Benkovic, 1978; Thatcher, 1989), i.e., the leaving group and the attacking nucleophile are barely or very weakly bonded in the transition state (see scheme 1.1). A dissociative transition state is dominated by bond cleavage; in the extreme case, the bond to the outgoing leaving group is fully or nearly broken and the bond to the incoming nucleophile is absent or barely formed. The dissociative extreme is

depicted by the single negative charge and two full double bonds to the nonbridging phosphoryl oxygens of the phosphoryl group being transferred, and by the absence of bonds to the incoming or outgoing groups. In contrast, in an associative transition state, the oxygen atom from the nucleophilic attacking water is bonded to the phosphorus in the γ–phosphate to form a stable pentacoordinate intermediate. The associative extreme is depicted by the three negative charges and single bonds to the nonbridging phosphoryl oxygens of the phosphoryl group being transferred, and by the presence of bonds to the incoming and outgoing groups. The characters of both dissociative and associative reactions are schematically shown in Scheme 1.1.

The dissociative or associative nature of a phosphoryl transfer reaction is defined by the extent of bond formation between the incoming nucleophile and phosphorus, and the extent of bond cleavage between phosphorus and the leaving group in the transition state. Empirically, it is often found that there is a linear relationship between the logarithm of the rate constants and pK_a of ROH where R is the leaving group (see e.g. (Kirby, 1965; Kirby, 1967; Hall, 1986)). This relationship is quite general and is a very fundamental concept in physical organic chemistry. The slopes of linear free energy relationships (also called Brönsted relationship) correlating the pK_a values (proportional to a standard free energy change) of a series of nucleophiles or leaving groups with log k (a linear function of the activation energy of breaking the P-O bridging bonds, where k is the rate constant for reaction) are known as Brönsted, or β, values. These β values provide a measure of the bonding present in the transition state and thus are useful probes of transition state structure (for reviews of linear free energy relationship, see (Jencks, 1987; Ritchie, 1990; Williams, 1992)).

Bond length and bond order are direct measures of the molecular structure. A change in bond length and bond order is always present prior to the macroscopic observation of a

reaction. Therefore monitoring the changes in bond length and bond order can be very informative in understanding how the reaction happens. For example, a dissociative transition state has a decrease in the combined bond order of incoming and departing groups relative to reactant, whereas an associative transition state has an increase in combined bond order.

There are several expressions of the correlation between bond order s and bond length L. Some of them are based on fitting of the data to the environment of individual cations; others are based on the use of universal parameters applicable to all crystals. Empirical parameters were given for the equation $s=(L/L_1)^{-N}$ for 84 different cations, where L_1 and N are the fitting constants (see (Brown, 1976) and references thereby). Specifically, for phosphate, L1 is 1.622 and N is 4.29.

Since normally the molecules are in solution, there is no way to tell exactly what the bond length is by crystallographic means. But with the correlation between bond length and bond order, bond length can be determined once bond order is known. People have tried to find a correlation between the bond order and the vibrational frequencies, that can be directly measured. As early as 1937, a linear relationship between valence bond order and the square of the stretching frequency of a bond was posed by Badger (Badger, 1937). The subsequent work by Gordy (Gordy, 1946) correlated bond order with vibrational frequency for a variety of simple molecules with very high accuracy. However, Gordy's original description fails in dealing with those molecules that contain multiple bonded atoms, for instance, phosphates and vanadates. It was first shown by Hardcastle and Wachs (Hardcastle, 1990; Hardcastle, 1991) that the vibrational frequency of V$\underline{\bullet\bullet}$O bonds can be related to bond length. Recently in our lab, a normal mode analysis combined with spectroscopy measurements postulated a bond order/stretching frequency correlation for phosphate non-bridging bonds, which holds accuracy over a

wide range of phosphate compounds (Deng, 1998). Therefore, we have a very useful tool to explore the properties of phosphate hydrolysis with sensitive spectroscopic measurements.

1.2 Introduction of Ras

Guanine nucleotide binding proteins are involved in many cellular processes such as signal transduction, cell growth and differentiation, protein transport, and polypeptide chain elongation. They all act as molecular switches (Gilman, 1987; Kaziro, 1978; Sprang, 1997). The Ras protein, like other proteins under G-proteins, is believed to be involved in a growth promoting signal transduction process (Barbacid, 1987; Bourne, 1997; Gibbs, 1984; Zhang, 1993). There are three different Ras proteins classified by the proto-oncogene type, i.e., Ki-, Ha- and N-ras. Since they all have a molecular weight of about 21 kDa, Ras is also called p21 or ras p21. It exists in two stable states complexed with Mg^{2+} ion, an 'active' GTP bound state and an 'inactive' GDP bound state. When bound to GTP, the Ras protein exhibits an intrinsic GTP hydrolysis (GTPase), which is common for all the G proteins. The rate of this reaction is crucial for the corresponding regulation process: the longer a guanine nucleotide binding protein remains in its active GTP bound state, the longer it will transmit and also amplify a certain signal. Hence, the rate of GTP hydrolysis is of great importance for the right timing of many processes in a cell. In vivo, this intrinsic activity can be greatly enhanced by GAP (GTPase activating protein) (Bollag, 1991; Trahey, 1987). However, mutations may slow the GTPase reaction rate in these biologically active signaling proteins. For instance, mutations at either one of position 12, 13, or 61 of Ras drastically reduce its GTPase activity (Fasano, 1984) and renders it insensitive to activation by GAP (Adari, 1988; McCormick, 1989). Therefore the protein remains in the active, growth promoting GTP-bound state, which

can lead to cancer. Ras genes with point mutations are found in approximately 30% of human tumors (Barbacid, 1987). Thus, an understanding of the mechanism of GTP hydrolysis catalyzed by Ras and how the reaction changes upon binding to GAP is very important for clarifying the molecular basis of cancer.

The biological properties of Ras have been studied extensively (for review, see (Grand, 1991). Expression of recombinant Ras-p21 proteins resulted in an abundance of sample that has made it feasible to investigate these proteins completely via X-ray crystallography, NMR and vibrational spectroscopy. It is very important to understand, at atomic level, how normal and mutant Ras proteins interact with GDP and GTP at active and inactive site, as well as how these interactions are involved in the GTP hydrolysis in proteins.

Detailed description of the three dimensional structure of Ras as well as its mutants is available through X-ray crystallographic studies. Much information on the active site and mechanism of GTPase are drawn from the structure of Ras protein bound with a GDP or a GTP analogue (deVos, 1988; Krengel, 1990; Milburn, 1990; Pai, 1989; Pai, 1990; Schlichting, 1990; Wittinghofer, 1991). The protein as crystallized contains five α-helices, one central β-sheet which contains five parallel strands and one antiparallel strand, and ten interconnecting loops (Figure 1.1). Five of the ten loops contribute side chains and backbone interactions essential to the binding of the nucleotide and metal ion. The structures show that Gln61 is on a loop and makes contact with a water molecule, which is perfectly placed to be the nucleophile attacking the phosphate of GTP. The Mg^{2+} ion is seen to be coordinated to six oxygen atoms in a perfect octahedral arrangement (Pai, 1989). X-ray structure studies also show several hydrogen bonding interactions between the nucleotide and Ras protein, both at the guanine ring moiety and at the phosphate moiety. These strong hydrogen-binding interactions are attributed to the high

affinity and specificity for GDP and GTP. The kinetic studies have shown that Ras does not tolerate many substitutions of GDP and GTP. The affinities of Ras for ADP and GMP are about six orders of magnitude smaller than that of GDP (John, 1990). The overall structures of mutant Ras (Gly12 →Val12; Gly12→ Asp12) are very similar to that of the wild type Ras.

1.3 Mechanisms of GTPase

Since Ras plays an important role in signal transduction, many kinetics and structural studies of wild type and mutant Ras proteins were conducted during the past years. However, the mechanism of Ras-catalyzed GTP hydrolysis remains unclear. Several possibilities have been proposed in the last few years.

The most controversial issue is whether the transition state of the intrinsic GTP hydrolysis is dissociative or associative. From the crystal X-ray structure, a water molecule was identified in a position favoring a nucleophilic attack to the γ–phosphate of bound GTP. In classical general base catalysis Ras might catalyze hydrolysis by abstracting a proton from the nucleophilic water, thereby activating it to attack the γ–phosphate. Historically, careful inspection of the GTP-bound active site of Ras suggests five possible candidates for the general base, which are Asp-38, Asp-57, Gln-61, Glu-62 and Glu-63. But studies of the GTPase activity for the mutants excluded their qualifications in general (Cales, 1988; John, 1993; Krengel, 1990; Schweins, 1995). The lack of a conclusive identification of the base has spawned alternative suggestions for the chemical mechanism. The γ–phosphate of GTP itself is then proposed by Warshel et al to be the general base (Schweins, 1994; 1995). A strong evidence is the linear free energy relationship and the predicted pK_a of the γ–phosphate. The idea that the γ–phosphate

might be the general base in Ras-catalyzed GTP hydrolysis reaction was described first in a computational study that calculated that the hydrolysis ΔG^* for this mechanism is 24±5 kcal/mol (Schweins, 1994), which is close to the experimental observed value (~22 kcal/mol) (Neal, 1988). Support for this theory was provided in a subsequent paper in which the ^{31}P-NMR of Ras-bound GTP was studied as a function of pH (Schweins, 1995). The α-, β-, and γ-resonances of GTP shift concomitantly with a pH midpoint of 2.9, which agrees, within error, with the midpoint obtained from pH rate studies of Ras-catalyzed GTP hydrolysis. pH rate studies of Ras k_{cat} mutants were used to construct a free energy plot (ΔG^* versus pK_a); the plot was linear, with a slope of 2.1 (Schweins, 1995). These observations are consistent with, but do not prove that, the observed midpoint is the pK_a of the γ-phosphate of the bound GTP. A further analysis of this observed linear free energy relationship prefers that the transition state is associative (Schweins, 1996). Besides, it seems that in the presence of GAP, the transition state is more associative (Scheffzek, 1997).

An alternative proposal about GTPase is that the transition state is mostly dissociative, which is believed to be the case for GTP hydrolysis in solution. Experiments show that most phosphate monoesters including GTP hydrolyze in solution through dissociative transition states (Admiraal, 1995; Maegley, 1996). In addition, the enzymatic reactions of tyrosine phosphatases from *Yersinia* and rat, *Escherichia coli* alkaline phosphatase and some other phosphatases also appear to proceed via dissociative transition states (Hengge, 1996; Hollfelder, 1995). That implies the localization of positively charged side chains and metal ions in an enzymatic active site may not change the dissociative transition state to a more associative one in some enzymatic reactions. Therefore, it is possible that a dissociative transition state is found in Ras and related GTPases. Based on this perspective, after evaluations of previous mechanistic proposals for Ras catalysis, a new catalytic picture is proposed: a hydrogen bond from the backbone

amide of Gly-13 to the β-γ bridging oxygen of GTP is strengthened in the transition state compared to the ground state. Other interactions between the β-nonbridging phosphoryl oxygen and the active site Lys-16, Mg^{2+} may also contribute to the catalysis of Ras (Maegley, 1996).

We have used both Raman and FTIR spectroscopic methods to investigate hydrolysis of phosphate monoesters in solution as well as of GTP in Ras protein. Based on the analysis of bond order and bond length, it seems that in the hydrolysis reactions in solution, the ground state has some signatures of the transition state with regards to the bonding of the bridging phosphorus and oxygen. A linear correlation of bond length to pK_a of the leaving group is found to hold for a broad range of phosphate monoesters. We also found the linear correlation of bond length and hydrolysis rate for PNPP and PP in a solvent of water/DMSO mixture. These results not only give us some new information about the hydrolysis of phosphates in solution, but also provide the basis for applying similar methods to investigate the nature of the transition state in GTPase. Our studies show that the GDP moiety of GTP in Ras is highly stabilized by the protein. Compared with the structure of GTP in water, the β-γ bridging bond is weakened upon binding, which indicates a dissociative transition state. We also measured the pK_a of the γ-phosphate of GTP in Ras. The value we estimated agrees well with the NMR result (Schweins, 1995). Combining the information we obtained, we would prefer a concerted (with both dissociative and associative features) transition state of GTPase. pH induced unfolding of Ras protein is also discussed.

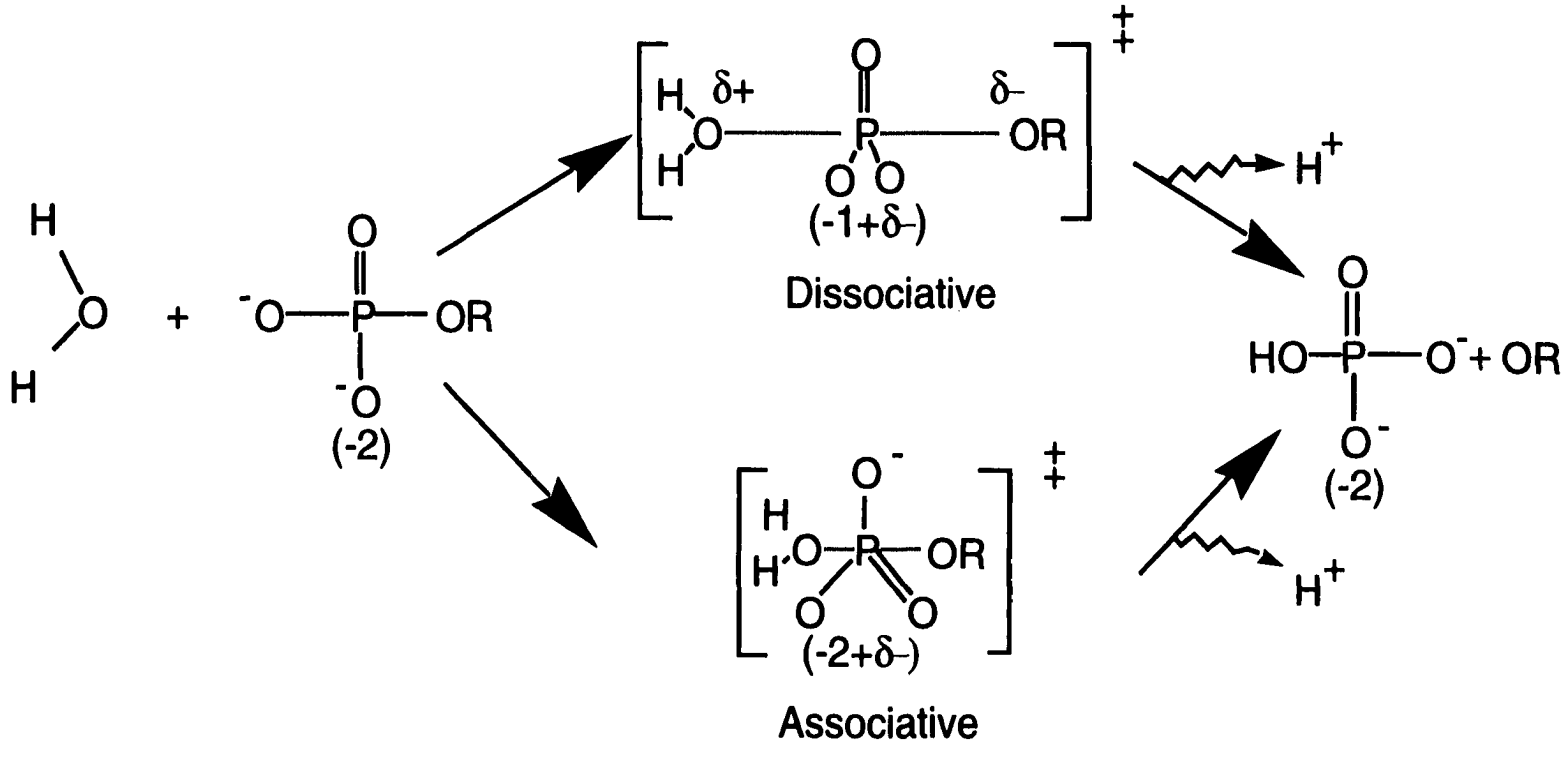

Scheme 1.1: Schematic drawing for phosphoryl transfer reactions with dissociative and associative transition states.

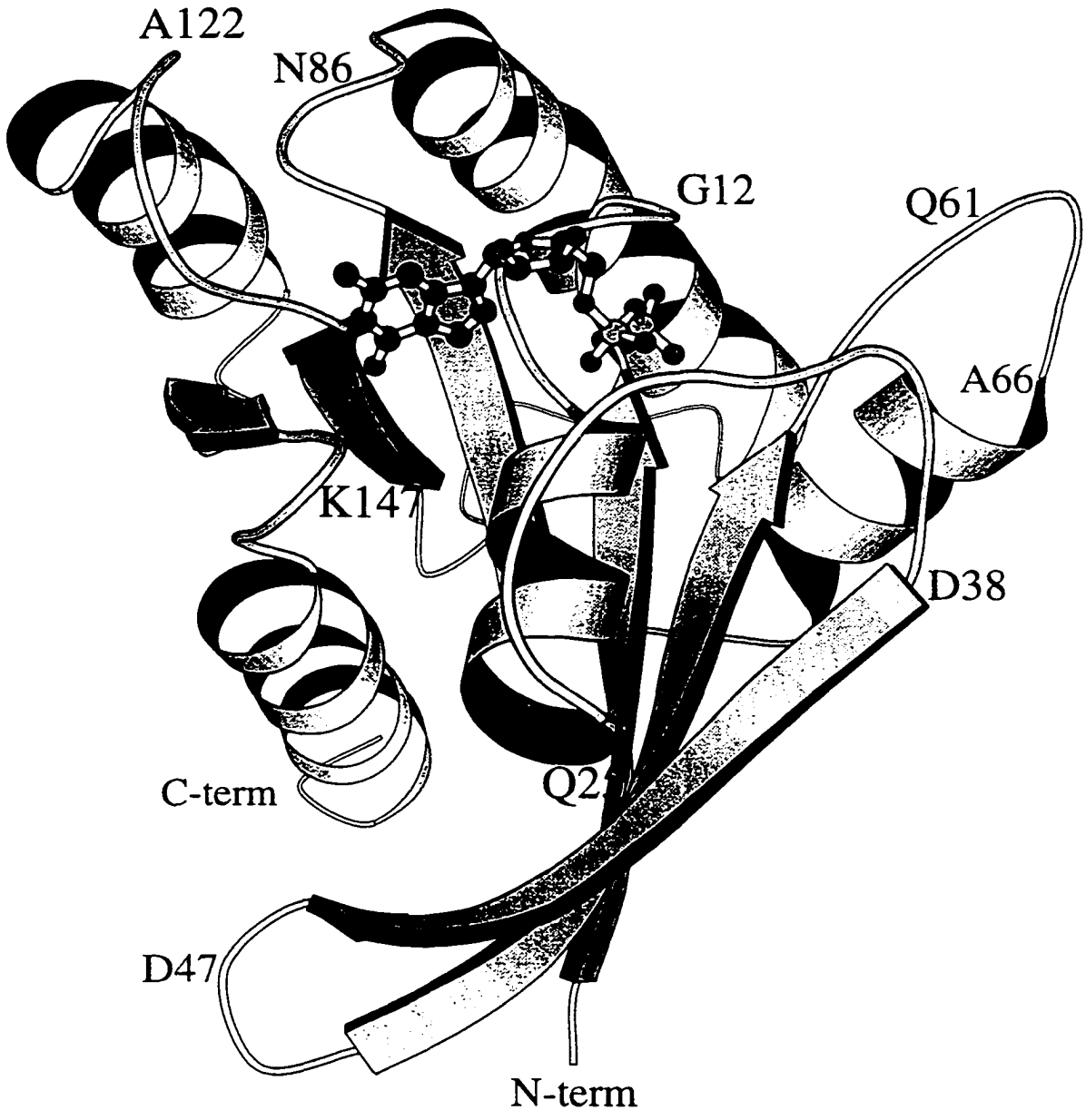

Figure1.1: Ribbon diagram of truncated human Ha-ras (1-166) complexed with GDP and Mg^{2+}, showing the secondary structure and the position of some key amino acids.

CHAPTER II

VIBRATIONAL SPECTROSCOPY

2.1 Introduction of Normal Mode Analysis

For a molecule of N atoms, there are 3N degrees of freedom of motion for all the nuclear mass in the molecule. After subtracting the translational and rotational degrees of freedom, there will be 3N-6 degrees of freedom left for a nonlinear molecule, and from a classical mechanical picture, these 3N-6 degrees of freedom correspond to 3N-6 independent normal modes of vibration. In each normal mode of vibration, all the atoms vibrate at the same frequency and pass through their equilibrium positions simultaneously.

The energy of molecular vibrations is of the magnitude of infrared light in the spectrum. The vibrational spectrum of a molecule has fruitful information about its structure. Every compound has its unique vibrational spectrum and any chemical changes or other minor changes in conformation and environment will be reflected in the spectrum. Therefore, vibrational spectroscopy has been a powerful tool in analyzing the structure and interactions. Raman scattering and infrared absorption are the experimental approaches for vibrational spectroscopy.

The symmetry of a molecule plays an important role in which vibrations are permitted and which excluded in a Raman or IR experiment. We can also determine the number and features of normal modes solely by the symmetry. For example, the unprotonated phosphate PO_3^{2-} has symmetry of C_{3v}, and we expect to see a sharp

symmetric band and a broad degenerate antisymmetric band. Group theory is the general mathematical tool to study molecule symmetry. For most compounds, certain chemical functional groups are found to be correlated with some characteristic vibrational frequencies, which are called group frequencies. The existence of group frequencies is attributed to the fact that the force constant for a specific chemical bond is transferable from one molecule to another.

2.2 Raman Scattering and IR Absorption

The phenomenon that a light is scattered with a shifted frequency is called the Raman Effect. The physical origin of Raman scattering is the inelastic collision between molecules and photons. The quantum mechanical picture of Raman scattering is depicted in Figure 2.1 (Spiro, 1987).

Ignoring the molecular rotational and translational energy, then the energy spectrum of a molecule is composed of the electronic energy and associated vibrational energy. Suppose the molecule is in the ground electronic state initially (but it is not necessarily to be in the vibrational ground state). If it is irradiated by a monochromatic light, some interactions between the molecule and the photons may happen simultaneously. One possibility is that a photon from the incident light excites the molecule to a higher virtual energy state. The lifetime of this virtue state is very short (typically $< 10^{-13}$ s), the molecule might return to a different vibrational energy level, releasing a photon with energy different from the original one by the difference of the two vibrational energy levels. This process is called Raman scattering. On the other hand, if the molecules are irradiated by a continuous wave, then the photons with energy equal to the energy difference of two vibrational energy levels will be strongly absorbed by the molecules,

showing an absorbance band in the spectrum of transmitted light. However, the photons absorbed by the molecules will not be released. Therefore, although associated with the molecular vibrations, the physics of the Raman effect and infrared absorption process are quite different. This dissimilarity leads to their different sensibility and resolution to certain vibrational modes.

2.3 Raman Spectroscopy

In a Raman spectrometer, the sample is irradiated with an intense source of monochromatic radiation usually in the visible part of the spectrum. The radiation scattered by the sample is collected and analyzed in the spectrometer. Figure 2.2 shows the typical instrumental setup of our Raman experiments. A laser beam is introduced through the sample. The scattered light is collected in 90° and focused on the entrance slit of a monochromator. The gratings in the monochromator disperse the incoming light into a spectrum of frequencies. This spectrum is transformed into an electronic signal by a detector, and then sent to a computer for analysis.

The laser sources available in our laboratory are a 4-Watt argon ion laser from Spectra Physics (Model 165), a 5-Watt krypton ion laser (Model INNOVA 400) and a 10-Watt argon ion laser (Model INNOVA 200, Coherent Radiation Inc.). The sample holder can hold a double or a triple split cuvette specially designed for measuring several spectra under the same conditions, and each sample space of the split cell has a dimension of 2.5mm×2.5mm. The cuvette is set on a computer-controlled stage that can be moved to within 1μm accuracy. Raman spectra are measured by a Triplemate spectrometer (Spex Industries), equipped with a solid-state detector system (Model DIDA-100 water cooled photodiode array and a model ST-100 detector controller;

Princeton Instruments), or a charge coupled device (CCD) system (CCD model LN/CCD-1152UV liquid nitrogen cooled and a model ST-135 detector controller; Princeton Instruments). Data are acquired stored, and analyzed on a Macintosh computer. Spectral lines are calibrated against known Raman lines of toluene and are accurate to within 2 cm^{-1}. The resolution of the instruments is typically set to 6 cm^{-1} full width at half height. Igor pro 3.1 (Wavemetrics Inc.) was used to process the data.

2.4 FTIR Spectroscopy

Compared with Raman spectroscopy, FTIR spectroscopy has a number of advantages. First of all, it needs much less time to achieve the same signal-to-noise ratio as Raman. This is of importance because for my study of the binding of GTP to Ras proteins, we prefer a quick measurement to reduce the effect of GTP hydrolysis. Secondly, there is no florescence background in the FTIR spectra because IR spectra are based on absorption rather than scattering. Thirdly, the sample volume needed for one measurement of IR is less than half of that for Raman. This may be crucial for limited sample. Finally, Raman and IR spectra are basically complementary: Raman is sensitive to nonpolar groups and symmetric modes while IR is sensitive to polar groups and antisymmetric modes. Therefore, combination of Raman with IR can give the full information of molecular vibrations. A more detailed look at IR absorption may be found in the appendix.

The FTIR instruments in our lab are a Bruker IFS 66 (Bruker Instruments Inc., Billerica, MA) and a Magna 760 (Nicolet Instrument Corp.). An MCT detector is used in each case. A Blachman-Harris three-term apodization and a Happ-Genzel apodization

were applied respectively. Opus 2.0 (Bruker Instruments, Inc.) and Omnic 4.0a (Nicolet Instruments, Corp.) were used for data collecting and analysis.

In order to observe IR allowed bands of substrates bound to proteins, we developed techniques for performing FTIR difference spectroscopy without using sample photolysis to switch the sample from one state to another. To study protein-ligand interactions, our laboratory developed isotope edited Raman difference spectroscopy to discern the differences between two spectra at the level of one part in 1000 (Callender, 1994). The operator can be represented by:

Spectrum (Protein•L) - Spectrum (Protein•L*) = Spectrum (L-L* bound in protein),

where L represents a cofactor, inhibitor or substrate of the enzyme and L* is the isotopically labeled cofactor at certain positions. There are no protein changes caused by isotope editing because L and L* have same chemical properties. This has permitted measurement of a single phosphate group within a ca. 60 kDa protein (Deng, 1993).

Two IR cells, made as identical as possible, are mounted on a stepping motor translation stage. One cell is moved into the IR beam and the IR absorption spectrum is taken. The cell holder is translated to bring the second cell into the IR beam, and the sequence is repeated. A reference spectrum of the residual water vapor is taken (which is quite low, on the order of 0.002 mOD), and this is subtracted from the protein spectrum. In general, the major difficulty in forming the difference spectrum is the strong water IR background. This will not be a problem for measurement of phosphate modes since, at their frequencies (ca. 1000 cm^{-1}), the water background is not too strong and is relatively flat. For other regions of the spectrum, studies of protein solutions in D_2O moves the

water band from ca. 1640 cm^{-1} to 1200 cm^{-1}. In a separate run, the water (or D_2O) background is measured, and this background is subtracted away.

Appendix: FTIR Spectrometry

The design of most interferometers used for infrared spectrometry today is based on that of the two-beam interferometer originally designed by Michelson in 1891. The Michelson interferometer is a device that can divide a beam of radiation into two paths and then recombine the two beams after a path difference is introduced. The intensity variation of the beam emerging from the interferometer can be measured as a function of path difference by a detector. The simplest form of Michelson interferometer is shown in Figure 2.3. It consists of two mutually perpendicular plane mirrors, one of which can move along an axis that is perpendicular to its plane. The movable mirror is either moved at a constant velocity or is held at equally spaced points for fixed short time periods and rapidly stepped between these points. Between the fixed mirror and the movable mirror is a beamsplitter, where a beam of radiation from an external source can be partially reflected and partially transmitted. Because of the effect of interference, the intensity of each beam passing to the detector depends on the difference in path of the beams in the two arms of interferometer. The variation in the intensity of the beam passing to the detector as a function of the path difference ultimately yields the spectral information in a Fourier transform spectrometer.

Consider a coherent monochromatic laser beam passes through the Michelson interferometer of Figure 2.3. If the movable mirror moves at constant velocity along the beam path, then the detected signal intensity, I (δ), will be modulated sinusoidally as a function of movable mirror position:

$$I(\delta) = \frac{1}{2} I_0(\delta)\left(1 + \cos 2\pi \frac{\delta}{\lambda}\right), \tag{2.1}$$

where I_0 is the intensity of the source beam, λ is the wavelength of the light, and δ is the amount of retardation, i.e., the path length difference. The factor of 1/2 in equation (2.1) arises from the loss of half of the source beam intensity back to the source by reflection at the half-reflective mirror. The d.c. component arises because the signal is detected by its energy.

The interferogram is formed by the addition of waves of different phase. However, photon detection is based on the energy of the light wave, which is proportional to the square of its amplitude. Since sample concentration is related to spectral intensity rather than amplitude in optical absorbance spectra, it is in fact the power spectrum that is of interest in optical interferometry.

A standard technique for calibrating the position of the moving mirror in a Michelson interferometer is to fix a visible-wavelength mirror to the back side of the moveable infrared mirror of Figure 2.3, and use that visible-wavelength mirror as the moving mirror of a second Michelson interferometer for which the source is (e.g.) a helium-neon laser. The infrared-wavelength interferometer detector may then be triggered to sample the interferogram signal whenever the visible-wavelength interferometer detector signal crosses zero. In Bruker IFS 66, the helium-neon laser and IR light use the same Michelson interferometer but different detectors. This is true for the Nicolet as well.

Since the maximum retardation Δ is restricted, the spectrum B (ν) is obtained from Fourier transform (FT) of the product of two functions,

$$B(\nu) = \int_{-\infty}^{+\infty} I(\delta) D(\delta) \cos(2\pi \cdot \nu \cdot \delta) \cdot d\delta \ , \tag{2.2}$$

here D (δ) is a truncation function satisfying $D(\delta) = 0$ for δ > |Δ|. It is called apodization function when it is not uniform (weighed) in the region of -Δ to +Δ. Proper choosing of apodization function can reduce the difficulty of detecting a small peak next to a large peak.

The interferogram signals are picked up by the detector and converted to digital signal. Then the frequency domain spectrum can be obtained by performing a fast fourier transform, with some additional procedures such as phase correction and zero filling.

Detailed discussion about signal to noise ratio, sources of noise, etc., can be found in the book (Griffiths, 1986).

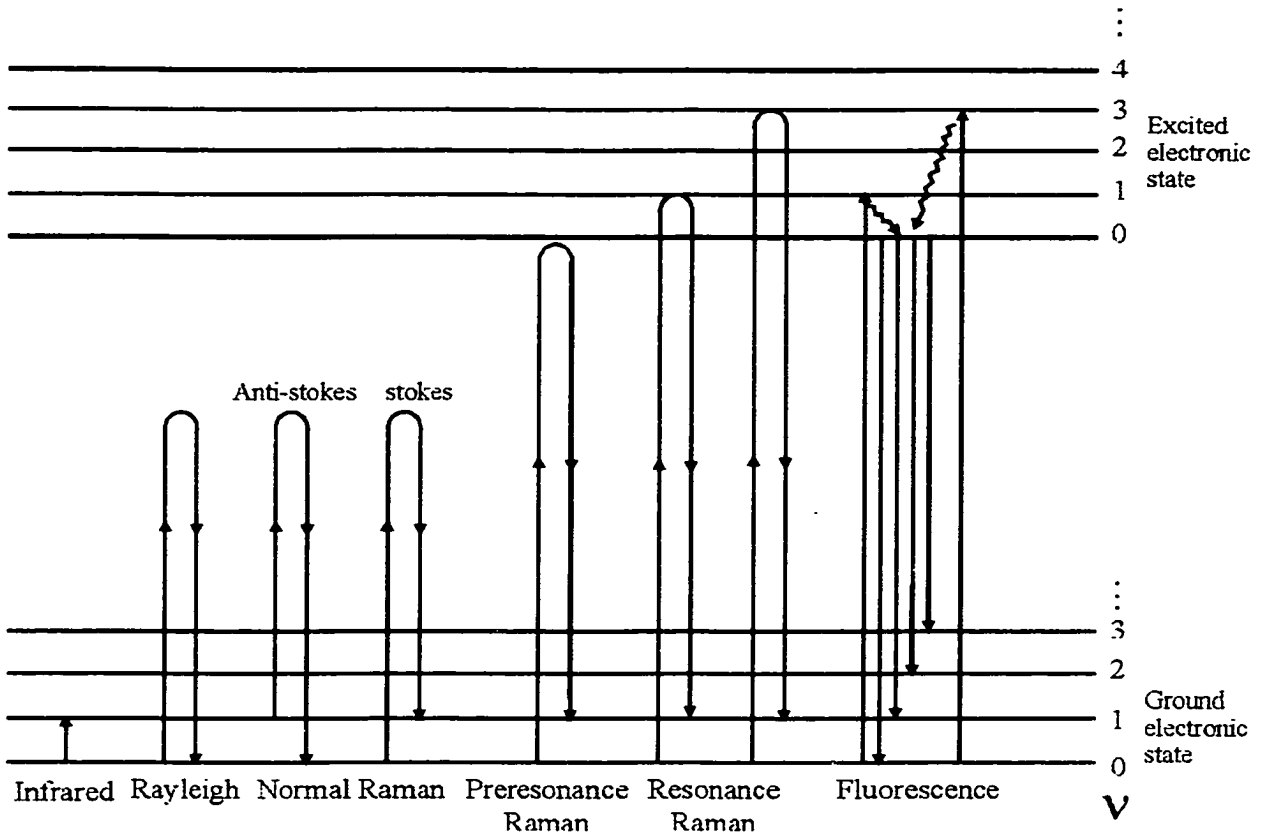

Figure 2.1: The energy diagram of various interactions between the photons and vibrational states of molecules. Let hν be the energy difference between the nearest vibrational states. The effects we are using are the infrared absorption in which the molecule takes on a photon with energy exactly equal to hν and goes to a excited vibrational state, and stokes Raman scattering in which the molecules is excited to an higher virtue state but comes back to a high level vibrational state, releasing a photon with energy equal to hν.

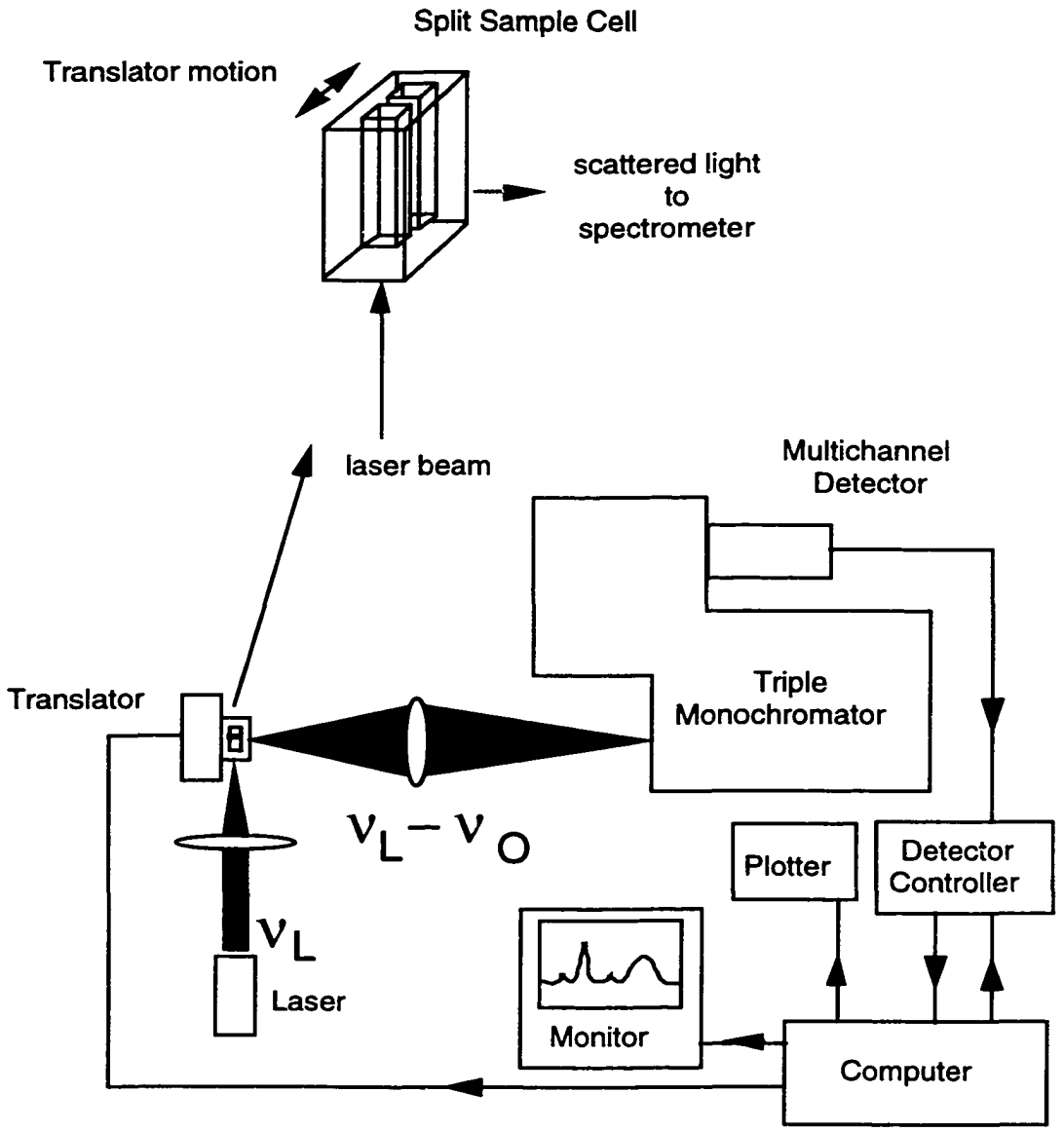

Figure 2.2: A scheme for the Raman measurement setup. The monochromatic light emitted from a laser source is introduced through the sample. The scattered light is focused on the entrance slit of a Triplemate monochromator. The spectrometer disperses the incident light into a spectrum and focuses it on to a detector. The spectrum is converted into electrical signals by a charge coupled device (CCD), and then transferred to an Apple computer for analysis.

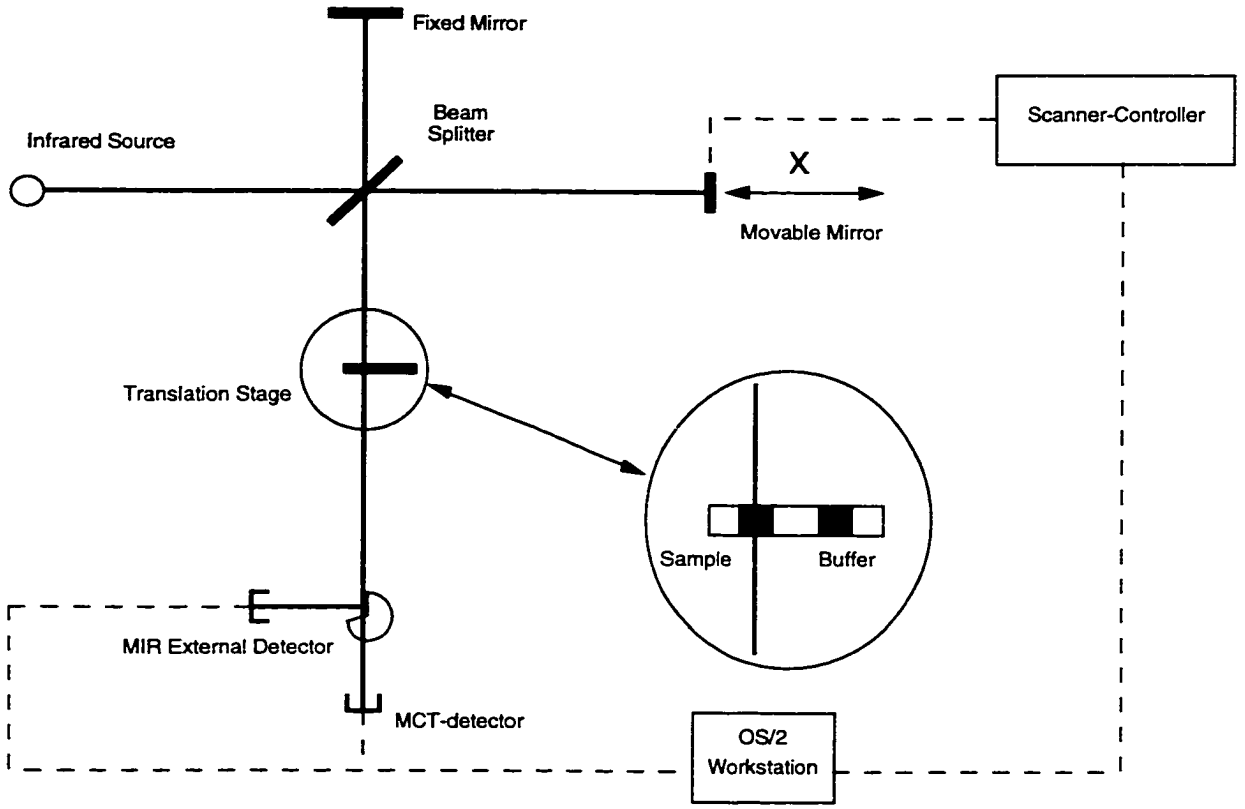

Figure 2.3: Experimental setup for FT-IR. Insert shows how the cells containing the sample and the buffer are positioned relative to the infrared beam.

CHAPTER III

VIBRATIONAL MODES OF PHOSPHATES

3.1 Introduction

If the phosphate is completely unprotonated, the three phosphorus oxygen bonds are then essentially identical and the symmetry of phosphate is C_{3v}. Group theory predicts that there is one symmetric vibrational mode and two antisymmetric vibrational modes (see, e.g. (Colthup, 1990)). The classical picture of normal modes gives the vibrations as shown in Figure 3.1. The symmetric vibrational mode is the simultaneous stretching along the P-O bond. The phosphorus atom is at rest. The antisymmetric vibrations, however, have different direction for each oxygen atom. The phosphorus atom also moves to keep the center of mass still. The symmetric frequency is lower and the band is narrow. The antisymmetric frequency is degenerate and the band is broad. In the experiments, Raman spectroscopy can only detect the symmetric vibrational mode while IR spectroscopy is sensitive to both symmetric and antisymmetric ones. If the phosphate is protonated, then the symmetry will be C_{2v}. Figure 3.1 also demonstrates the two vibrational modes we expect to see: one symmetric and one antisymmetric. Since in most of our experiments, the phosphate stays in dianionic form, we will only focus on the C_{3v} case in our discussion hereafter.

Using empirical Wilson-FG method, people in our lab have derived the equations that connect vibrational frequencies to the force constant (Deng, 1998a).

$$\nu_s^2 = \left(\frac{1}{\mu} + 2\frac{\cos\theta}{M_P}\right)(f_S + 2C_{SS}) \tag{3.1}$$

$$\nu_a^2 = \left(\frac{1}{\mu} - \frac{\cos\theta}{M_P}\right)(f_S - 2C_{SS}) \tag{3.2}$$

with $q \equiv \frac{f_S}{C_{SS}}$, $p \equiv \frac{M_P}{\mu}$, where θ is the angle between two nonbridging P••O bonds, f_s is the stretching force constant for the P••O bond, μ is the reduced mass, M_p is the mass of phosphorus and C_{ss} denotes the coupling constant for the three stretching modes.

In most cases, the electrostatic interactions between the phosphate and other atoms in the molecule or the environment will distort the symmetry to some extent and as a result, the degeneracy of two antisymmetric vibrational modes is broken. In this case, we might resolve two antisymmetric frequencies in the relatively broad band.

3.2 Vibrational modes of phosphate in monoesters

Figure 3.2 panel A shows the IR spectrum of a simple dianionic phosphate monoester: methyl phosphate in solution at pH > 10. The band at frequency 980 cm^{-1} is assigned to be the symmetric one. The bandwidth is about 18 cm^{-1}. The broad band (bandwidth > 50 cm^{-1}) centered at 1100 cm^{-1} corresponds to the antisymmetric vibrational modes. One can easily find two peaks with relatively similar intensity in that broad band. If the bands are not too close, performing second derivative to the spectrum is a good method for resolving the intrinsic bands and correctly assigning the frequencies. The second derivative method applied to the spectrum shows that there are two intrinsic bands with frequencies of 1084 cm^{-1} and 1109 cm^{-1} respectively (Figure 3.2 Panel B). For all the phosphate monoesters we studied, the two antisymmetric vibrational modes can be

resolved due to the break of degeneracy. The antisymmetric frequencies are all around 1100 cm^{-1}. And the symmetric frequencies are around 980 cm^{-1}.

3.3 Vibrational modes of phosphate in GTP and GDP

Figure 3.3 shows the FTIR spectra of both GDP (panel A) and GTP (panel B) in solution at pH 7.5. All the vibrational modes of the terminal phosphate have been previously assigned (Wang, 1998b). The symmetric frequency is 943 cm^{-1} for GDP and 927 cm^{-1} for GTP (not shown in the spectra); and the antisymmetric frequency is 1112 cm^{-1} and 1120 cm^{-1} respectively. The 1208 cm^{-1} band in the GDP spectrum is the antisymmetric stretching of the β-PO_2 group. For GTP, the 1087 cm^{-1} band is from the out-phase coupling of the symmetric stretch modes of the two inner PO_2 group while the 1232 cm^{-1} is due to the antisymmetric stretching of the PO_2 group (Wang, 1998b). Since the terminal phosphate is coupled with the β- and α- PO_2 weakly, the symmetric vibrational frequency is lower than that for phosphate monoesters.

3.4 Correlation of Bond Length to Stretch Frequencies

In general, a highly accurate determination of bond lengths of molecules in solution from vibrational frequencies, under proper conditions, is feasible, although this approach has not seen wide use in recent years. For this reason, we discuss the details of relating frequencies to bond lengths and bond orders here. Gordy (Gordy, 1946), based on the earlier work of Badger (Badger, 1937), established empirical correlations relating the frequencies of vibrational modes (through the force constant of the mode) to bond length and bond order. These correlations hold up quite well for relatively simple molecules or molecular fragments whose vibrational coordinates can be treated as approximating a

diatomic oscillator (i.e., the measured frequency is proportional to the square root of the bond's force constant divided by a suitable reduced mass). In these cases, the accuracy of calculating a bond length from vibrational frequencies found to be as good as the accuracy of direct measurement of bond length by crystallography, about 1.2% at the time of Gordy's work. In general, bond length versus frequency correlations are less accurate for polyatomic molecules because of interactions between non-bonded atoms that show up in mode-mode coupling between internal coordinates of the molecule. Hence, the normal mode for a polyatomic molecule is typically not a simple diatomic oscillator but, rather, involves contributions from several internal coordinates. For phosphates of varying ionization states, including dianionic phosphate monoesters, and likewise for vanadates, the normal modes of the stretch motions of non-bridging P–O and PO bonds are not simple diatomic oscillators. The individual frequencies of the phosphate symmetric, ν_s, and antisymmetric, ν_a, stretch modes depend on both the force constant and reduced mass of the relevant P–O bond but also on other factors (primarily on the geometry of the bond). However, it has been found that these other factors cancel out (Deng, 1998a) for the geometric average frequency of the phosphate stretch, or the so-called 'fundamental frequency'. The fundamental frequency, called ν here, is proportional to the square root of the P••O force constant divided by the reduced mass to a very high degree of accuracy. There are three independent non-bonded P••O stretch modes of the $-PO_3^{2-}$ moiety. For dianionic phosphate monoesters that preserve the C_{3v} symmetry of the $-PO_3^{2-}$ moiety, the normal modes are characterized by two doubly degenerate antisymmetric stretches, ν_a, located near 1110 cm^{-1}, and one symmetric stretch, ν_s, located near 970 cm^{-1}. The fundamental frequency is given by:

$$\nu = [(\nu_s^2 + 2\nu_a^2)/3]^{1/2} \qquad (3.3)$$

In this case, the bond length of each nonbridging P••O bond is equal. When the C_{3v} symmetry is not retained, the degeneracy of the antisymmetric stretch modes are lifted, and three frequencies are measured for the stretch modes of the $-PO_3^{2-}$ fragment. Typically, one is 'symmetric-like' and two are 'antisymmetric-like' in their polarization attributes as well as relative band intensities in the Raman and IR spectra. In any case, the fundamental frequency is then defined by:

$$\nu = [(\nu_s^2 + \nu_{a1}^2 + \nu_{a2}^2)/3]^{1/2} \tag{3.4}$$

The relationship linking the length of the non-bridging P••O bond (or average bond length in the case of a non-symmetrical $-PO_3^{2-}$ fragment) is (Deng, 1998a):

$$L_{PO} = 0.2835 \cdot \ln(224500/\nu) \tag{3.5}$$

A similar relationship exists for vanadates with somewhat different values of the constants in Eq. 3.5 (Deng, 1998a). The error in the absolute value of the bond lengths obtained from this method has been estimated at ±0.004 Å by comparing spectroscopically determined bond lengths to small molecule diffraction studies and from theory (Deng, 1998a). A large part of this error has to do with mode coupling between P••O stretches and other modes that affect the character of the stretch mode. These couplings vary amongst various phosphate compounds to some extent. An accuracy of ±0.004 Å relates to an error of ±13 cm^{-1} using Eq. 3.5 to relate frequency to bond length. The precision of the measurement of vibrational frequencies is much better than this, about ±2 cm^{-1}, and the issue of mode-mode coupling is not as important for the same molecule in different environments (i.e., the coupling parameters remain essentially constant). Hence, calculating bond length changes when a specific molecule undergoes a change in environment are most likely more accurately determined. It is unclear what

the accuracy is since there are no experimental benchmarks. However, an accuracy of better than ±0.001Å is possible using the ultimate accuracy provided by the precision in the measurement of frequency.

It is not possible to determine directly from these methods the bond length of the bridging P–O bonds because this mode is typically highly extended and, hence, does not conform to a simple diatomic oscillator. However, both the bond length and bond order of this bond can be inferred from an analysis of the non-bridging P••O bonds. The first leg in this analysis rests on the network theory developed by Brown and co-workers (Brown, 1973; Brown, 1992; Brown, 1976), developed as a refinement method of small molecule crystallography, which imposes the constraint that the sum of the bond orders of all the bonds of a specific atom is fixed to the atomic valence, which for phosphates is 5.0. Such a bond valence paradigm has been shown to yield very accurate bond length refinements in small molecule crystallographic studies. The bond orders (bond strengths) are given in terms of valence units (vu). The second leg of the analysis rests on relating vibrational frequencies to bond orders and bond orders to bond lengths. The equations that define these relationships for phosphates are:

$$s_{PO} = (L_{PO} / 1.620)^{-4.29} \tag{3.6}$$

$$s_{PO} = [0.175 \ln(224500 / \nu)]^{-4.29} \tag{3.7}$$

where S_{PO} is the bond order of the PO bond (either bridging or non-bridging), L_{PO} is the length of the PO bond (either bridging or non-bridging), and ν, the same fundamental frequency for the non-bridging P••O bonds as above. Equation 3.6 holds for either bridging or non-bridging bonds while Eq. 3.7 holds for only the non-bridging bonds. Hence, the total bond order of the non-bridging bonds in the $-PO_3^{2-}$ fragment are

determined from the empirical relationships using Eq. 3.7, and the bond order of the bridging bond is then inferred by subtracting this number from 5. The bond length of the bridging P–O bond is then calculated through the use of Eq. 3.5. To find the angle between the two vibrating P••O bonds, we can divide Eq. 3.1 by Eq. 3.2 and get:

$$\frac{\nu_s^{\,2}}{\nu_a^{\,2}} = \frac{p+2\cos\theta}{p-\cos\theta}\frac{q+2}{q-2} \tag{3.8}$$

With all these equations, the geometry of the phosphate group is completely revealed by the antisymmetric and symmetric stretching frequencies. Therefore, we are able to determine the tiny difference in structure when the phosphate is bonded to different groups. We can also readily resolve the tiny change of structure when the phosphate goes from aqueous solution to the active site of a protein.

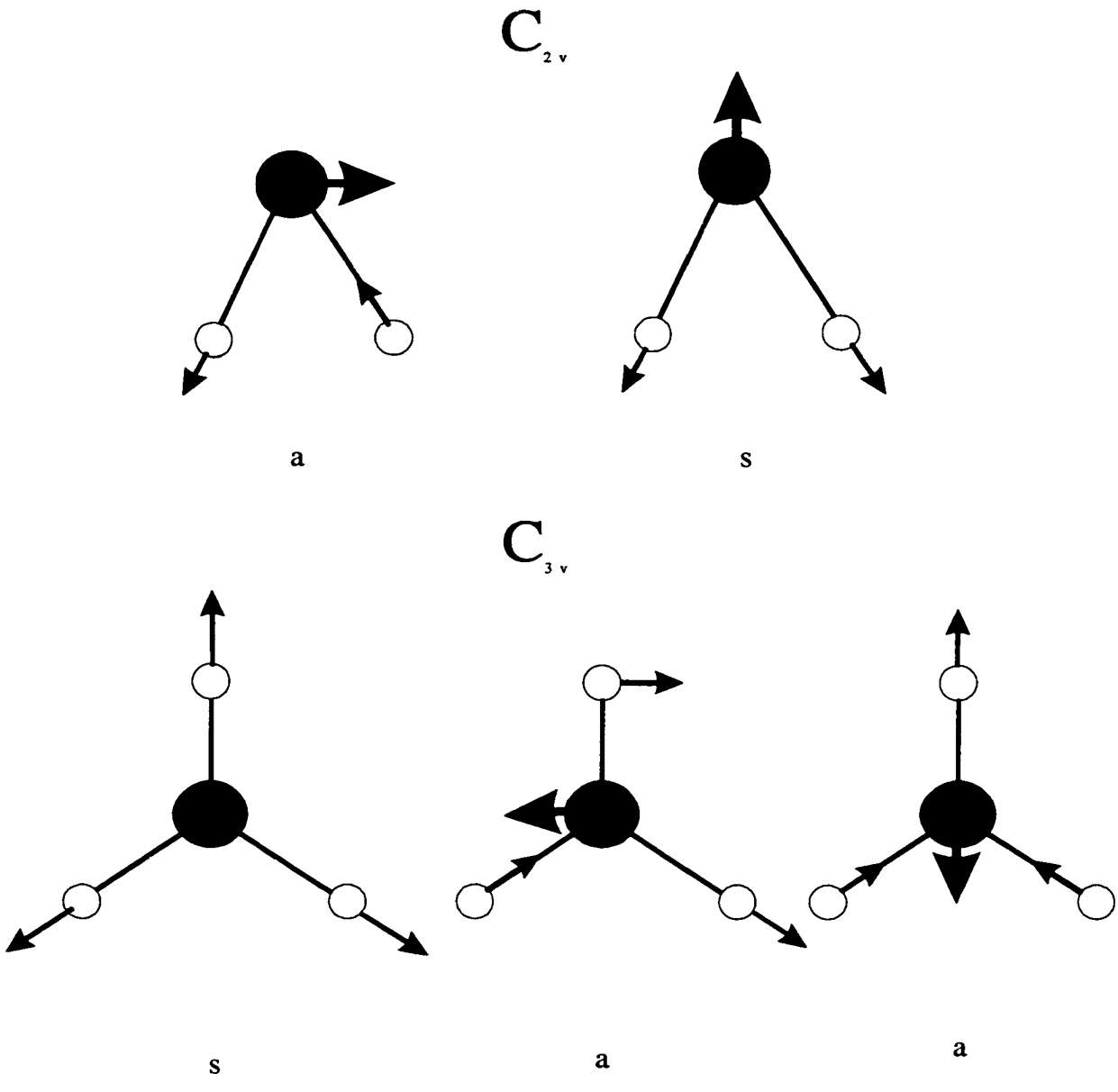

Figure 3.1: Schematic drawing of the symmetric and antisymmetric vibrational modes of molecules with C_{2v} and C_{3v} symmetry. Here 'a' represents antisymmetric modes and 's' represents symmetric modes.

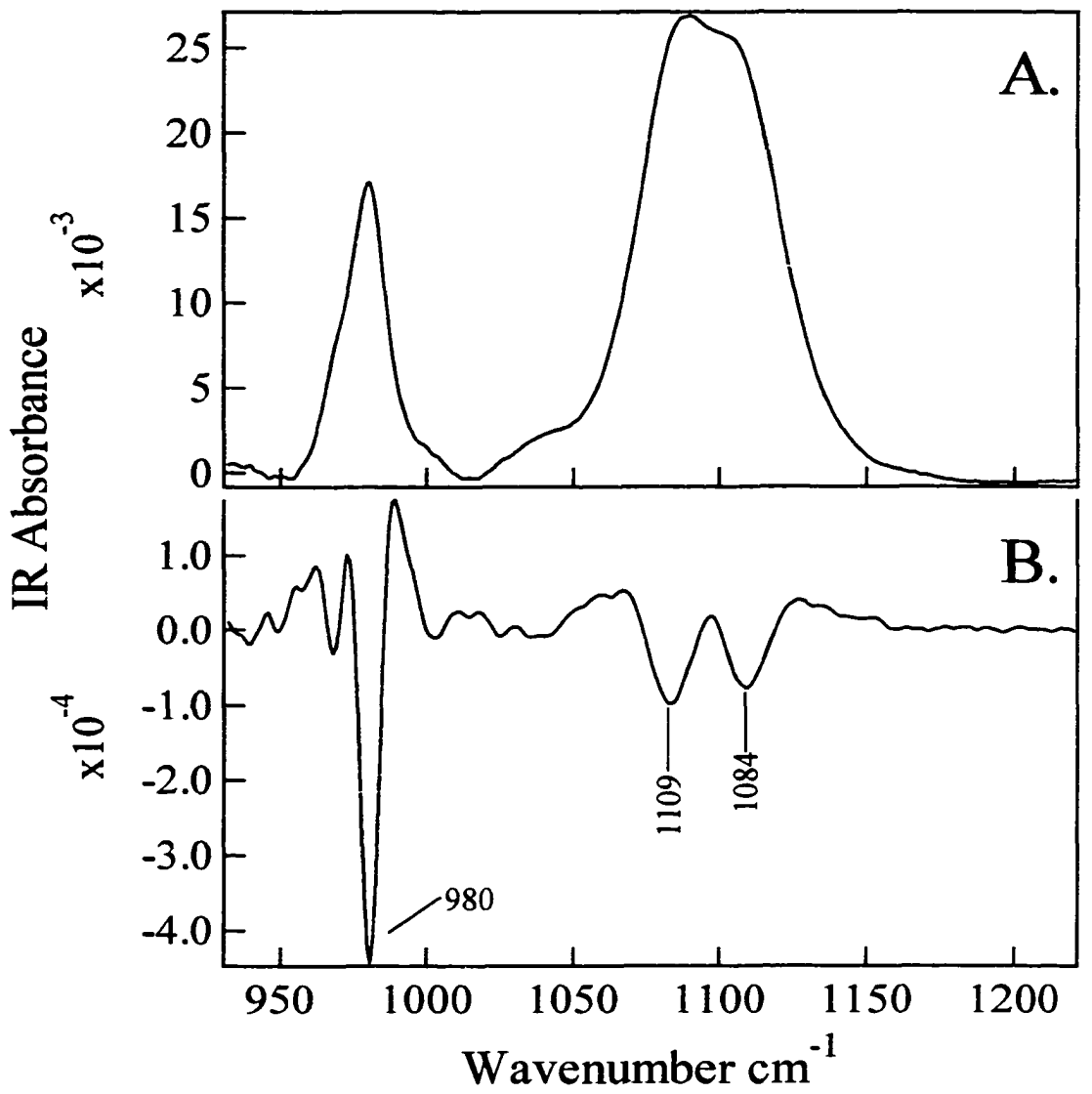

Figure 3.2: A. IR spectrum of allyl dianionic phosphate; B. the corresponding secondary derivative spectrum.

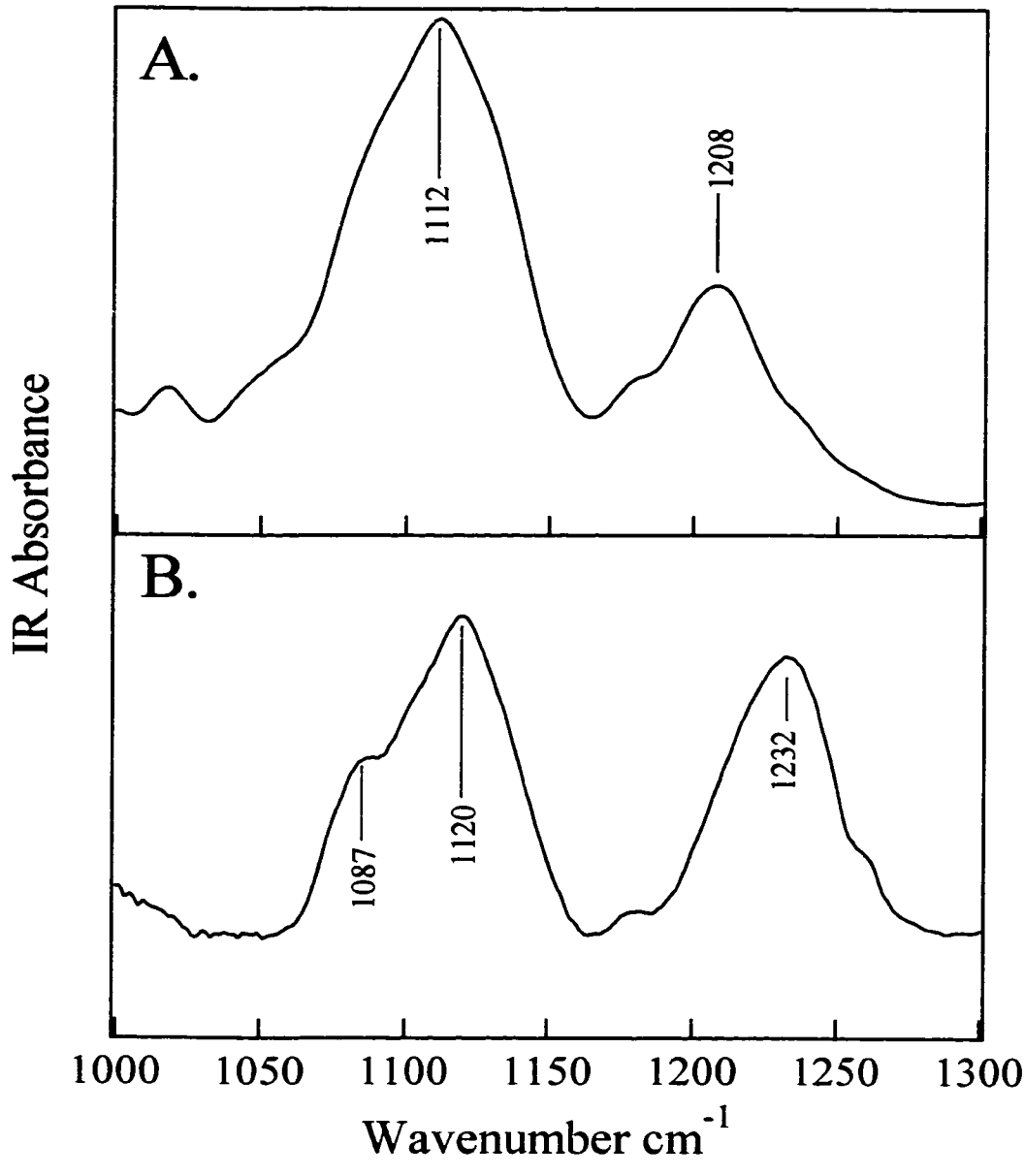

Figure 3.3: Spectrum of GDP (panel A) and GTP (panel B) in aqueous solution. PH = 7.5.

CHAPTER IV

HYDROLYSIS OF DIANIONIC PHOSPHATE MONOESTERS

The bond length (and bond order) of the bridging bond in a wide series of dianionic phosphate monoesters, RO- PO_3^{2-}, in aqueous solution and in mixed water/DMSO solvents was determined from the vibrational frequencies of the $-PO_3^{2-}$ fragment. The rates of hydrolysis, k_{hyd}, of some of the compounds were measured in parallel in order to construct plots of bridging bond length versus $\log(k_{hyd})$, and the pK_a of the various leaving groups was either measured or its value taken from the literature to likewise construct relationships between the bond length of the bridging P-O bond and leaving group pK_a.

4.1 Materials and Data Processing

A preliminary study of over 20 various compounds of phosphate monoester in our lab has found a linear relationship between the bond length of bridging P-O and the pK_a of the leaving group. To get more insight on this finding and to simplify the discussion, here we added the alkyl phosphates. Nine different alkyl phosphates, Allyl, butyl, isopropyl, 2-Methoxy ethyl, trifluoroethyl, methyl, propargyl, trichloro ethyl, F5 propyl, and phenol phosphate were synthesized by our collaborators: Daniel Herschlag and Ivana Danilo Nikolic at Stanford University. These compounds are in disodium forms. After dissolving them into water to get a 10 mM solution, NaOH was added to make the phosphates dianionic. The final concentration of NaOH was 20 mM. Then FTIR spectra of both sample and reference (20 mM NaOH solution) were taken at 25 C. The difference spectra (sample minus reference) will feature the IR absorption of these compounds.

We also studied the solvent-facilitated hydrolysis of PNPP (*para*-nitrophenyl phosphate) and PP (phenyl phosphate). It is well known that some solvents can increase hydrolysis drastically. It is of interest whether a linear correlation holds between the bond length of bridging P-O and the hydrolysis rate. 4-Nitrophenyl phosphate, disodium salt hexahydrate, was purchased from Aldrich and used without further purification. FTIR spectroscopy of 5 mM PNPP and PP were performed in water-DMSO mixture solvent with different compositions from 0% DMSO to 95% DMSO. An NaOH concentration of 20 mM was maintained in all experiments. The final pH values of the solution were around 11, much bigger than the highest pK_a of the phosphates. The measurements of PNPP were done at 25 °C while these of PP were samples were done at both 25 °C and 95 °C.

Omnic 4.0a (Nicolet Instruments, Corp.) and Igor pro 3.1 (Wavemetrics Inc.) software were used to analyze and process the data. Spectra subtraction, second derivative, and Fourier self-deconvolution (FSD) were performed with the Omnic 4.0a software. Since the conditions for sample and reference were the same, a direct subtraction of reference from sample usually resulted in a good difference spectrum. Particularly, since water has no peak around the phosphate bands, it is very safe to perform a direct subtraction if water is the solvent. The spectrum of DMSO contains substantial absorbance near the phosphate antisymmetric bands. Hence, for experiments in water/DMSO mixtures, the reference spectrum was multiplied by a factor near one when the subtraction was performed. The subtraction criterion being to cancel out the DMSO peak at 1316 cm^{-1} and 1400-1450 cm^{-1}.

The phosphate mode positions were determined by calculating the spectral second derivative and by Fourier spectral deconvolution. The software fits automatically found

the optimized positions. The symmetric band of phosphate in IR is very distinct; the frequency can be read directly from the spectrum. However, the positions of the antisymmetric bands are more difficult to determine for PNPP because the two antisymmetric modes sometimes overlap another mode arising from the phenyl moiety. It was found useful here to employ Gaussian curve fitting of the FTIR spectra, using the peak positions found by second derivative and spectra deconvolution as initial peak placement, using Igor pro 3.14 software to disentangle the overlapping spectra. The corresponding Raman spectrum was taken to eliminate observed bands that were simultaneously Raman active. For PP, we resolved three components in the antisymmetric region. As an approximation, we fit the spectra with three Gaussian waves and calculated the average frequencies based on the weight of their corresponding area. The average frequency was taken as the degenerate antisymmetric frequency.

4.2 Hydrolysis of dianions of phosphate monoesters

Linear free energy theory. Empirically, in general catalysis, it is often found that there is a logarithmic relationship between the rate constant, k_{HA}, for a series of acids, or k_A, for a series of bases, and the equilibrium constants for acid ionizations, K_{aHA} of the acids or conjugate of the bases. Both of these equations are called Brönsted relationships (see e.g. (Ritchie, 1990)). Similarly, for the hydrolysis of dianionic phosphate monoesters $R\text{-}PO_3^{2-}$, it was first found by Kirby that the kinetic plot of $\log(k_{hyd})$ vs. pK_a of ROH gives a good straight line of slope –1.23 (Kirby, 1967). The equation was $\log k_{hyd} = 2.64 - 1.23pK_a$. Although these equations were observed from a series of substituted benzoyl phosphates studied by Kirby et al, it is believed they hold for a wide range of phosphate monoesters. Since both sides of the linear equation are related to the free energy, the correlation is called a linear free energy relationship. Basically, this relationship is

phenomenological without a theoretical basis. The chemical origin of this relationship was discussed by Marcus et al(Marcus, 1964; Albery, 1980).

Most work on ionic reactions emphasizes the description of the transition state. However, Kirby et al (Allen, 1984; Briggs, 1983; Jones, 1984a), have shown that the ground state of a reacting system may contain the valuable mechanistic information for the reaction. It is possible, in appropriate cases, to characterize the reaction from the length of a bond being broken. In those papers, the correlation of bond length to reactivity was discussed for a different system R_1-OR_2. The bond lengths of the bridging C-O bond in crystal structures were analyzed for a considerably large number of R groups from methyl through primary, secondary, and tertiary alkyls. Linear relationships of C_1-O bond length versus pK_a of R_2OH were obtained for each class of R1 groups (methyl, primary, secondary, tertiary). Despite the displacements in the plots for different groups, the values of the slopes were quite close (Allen, 1984). A plot of P-OR bond length versus the pK_a of ROH for phosphate monoester dianions was also given in a subsequent paper (Jones, 1984). However, the bond length is from the crystal structure and only four data points were presented.

Given the formula connecting vibrational frequencies of phosphates to the bond order of P••O, and knowing that the summation of all bond orders of the phosphoryl bonds is 5.0, we are able to calculate the bond order of the P-O bridging bond. With the bond order-bond length relationship for phosphates, we will consequently find bond length of the P-O bridging bond from the vibrational frequencies.

pK_a of the leaving group. Tables 4.1 and 4.2 tabulate the vibrational frequencies of the nonbridging P••O stretches, the calculated bridging P-O bond length, and the pK_a of the ROH leaving group for a number of RO-PO_3^{2-}compounds in water. Table 4.1 is

comprised of the data obtained earlier in our lab by Jianghua Wang for various compounds. Table 4.2 presents the data obtained in this study. Figure 4.1 is a graph of the bridging bond length versus pK_a of the leaving group. A linear least squares fit to the data in Table 4.1 yields L = 1.644 - 0.00286* pK_a (solid line). The accuracy of the fit to the data is ±0.002 for the y-intersection and ±0.00017 for the slope. It is very interesting that the slope we obtain here is close to the value (~0.0025) obtained by Kirby for the C-O bonds of several series of acetals and glucosides.

This study represents a wide variety of leaving groups with a large range of pK_a values (from 4.76 to 16.4). The linear relationship of bond length and pK_a of the leaving group is promising. Although the compounds are different, Kirby's explanation of the linear relationship in the R_1-OR_2 system does shed some light in our understanding of this phenomenon. We will discuss this in several aspects. First, we would like to review the theory proposed by Kirby (Jones, 1984). The effective electronegativity of the oxygen atom in the RO group can be approximately measured by the pK_a of its acid form ROH. The bigger the pK_a, the smaller the value of the electronegativity. Hence, the oxygen in which ROH has a smaller pK_a value will have greater ability of attracting electrons in a covalent bond, making the bond more polar or ionic. In the case of C-O, increasing ionic character weakens and lengthens the bond. If applying the arguments to our studies of phosphate esters: the oxygen atom withdraws electrons from the phosphorus atom. The greater the effective electronegativity of the oxygen atom of the OR group, and the greater the stability of the phosphocation P^+, the greater will be the possibility of forming the structure of $RO^-P^+O_3^{2-}$, this P-O bond will be more susceptible to heterolytic cleavage. We may also take another view of this problem. Although the electronegativity of the oxygen atom varies due to the character of the leaving R group, the bond of OH is always covalent in ROH. The longer the bond, the easier will be the cleavage of the bond, and therefore, the easier the hydrogen loss in ROH. If we replace the hydrogen in ROH

with a phosphate PO_3 group, the character of the electronegativity and covalent R-O bond does not change a lot, so the R group in $ROPO_3$ which has longer P-O bond will correspond to the R group in ROH which has longer O-H bond, or, a smaller pK_a value. Therefore, a negative slope found is expected in Figure 4.1. At a first approximation, the bond length is found to be linearly correlated to pK_a.

The dashed line in Figure 4.1 is the linear fitting of the data for bond length versus pK_a for alkyl phosphates. The slope is 0.003981 Å, which is much bigger than the average value for various phosphates. This raises the issue of what the slope indicates and whether it is a constant for all the phosphate monoesters. To resolve this, we have to take into account the interaction between the nonbridging P••O stretches and the internal coordinates amongst the leaving groups. First of all, if we take a close look at the data for various phosphate compounds, we find that the points marked with ◆ in Figure 4.1 can be divided into two groups having the same slope but different intersections. This is demonstrated in Figure 4.2. The data for the alkyl phosphate is represented with ▲. The three lines are parallel, indicating one value of the slope can describe the correlation for all phosphate monoesters. The difference in intersection clearly shows the effect of the leaving group. Different types of leaving groups will have slightly different steric effects and electrostatic interactions. The line crossing the ▲ corresponds to the various alkyl phosphates. The line which spans from pH 4 to pH 13 is surrounded by the data of phenyl-related leaving groups. The line between the other two, gathers the points for some aliphatic compounds with a few hydroxyl groups on the chain. The three type of leaving groups, have different chemical properties, making the intersections vary a little. This kind of phenomenon is quite general in the linear free energy correlation plots, i.e., different leaving groups result in different intersections in the Brönsted plot (see, e.g. (Allen, 1984; Hoff, 1998)). We have included so many varieties of leaving groups, it is not surprising that in Figure 4.2, although we have three lines representing the

correlations, the data points are quite scattered. Even for alkyl phosphates, there are some scatters since the leaving groups are very heterogeneous.

We believe that our data all give the same slope in the L-pK_a plot. However, it is worthwhile to point out that the slope may be not uniform for all the leaving groups. It depends on how the reaction happens. Depending on the ionization of the phosphates, the β value can be very different (Kirby, 1967; Bourne, 1984). Other factors also affect the linear free energy relationships. For instance, β = -1.2 for hydrolysis of aryl and benzoyl phosphates (Di Sabato, 1961; Kirby, 1967); β = -(1.0-0.9) for reactions of aryl phosphates with amine nucleophiles (Kirby, 1968) and β = (-1.1±0.2) for phosphoanhydrides and related compounds (Admiraal, 1995). These differences in β indicate that both the charge distribution of the leaving group and the electrostatic properties of the solvent will affect the characteristics of the transition state. Usually, a large value of the β means there is a small amount of bond making but a large bond breaking in the transition state. So the linear relationship reflects the central role of the electronegativity of the oxygen atom attached to the leaving group; while the different β values are consequences of the structural difference in forming transition state. This, of course, will reflect in our bond length correlations.

4.3 Hydrolysis of PNPP and PP in DMSO/water mixture

The empirical equation connecting bond length to vibrational frequencies is quite accurate. The crystal structure of PP has shown that the real bond lengths are 1.53 Å, 1.53 Å, 1.51 Å for the three nonbridging P••O bonds and 1.64 Å for the bridging P-O bond (Jones, 1984). From the IR spectrum of the crystal (Pouchert, 1985), one antisymmetric frequency is found to be 1118 cm^{-1}. We estimate the second antisymmetric frequency is

either 1142 cm^{-1} or 1160 cm^{-1}. The two sets of the bond lengths are calculated out with Euation 3.5. One is 1.511 Å for non-bridging bonds and 1.636 Å for bridging bond. Another is 1.510 Å and 1.640 Å respectively. In both cases, the error of the bridging bond length is within 0.004 Å.

Hydrolysis. Table 4.3 lists the measured hydrolysis rates for *para*-nitrophenyl phosphate in various water/DMSO mixtures. The rates are very sensitive to the percent DMSO and increase dramatically for DMSO concentrations greater than 70-80%. This has been noted before (Abell, 1986; Catrina, 1999). Also given in the Table are the nonbridging phosphate stretch modes, the calculated fundamental frequency, and the calculated bridging bond length that results from applying the correlations discussed above that relate the measured frequencies to bond lengths (Equation 3.5). Table 4.4 provides the same numbers for phenyl phosphate. It should be noted that the frequencies are quite insensitive to temperature while the hydrolysis rates are quite sensitive. This is expected if temperature has little affect on the structure of either the ground state or the transition state but simply raises the percentage of molecules that are activated as generally assumed in studies of chemical kinetics.

Figure 4.3 plots the bridging bond length versus the log of the hydrolysis rate for both p-nitrophenyl phosphate and phenyl phosphate. The correlation is striking, and a linear least squares fit to the data yields $L = 1.636 + 0.003823*\log(k_{hyd})$ at 20 °C. The scatter in the data from the fit is about ±0.001 Å, which is what is anticipated (see above). The fit to the high temperature data for phenyl phosphate is essentially parallel but 'shifted' compared to the low temperature data, which is the expected result for a temperature activated process.

The average angle of the O••P••O bonds can be calculated with Equation 3.8. Here we are mostly interested in the change caused by the solvent, this turns out to be only weakly affected by choosing of the original angle if stretching angle is close to the real number. Using 114° (this value is from the crystal structure of Bis 4-nitrophenyl phosphate dihydrate (Jones, 1984)) as the average angle for PNPP in water, and taking the average of the two antisymmetric frequencies as ν_a in Eq. 3.8, then we get that from 0% to 90% DMSO, the change of angle is about +0.5°. So DMSO makes the structure of PO_3^{2-} a little more planar. Actually, we do expect this result from the lengthening of the P-O bridging bond because it reduces the repulsions between the oxygen atoms. In the dissociative mechanism that is assumed for all phosphate monoesters, a metaphosphate-like intermediate in the transition state is formed. The DMSO-driven opening of the P••O/P••O angle suggests that for dissociative mechanisms: (1) the more the ground state is like the transition state, the less is the activation energy of the reaction; (2) the energy cost of destabilizing the ground state is small.

The rate enhancement has been attributed to decreased ability of the mixed solvent in stabilizing hydrogen bonding interactions (Abell, 1986). In aqueous solution, the oxygen atoms of the nonbridging P••O group will form hydrogen bonds with water molecules. If part of the water is replaced by DMSO, which has no hydrogen bonding sites, the amount of hydrogen bonding between the phosphate group and the solvent will then decrease. On the other hand, since the bond order of oxygen is fixed, the decrease of hydrogen bonding will lead to the increase of the bond order of the P••O bond. This gives a rough picture of the bond order changes. The hydrolysis rate increase, however, has to be considered in a comprehensive picture since the activation energy change is associated with the whole system including both solvent and solute. The reduced activation barrier could be due to raising the energy of the reactant or lowering the energy of the transition state, or a combination of both. Hoff and Hengge (Hoff, 1998) have compared the energy of the

tetrabutylammonium salt of *para*-nitrophenyl phosphate in water and in *tert*-amyl alcohol. The activation energy is 29.5 kcal/mol in water and 23.7 kcal/mol in the alcohol. The contribution to the reduction is ~1 kcal/mol from the aqueous reactants and ~5 kcal/mol from the transition state. Currently, several models are consistent with the data we obtained for PNPP and PP. (1) This model was recently presented in a paper by Rucker & Byers (Rucker, 2000), and involves consideration of the rearrangement of the solvent molecules in going from the ground state to the transition state. If n molecules of water are hydrogen bonded to the ground state phosphate, and this number goes to n′ when the phosphate is in the transition state, then (n - n′) molecules of water undergo reorganization as the transition state is approached. This reorganization is achieved more easily in DMSO than in water due to the fact that DMSO is not a hydrogen donator. (2) The dissociative transition state for the hydrolysis of PNPP is destabilized less than the ground state PNPP by removal of water; this can be viewed from the difference in bond order of each nonbridging phosphorus oxygen bond. In the ground state of phosphate, the average bond order of the nonbridging P••O bond is 4/3, while in the metaphosphate-like transition state, the bond order per P••O bond is 5/3. However, the development of negative charge on the leaving group oxygen on the PP substrate as the transition state is approached (Scheme 4.1, reaction I) has an opposite effect relative to the decreasing charge on the non-bridging oxygens, in that the transition state is destabilized more by removal of water than the ground state. Charge development on the PNPP leaving group oxygen is reduced compared to the PP hydrolysis transition state, due to delocalization of charge throughout the phenyl ring and to the *p*-nitro group. This is depicted in Scheme 4.1, reaction II. Therefore, PNPP exhibits a larger rate enhancement than PP does. (3) The nucleophilicity of water may also be increased in DMSO, as the lone pairs on the oxygen are more readily available for attack at the phosphorus, rather than being involved in a network of hydrogen bonds when water is the sole solvent. However, this is not

expected to be a large effect for dianionic phosphate monoesters, in the light of negligible nucleophilic participation in the dissociative transition state.

Besides the observation of a linear relationship of bond length to log(k_{hyd}) in the hydrolysis of PNPP and PP in a DMSO/water mixture, there is a general linear relationship between the activation energy of the cleavage of the P-O bridging bond and the pK_a of the acid form of the leaving group. Therefore, the linear relationship of P-O bond length to the pK_a of ROH in various compounds of $ROPO_3$ also establishes the linear correlation between the bond length of the bridging bond and the activation energy to break this bond. The change of bond length or angles is just an effect of the destabilization of the ground state. From ab initio calculations, a change in P-O bridging bond of 0.1 Å corresponds to a change in energy of about 1 kcal/mol, therefore, the energy needed to generate these small changes of the bond length or bond order in the ground state is negligibly small (~0.13 kcal/mol) compared with the activation energy. Comparisons of the hydrolysis of dianionic *para*-nitrophenyl phosphorothioate and *para*-nitrophenyl phosphate in both water and DMSO/water mixture show that the transition state effects are much more important (Catrina, 1999). Consequently, why the bond order or bond length of the P-O bridging bond in the ground state is associated with the activation energy becomes a very interesting issue. There is no theoretical work to predict this kind of linear relationship. One way to think about this problem is to assume a general function of the chemical potential of this reaction (Jones, 1984). The reaction coordinate is chosen to be the bond length of the bridging P-O. If we equalize the free energy for all the transition states on the energy surface, then both coordinates characterize the minimal point at the energy surface for each individual compound: the activation energy and the bond length. If the energy surfaces for all the compounds adopt some similar shapes, the bond length is related to the hydrolysis subsequently in a regular manner. For instance, the interaction between the phosphorus and oxygen can be

described by the Morse function (see Figure 4.4), where the y-axis is the free energy of the system and the x-axis is the bond length. The ground state is at the minimum. These minima are separated by their different bond lengths in the ground state. The right of the minimum corresponds to the reaction path. Hence, the same hydrolysis path requires the curves to superimpose on the right branch as much as possible. Since the energy for transition states are all set to zero in the graph, the absolute y value of the minimum is the activation energy. The dashed straight line in Figure 4.5 shows that all the minima are lined up, indicating a linear relationship between the ground state bond length and the activation energy to break the bond. Of course, the Morse function is just a good description of the potential energy of simple diatomics in the gas phase; it might not give the true profile of the free energy from ground state to the transition state in the hydrolysis of phosphate monoesters. The reaction, which is involved with not only the leaving group and phosphate, but also the solvent, is far too complicated to be described in a simple function of the bond length of the bridging P-O bond. But the picture here may help to explain the origin of the linear relationship.

If we use Kirby's linear free energy relationship (Kirby, 1967), log k_{hyd} = 2.64 – 1.23pK_a, we can convert the bond length- pK_a relationship for the various phosphate monoesters to a bond length-hydrolysis rate relationship and compare this with the correlation we obtained for PNPP in a DMSO/water mixture. Since only the slope is associated with the mechanism, we will ignore the constant 2.64 in that equation. The slope in Figure 4.2 is –0.003981, divided by 1.23 to get the slope for bond length-log(k_{hyd}), we get the slope of –0.003236, which is only 2% off the slope (-0.003177) in Figure 4.4. This coincidence is not trivial at all. A study of the aqueous reaction of phosphonates with *p*-nitrophenyl acetate (pNPA) shows β_{nuc} = 0.3 in the Brönsted plot (Rucker, 2000). Here the subscript 'nuc' means the PO_3^{2-} group in the phosphonates acts as a nucleophile. Investigation of the effect of various DMSO/water mixtures on the

reaction of chloromethylphosphonate with pNPA shows increasing the DMSO concentration from 1% to 90% (v/v) increases the second order rate constant by over a factor of 5000. Taking into account that there is a linear increase in the pK_a with increasing mole fraction of DMSO (Buncel, 1989), the β_{nuc} turns out to be 0.8, which is considerably larger than the value for aqueous reaction. The difference in β_{nuc} reveals that factors other than pK_a values influence the effect of solvent variation on reaction rates. The solvent may in fact change the properties of the transition state. DMSO is believed to play a similar role in the reaction of PNPP hydrolysis. It is very interesting that we obtained the same value of slope. The coincidence we observed might show that this relationship is more fundamental than the linear free energy relationship.

The temperature studies of the bond length versus hydrolysis rate show that the correlation (characterized by the slope in the plot) is temperature independent. Since hydrolysis rate is a function of the ratio of activation energy to temperature, without structure modification, the activation energy changes little, leaving the hydrolysis rate solely a function of temperature. Hence, we observed just a displacement of the straight lines in Figure 4.2. This strengthens our argument that the bond length is related to the hydrolysis through the activation energy. The tiny change in bond length does not contribute to the bond breaking in the transition state. It is a kind of signature of the transition state properties.

4.4 Raman Spectroscopy Study of Hydrolysis of PNPP

We have successfully determined the bond lengths of the non-bridging P-O bond for PNPP in DMSO/water mixtures from the vibrational frequencies of the P••O stretch. In this approach, we use the fact that the total bond order of the phosphorus atom is five.

However, this is not a constraint when the bond order/frequency relationship was derived. Therefore, the empirical formula does not necessarily guarantee that the summation of bond order over all the phosphorus oxygen bonds is equal to 5. On the other hand, we believe that, as in the case of P$\underline{\bullet\bullet}$O stretches, the bond order of the P-O bridging bond is also related to its stretch frequency. The stretch mode of the P-O bridging bond is quite weak in Raman and not observable in IR. By using isotope edited PNPP in Raman spectroscopy, we determined the P-O stretch mode and measured the frequencies in the water/DMSO solvent with different percentages of DMSO. To avoid the large signal of normal DMSO around 740 cm^{-1}, 6-d deuterized DMSO was used in the experiments. If we use the same equation of Equation 3.7 as an approximation, the bond order, and consequently, the bond length, can be obtained from the stretch frequency. The results are listed in Table 4.6. The bond orders calculated from the frequencies of P$\underline{\bullet\bullet}$O mode are also listed as a comparison. The differences are of order of 0.005 vu, which is smaller than the total bond order change. In addition, there are both positive and negative differences, so we can exclude the possibility of a systematic error from the formulae we use. The bond length derived this way is also plotted versus the logarithm of hydrolysis rate in Figure 4.3. We used the same hydrolysis rate data of PNPP in normal DMSO since the interaction between the hydrogens of DMSO and the phosphate will not affect the hydrolysis rate very much. Again, we see a linear correlation here.

We would like to mention that generally the stretching mode of the bridging P-O bond is quite extended, which means it is coupled to some other modes. As a result, the frequency/bond order relationship for P$\underline{\bullet\bullet}$O bonds may not be the best way to describe the relationship for the bridging bond. We are unable yet to derive an appropriate empirical equation connecting the P-O stretch frequency to the corresponding bond order. In the case of PNPP, the oxygen atom is bonded to the ring of *para*-nitrophenol. The vibrational frequency of P-O stretching is below 750 cm^{-1}. While the stretch mode of O-C

is around 1100 cm^{-1}. Besides, there is an angle between the two stretches. So we would expect the coupling is small. This Raman study can be regarded as a complementary proof of that the bridging bond lengthening in the ground state is related to a rate enhancement.

Table 4.1: The non-bridging P••O frequencies of the $-PO_3^{2-}$ moiety of various dianionic phosphate monoesters, the antisymmetric mode, ν_a, the symmetric mode, ν_s, the resulting fundamental frequency, ν, in cm^{-1}, the calculated bond lengths of the bridging P-O bond (see text), and the measured pK_a of the leaving group alcohol.

[a] N. Bourne and Williams J. Org. Chem. 1984, **49**, 1200-1204.

[b] The pK_a of "enol pyruvate" is assumed to be equal to that of hydroxyehtylene (Guthrie, J. P.; Cullimore P. A. Can. J. Chem. 1979, **57**, 240; Guthrie, J. P. lbid. 1979, **57**, 797.)

[c] The pK_a of H_2O is taken from Sauers, C. K.; Jencks, W. P; Broh, S. J. Am. Chem. Soc. 1975, **97**, 5546.

Other values of pK_a are from the CRC Handbook of Biochemistry and Molecular Biology.

Table 4.1

Compounds	ν_s	ν_a	ν	l_{br}	pK_a
Acetyl-Pi	983	1130	1083	1.632	4.76
4-Nitrophenyl-Pi + Ca^{2+}	984	1122	1078	1.626	6.65
4-Nitrophenyl-Pi + Mg^{2+}	984	1120	1077	1.624	6.9
4-Nitrophenyl-Pi	983	1120	1076	1.625	7.15
4-Cyano-phenyl-Pi	983	1118	1075	1.622	7.95
3-Nitrophenyl-Pi	985	1118	1076	1.622	8.38
1-Napthyl-Pi	980	1110	1068	1.615	9.3
4-Br-phenyl-Pi	982	1108	1068	1.614	9.34
2-Napthyl-Pi	986	1112	1072	1.619	9.57
Phenyl-Pi	982	1108	1068	1.614	9.95
4-F-phenyl-Pi	983	1109	1069	1.616	9.95
Phosphorylchloline chloride	986	1103	1065	1.612	10
4-Methyl-phenyl-Pi	983	1108	1068	1.615	10.26
Phosphoenolpyruvic	976	1112	1069	1.615	11.1 [b]
2-Cyanoethyl-Pi	982	1100	1062	1.608	12
GMP	978	1098	1060	1.605	12.33
Glucose-1-Pi	968	1106	1062	1.608	12.4 [a]
2-Aminoethyl-Pi	981	1105	1065	1.612	12.65 [a]
Uridine-5-Pi	980	1100	1062	1.608	13
Glycerol-2-Pi	978	1098	1060	1.605	14.15
Glucose-6-Pi	980	1095	1058	1.604	14.7 [a]
HPO_4	984	1084	1052	1.597	16.4 [c]

Table 4.2: The non-bridging P••O frequencies of the $-PO_3^{2-}$ moiety of various alkyl dianionic phosphate monoesters, the two antisymmetric like modes (labeled ν_a), and one symmetric like mode (labeled ν_s), the resulting fundamental frequency, ν, in cm^{-1}, the calculated bond lengths of the bridging P-O bond (see text), and the measured pK_a of the leaving group alkyl alcohol.

Alkyl group	ν_s	ν_a	ν	l_{br}	pK_a
F5-propyl	983	1110	1069	1.616	12*
Trichloroethyl	981	1106	1066	1.612	12.2
Trifluroethyl	985	1112	1071	1.619	12.4
Propargyl	980	1104	1064	1.611	13.6
2-Methoxy	981	1094	1058	1.603	14.8
Allyl	980	1096	1059	1.605	15.5
Methyl	983	1095	1059	1.605	15.5
Butyl	973	1092	1053	1.599	16.1
Isopropyl	971	1089	1050	1.596	17.1

*: data not sure.

Table 4.3: The non-bridging P••O frequencies of the $-PO_3^{2-}$ moiety of *p*-nitrophenyl phosphate, PNPP, (two antisymmetric like, labeled ν_a, and one symmetric like, labeled ν_s), the resulting fundamental frequency, ν_a, in cm^{-1}, the calculated bond lengths of the bridging P-O bond (see text), and the measured hydrolysis rate (s^{-1}) in various water/DMSO solutions.

%DMSO	ν_{a1}	ν_{a2}	ν_s	ν	$l_{bridging}$	$logk_{hyd}$
0	1111	1133	981	1077	1.625	-6.959
25	1110	1136	980	1077	1.625	-6.62
50	1110	1137	978	1077	1.625	-6.009
60	1112	1139	978	1078	1.627	-5.668
70	1113	1141	977	1079	1.628	-5.026
80	1119	1146	977	1082	1.632	-4.168
90	1125	1156	976	1088	1.638	-2.523

Table 4.4: The non-bridging P••O frequencies of the $-PO_3^{2-}$ moiety of phenyl-phosphate, PP, (one doubly average antisymmetric like as described in the text, labeled ν_a, and one symmetric like, labeled ν_s), the resulting fundamental frequency, ν_a, in cm^{-1}, the calculated bond lengths of the bridging P-O bond (see text), and the measured hydrolysis rate (s^{-1}) in various water/DMSO solutions.

%DMSO	Temperature (°C)	ν_s	ν_a	$l_{bridging}$	$logk_{hyd}$
0	25	981	1110	1.615	-9.4
	95	980	1111	1.616	-5.28
90	25	974	1123	1.623	-6.96
	95	975	1125	1.625	-2.82
95	25	974	1127	1.626	-5.8
	95	973	1131	1.630	-1.68

Table 4.5: The stretching frequency (in cm^{-1}) of the bridging P-O bond of PNPP, the bond order, S_{P-O} (in vu) calculated with Eq. 3.7, the bond order, S'_{P-O} (in vu) calculated from the frequencies of non-bridging P••O bonds, the difference of the two approaches, $S_{P-O} - S'_{P-O}$, the bridging P-O bond length, $l_{bridging}$ (in Å), and the measured hydrolysis rate (s^{-1}) in various water/DMSO solutions.

%DMSO	ν_{P-O}	S_{P-O}	S'_{P-O}	$S_{P-O} - S'_{P-O}$	$l_{bridging}$	$logk_{hyd}$
0	733	0.9924	0.9871	0.0053	1.623	-6.959
25	730	0.9893	0.9861	0.0032	1.624	-6.62
50	726	0.9853	0.9856	-0.0003	1.626	-6.009
60	722	0.9812	0.9827	-0.0015	1.627	-5.668
70	720	0.9792	0.9798	-0.0006	1.628	-5.026
80	715	0.9750	0.9693	0.0057	1.630	-4.168
90	704	0.9639	0.9534	0.0105	1.634	-2.523

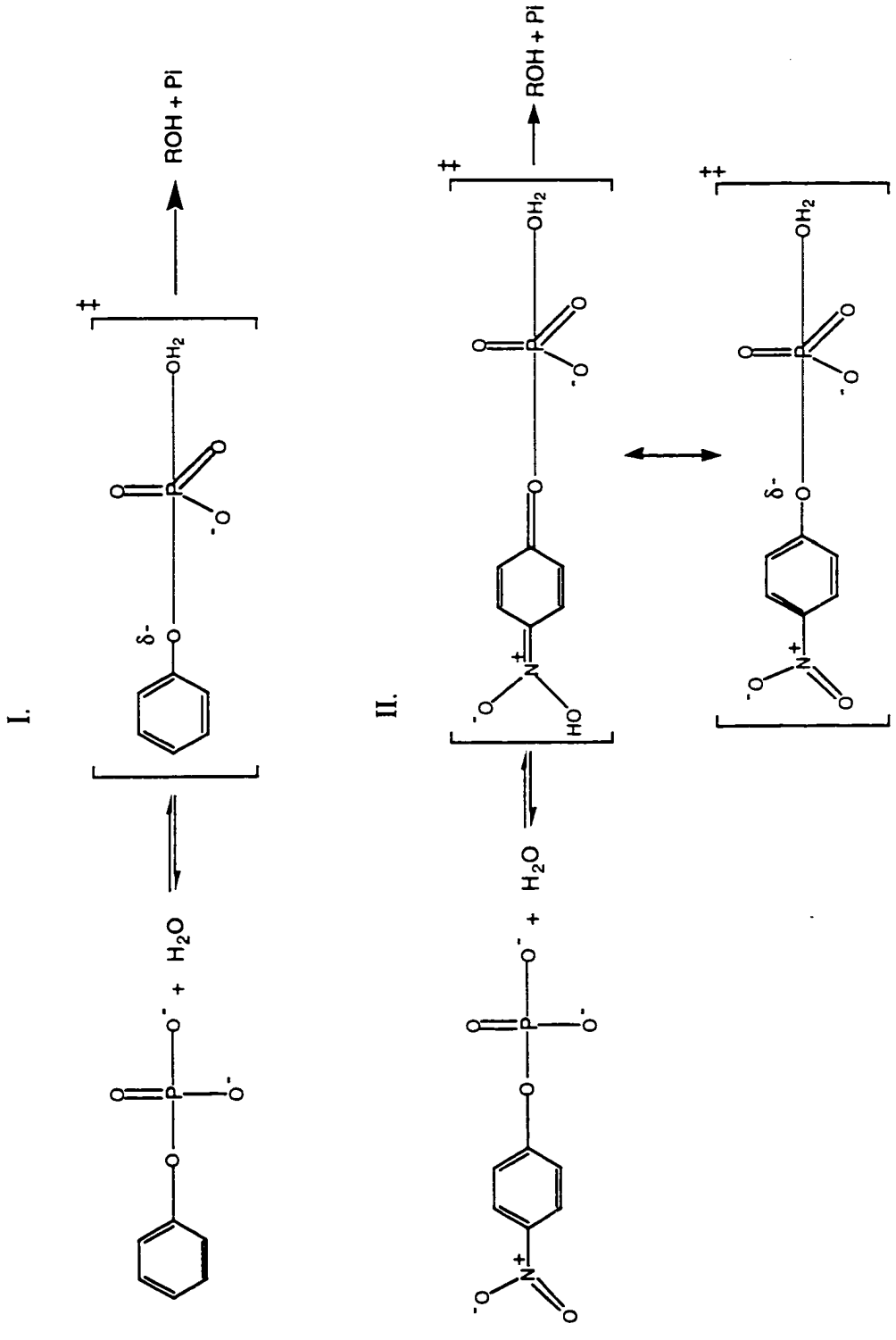

Scheme 4.1: Schematic drawing of the reaction path of the PP (I) and PNPP (II) in water.

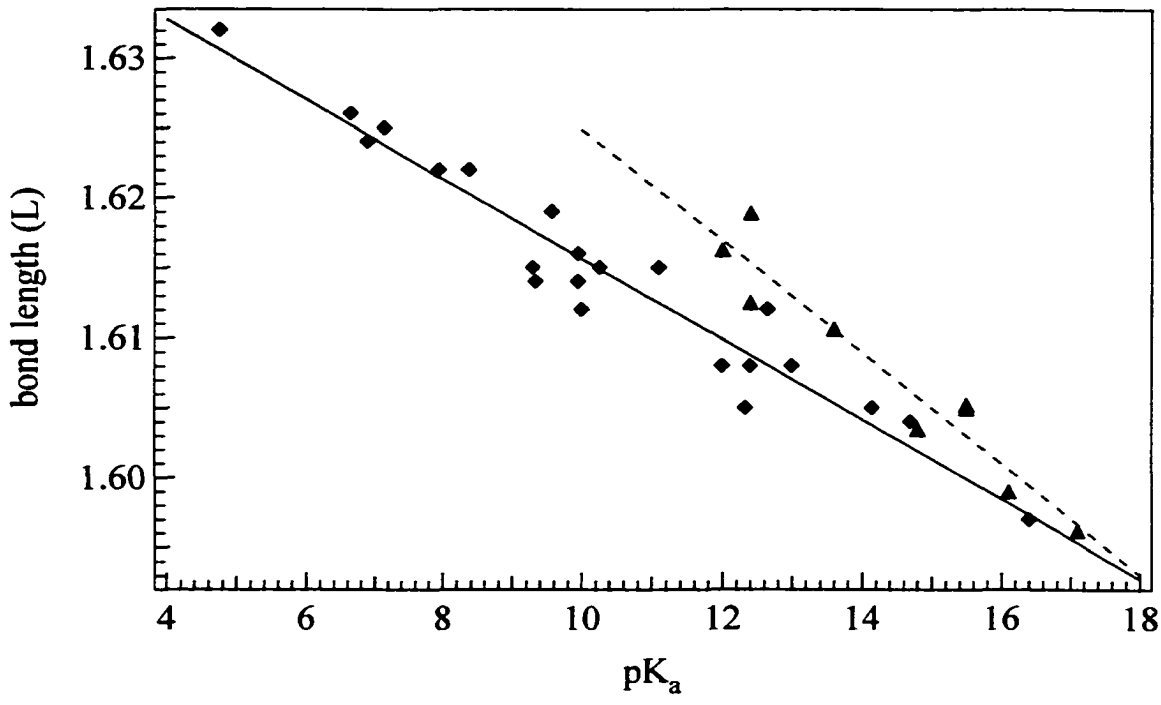

Figure 4.1: The bond length in Å of the bridging phosphate ester bond for various dianionic phosphate monoesters, RO-PO_3^{2-}, plotted versus the pK_a of the alcohol leaving group, ROH. The data is taken from Table 4.3 for alkyl phosphates (▲) and others from Table 4.1 (◆). The line is a least squares fit to the data with L = 1.644 (±0.002) - 0.00286 (±0.00017)* pK_a (solid line) and L = 1.6647 (±0.006) – 0.003981 (±0.00045)* pK_a (dashed line)

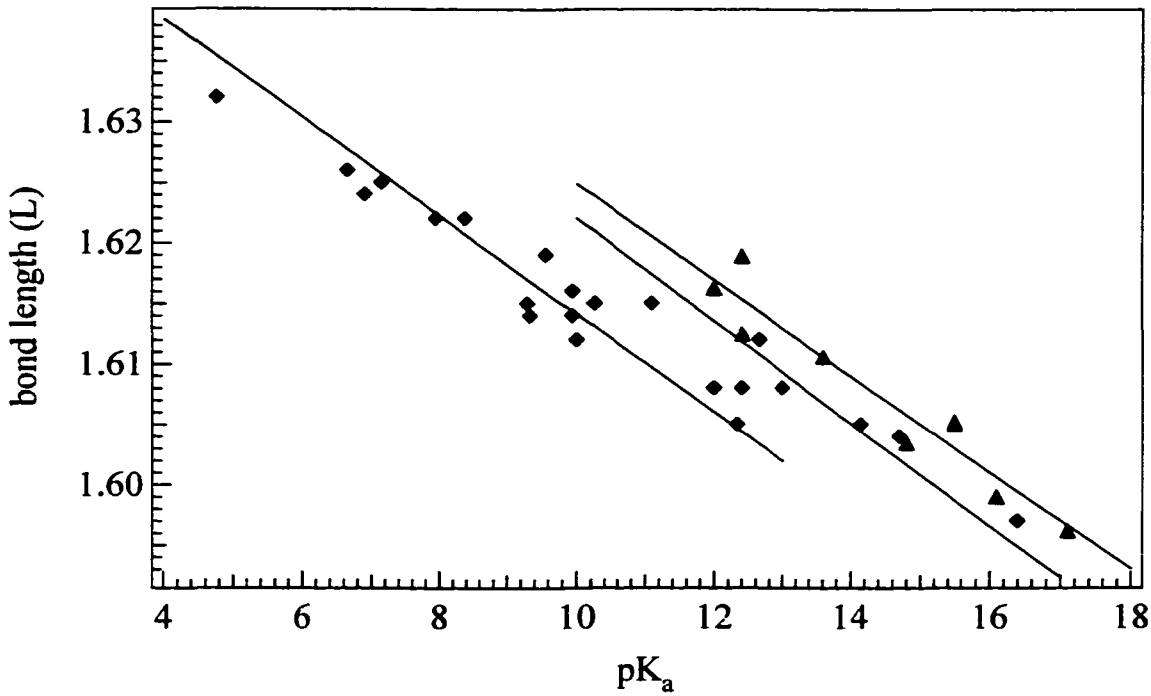

Figure 4.2: Using the same slope for alkyl phosphate, the data of various compounds can be fit to two lines. The data is taken from Tables 4.3 for alkyl phosphates (▲) and others from Table 4.4 (◆).

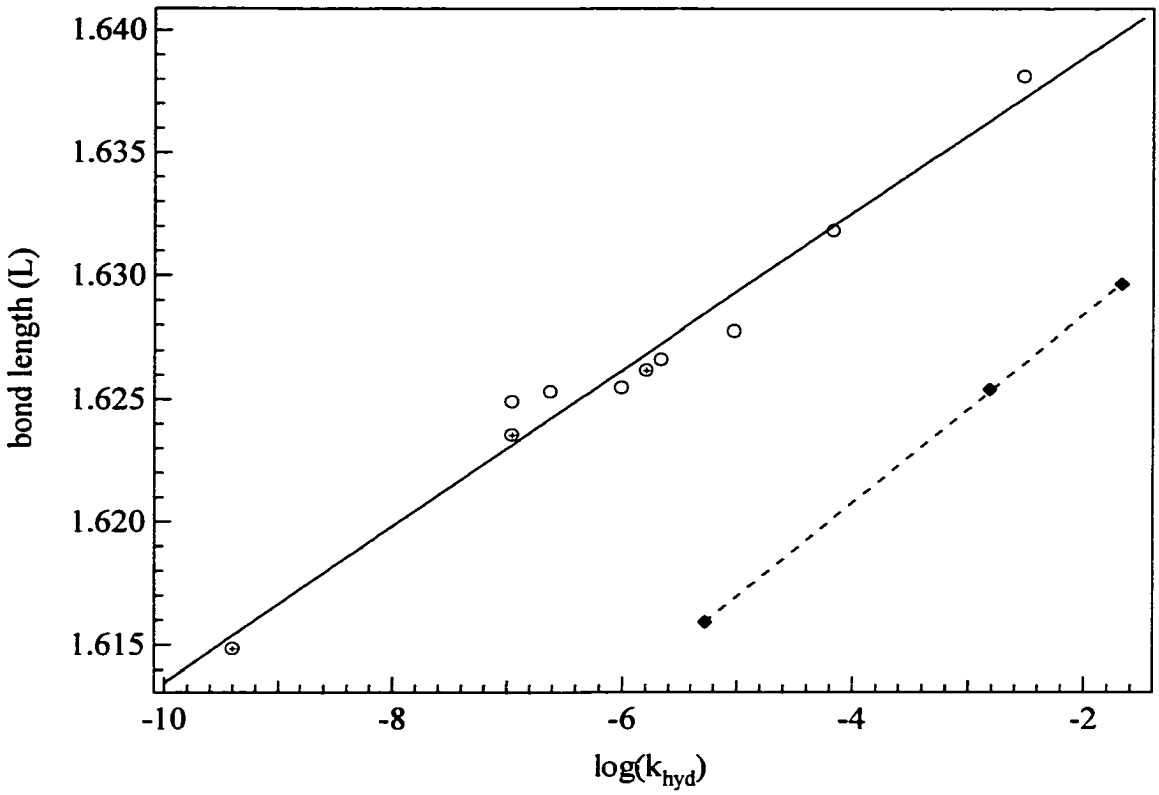

Figure 4.3: The bond length in Å of the bridging phosphate ester bond plotted versus the log of the hydrolysis rate in s^{-1} for phosphoryl transfer. The data is taken from Tables 1 and 2 with points for PNPP (○), phenylphosphate at 25 °C (+) and 95 °C (◆). The lines are least squares fit to the data with L = 1.645 (±0.001) + 0.003177 (±0.000196)*log(k_{hyd}) (solid line) and L = 1.636 + 0.003824 (±0.000038)*log(k_{hyd}) (dashed line).

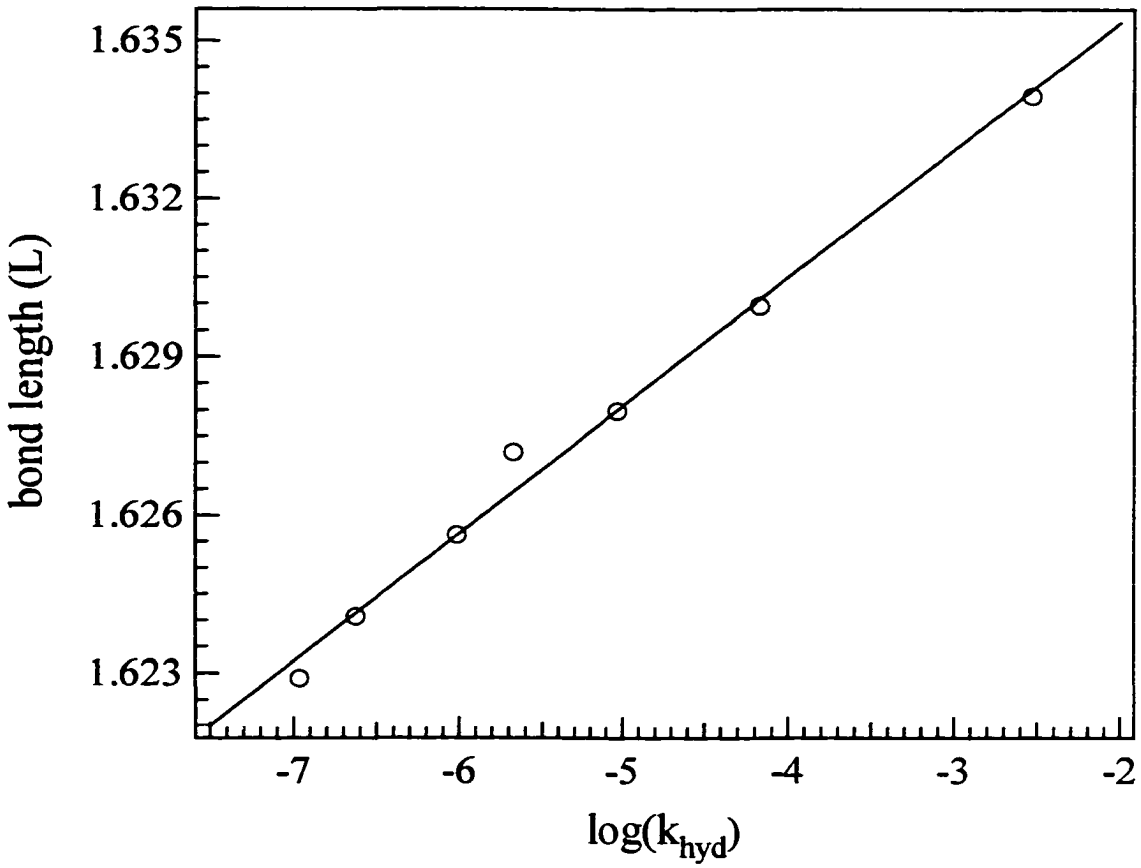

Figure 4.4: The bond length in Å of the bridging phosphate ester bond plotted versus the log of the hydrolysis rate in s^{-1} for PNPP hydrolysis. The data is taken from Tables 4.5. The lines are least squares fit to the data with L = 1.6402 (±0.0006) + 0.0024243 (±0.0001)*log(k_{hyd}).

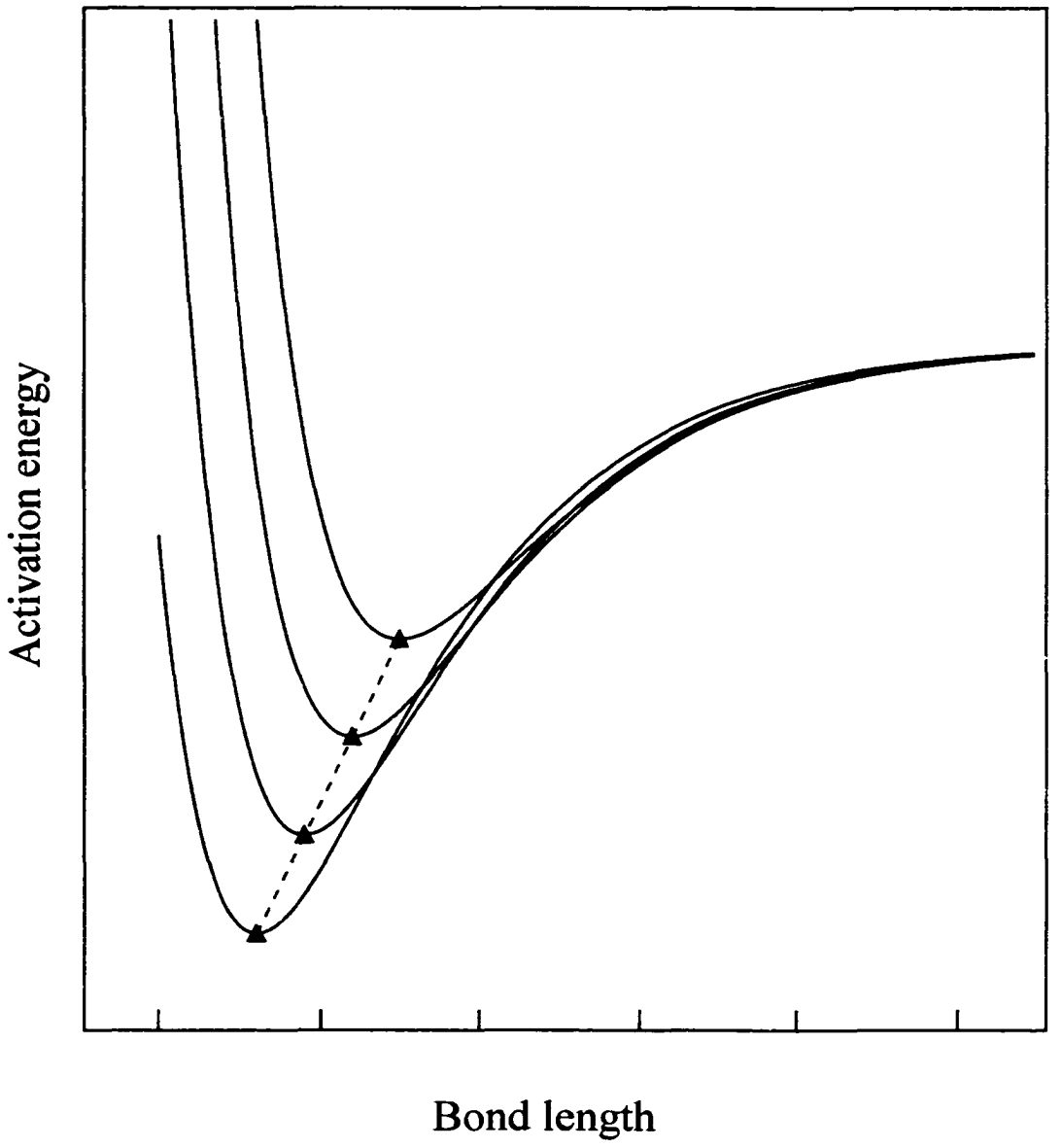

Figure 4.5: Illustration of the linear relationship between bond length and activation energy. The profile of the free energy against reaction coordinate of bond length is assumed to be described by the Morse function. The right branch of the curves are superimposed as much as possible to imitate the similar reaction paths in the hydrolysis of phosphate monoesters. The minima of each curve correspond to the ground state.

CHAPTER V

VIBRATIONAL STUDIES OF GTP and GDP BOUND TO RAS

5.1 Introduction

In general, GTP-binding proteins are in an 'active' state when complexed with GTP and in an 'inactive' state when complexed with GDP. The longer Ras protein stays in its active state, the longer the signal of growth will be transmitted and amplified. Therefore, the rate of GTP hydrolysis is of great importance for the correct timing of cell activities. This, in turn has led to great interest in understanding the mechanism of the GTPase in Ras. Despite of much progress from x-ray and other structural studies, the interaction between guanine nucleotides and the apoprotein that are responsible for binding and bringing about the protein GTPase activity is still not clear. As a result, although the phosphoryl transfer involving monoester dianionic phosphates in aqueous solution is known to be via a dissociative pathway, the mechanism of the GTPase activity in the enzyme is far from clear.

Understanding the bonding changes a substrate undergoes when it adds to an enzyme's active site, is fundamental to understanding how that enzyme accomplishes catalysis. The bond changes, and the attendant changes in bond lengths, angles and charge distribution that occur upon binding are typically small, and require a high-resolution structural technique to determine them. Vibrational spectroscopy is well suited for assess these small changes. A complete vibrational description of bonding requires the assignments of both the symmetric and antisymmetric vibrational modes. To study the nucleotide-enzyme interaction of Ras, Raman difference spectroscopy and FTIR

difference spectroscopy were applied to both GTP/GDP in aqueous solution and GTP/GDP bound to Ras. The vibrational modes of GDP and GTP in aqueous solution were completely assigned (Wang, 1998b), giving considerable information for further study of these compounds bound to enzyme. The antisymmetric vibrational modes of GTP and GDP bound to Ras were also obtained by both Raman difference spectroscopy and FTIR spectroscopy. Resort to caged GTP and GDP compounds, the antisymmetric frequencies were able to be measured (Cepus, 1998; Du, 2000). However, this method can introduce some ambiguity (which bands are from the caged compound and which from the liberated phosphate and caged fragment). Here we use isotope-edited FTIR difference spectroscopy to study nucleotide bound p21-Ras. The three oxygens of the terminal phosphate group of GDP or GTP bound to Ras are isotopically labeled with ^{18}O, the IR spectra of the enzyme-bound ^{16}O and ^{18}O-nucleotides are taken, and a difference spectrum is obtained by suitable subtraction of the $^{16}O/^{18}O$ pair. Consequently, this difference spectrum contains only bands from normal modes involving motions of non-bridging oxygens of the phosphate group, all others have cancelled out. There are, however, a number of experimental constraints that apply to this procedure if an accurate difference spectrum is to be obtained. In the first place, water has a substantial IR absorbance. Its IR spectrum in 500-2000 cm^{-1} region contains a strong peak near 1630 cm^{-1} and several overlapping bands centered at approximately 750 cm^{-1}. Fortunately, the water absorbance is lower (OD ~ 0.4 OD for 25 μm pathlength) and, importantly, relatively flat between about 1000 cm^{-1} and 1500 cm^{-1}. We found that this background spectrum can be well nulled within this frequency range. Fortunately also, this spectral range is also suitable for the study of phosphates. Second, the IR spectra must contain sufficient signal to noise so that the small spectral differences in the two parent spectra are not lost in the noise. That is, the background protein spectrum must subtract away sufficiently well. Our previous studies (Callender, 1994) on isotope edited Raman spectroscopy suggest that, for small to medium size proteins, a signal to noise ratio of

about a 1000/1 is sufficient to observe reasonably intense bands in the difference spectrum. Hence, for a parent spectrum having an OD of one, the spectrometer should be able to measure a protein spectrum of better than 1 mOD, which is easily achievable with most modern FTIR spectrometers. This signal to noise consideration, however, requires the protein signal to be comparable to the background water spectrum. For a protein like Ras, a concentration of several milimolar is required to achieve optical density at major protein peaks, like the amide-II band at 1550 cm^{-1}, of a few tenths of an OD for the 25 μm pathlength spacer used in this study.

In order to avoid systematic drift or mismatch in the spectral registry of the sample and reference parent spectra, we built a computer controlled shuttle attached to the plate of the sample holder area which brings the sample cell and reference cell into the IR beam of the spectrometer. Thus the spectrometer, particularly the cell holder area, was minimally perturbed during the experiment. Keeping a tight spectral registry is crucial and minimal disturbance of the spectrometer system during the experiment is important. This issue is discussed quite fully in the studies on Raman difference spectroscopy (Callender, 1994).

Lastly, it is necessary to null out residual water vapor bands from both parent spectra. In our case, the IR spectrometer was well purged with dry air to minimize water vapor in the IR path within the spectrometer. In our hands, these bands were typically a few mOD in the parent spectra and could be nulled out to a very high degree, better than about 0.1 mOD, by subtracting their spectrum as measured in a separate run. On the other hand, it is very difficult to have two cells (reference and sample) optically identical. Invariably, one cell's path length is slightly different than the other. Hence, the difference spectrum formed by simply subtracting the reference spectrum from that of the sample contains residual background protein, water and/or buffer spectral features that are

incompletely subtracted. In this case, we apply a small correction factor to one of the parent spectra which is varied until the background peaks are null.

The Ras protein was purified by Sean Sukal in the lab of Dr. Thomas Leyh in Albert Einstein College of Medicine. The isotope labeled nucleotides were also synthesized by them. Purified Ras were centrifuged in a Centricon 10 (Amicon) filter to a high concentration, then washed with buffer I (200 mM Tris-HCl; 200 mM $(NH_4)_2SO_4$; 0.55 mM DTT; 0.5 mM NaN_3; 0.6 mM EDTA; pH 7.5) one or two times to make sure the GDP and Mg2+ were almost gone. The protein was diluted with buffer I to a concentration of ~0.5 mM and then incubated with 10 fold molar excess of (^{18}O)GDP (GTP). The incubation time was set 30 minutes at room temperature. After the exchange was carried out, excessive GDP was washed out with buffer II (20 mM Tris-HCl; 10 mM $MgCl_2$; 0.5 mM NaN_3; pH 7.5) three times. The final concentration was raised to 2 ~ 4 mM for better resolution in the IR spectra.

Figure 5.1 and 5.2 provide an example of spectral subtraction in the Ras system. Figure 5.1 shows the spectrum of Ras•GDP•Mg^{2+} and labeled Ras• (β-^{18}O)GDP•Mg^{2+} in 25 μm pathlength cells. These two spectra, virtually superimposed (although a close look near 1100 cm^{-1} suggests a small difference) as shown in figure 5.1a, are the starting spectra of the subtraction process. Panel b of figure 5.1 shows the same two spectra after the water/buffer spectrum, separately taken, has been subtracted. The relatively large protein peak near 1550 cm^{-1} is the well-known amide II peak of proteins. Panels a and b of figure 5.2 show, individually, the two spectra given in figure 5.1b. Panel c-e show the result of subtracting these two parent spectra, scaled by a factor of ten. Because of slight differences in cell pathlengths, a small scaling factor between the two parent spectra is adjusted until the protein peaks, which are easily identified and are not affected by substitution of ^{18}O on the substrate phosphate, are well nulled. Note that the amide-II

peak does not entirely subtract but yields a small 'derivative' looking signal in the difference spectrum of Panel d. This indicates a small amount of misregistry in the frequency calibration of the two parent spectra. It is probable that the misregistry results from the substantial water background slope that begins near 1500 cm^{-1}. In such a series of difference spectra, it is most important to observe that the modes assigned to labeled phosphate groups (here, from 1050-1150 cm^{-1}) remain relatively constant as the background protein peaks range through an under to an over subtraction.

5.2 GDP Bound to Ras

Figure 5.3a shows the IR difference spectrum formed by subtracting the solution spectrum of Mg•[β-$^{18}O_3$]GDP from that of Mg•[β-$^{16}O_3$]GDP; panel b shows the analogous difference spectrum for GDP bound to Ras (this is the same as Figure 2d except over a narrower spectral range). A symmetric PO_3^{2-} moiety, as is reasonably well approximated for the terminal phosphate of GDP and GTP in solution, has three P••O stretch normal modes, a doubly degenerate antisymmetric stretch,ν_a, and one symmetric stretch, ν_s (Deng, 1998a). As for the phosphates in monoesters, the antisymmetric stretch lies in the 1000-1200 cm^{-1} region and is strongly allowed in the IR. Therefore, the positive peak found in the solution difference spectrum at 1143 cm^{-1} arises from the antisymmetric stretch for Ras•[β-$^{16}O_3$]GDP, while the negative feature at 1086 cm^{-1} is ν_a for Ras•[β-$^{18}O_3$]GDP. The antisymmetric bands for Mg•GDP have been previously measured and lie at 1123 and 1089 cm^{-1} for [β-$^{16}O_3$]•GDP and [β-$^{18}O_3$]•GDP, respectively (Wang, 1998b). The fact that the peaks in the difference spectrum do not correspond to the actual frequencies found in the parent spectra has to do with the fact that the antisymmetric bands are broad relative to the 34 cm^{-1} shift that arises from the isotope labeling. In this case (Manor, 1991), the apparent band positions in the difference

spectra are shifted, and the difference in frequency between the positive and negative couplet is greater than the isotope shift. The positions and bandwidth (full width at half-maximum, Γ) of the P••O stretches for GDP•Mg^{2+} in water and bound to Ras have been summarized in Table 5.1. The symmetric stretch parameters have been taken from refs (Wang, 1998b) and (Wang, 1998a). A previous time-resolved IR study, which employed caged GTP compounds of individually labeled ^{18}O P••O bonds and kinetic difference spectroscopic techniques, placed the IR modes of GDP bound to Ras at 1100 and 1236 cm^{-1} (Cepus, 1998). We do not know the reason for this discrepancy between the two studies, although (1) individually labeling the oxygens distorts the symmetry of the β-phosphoryl group, making a strict comparison difficult and (2), assignments of GDP bands rest on double difference spectra that are somewhat difficult to interpret (Du, 2000). On the other hand, our results are in good agreement with a second study using caged compounds (Du, 2000).

As ligands bind to proteins, their vibrational motion becomes restricted by interaction with the binding site. This increased order narrows the bands within the spectrum due to a reduction of the bandwidth compared to solution (particular water). Comparison of panels a and b of Figure 5.3 demonstrates this narrowing effect on the β-phosphoryl group of GDP. The bandwidth in the protein difference spectrum is small enough that the apparent band positions lie at their true positions.

It is clear from the observation of two positive/negative couplets in the isotope difference spectrum, which are separated by the expected ^{16}O-^{18}O isotope shift, that the degeneracy of the antisymmetric modes is lifted by ligand binding interactions, and that the two frequencies lie at 1138 and 1100 cm^{-1}. This means that the approximate C_{3v} symmetry of the PO_3^{2-} moiety has been broken as would happen if, for example, one of the oxygens interacted through hydrogen bonding interactions with protein moieties that

were stronger than the interactions with the other two. Such symmetry breaking has been observed for vanadate bound to the ATP binding site of myosin (Deng, 1998b).

5.3 GTP Bound to Ras

Figure 5.4a shows the IR difference spectrum formed by the subtracting the solution spectrum of Mg•[γ-$^{18}O_3$]GTP from Mg•[γ-$^{16}O_3$]GTP, while panel b shows the phosphate difference spectrum for GTP bound to Ras. Although Ras catalyzes the hydrolysis of GTP to GDP, the half-time of the reaction on the enzyme is about 34 hours at 4 °C, which is substantially longer than the time for these measurements (typically a few hours). In contrast to the GDP spectra, the solution and Ras-bound GTP difference spectra are similar. The C_{3v} symmetry of the PO_3^{2-} does not appear to be broken when GTP binds to Ras, and the degenerate ν_a bandwidth of both spectra is broad, causing the true peak positions to lie at somewhat different positions from the positive/negative positions of the couplet in the difference spectra. Figure 5.4 list the positions of the couplet observed in the difference spectrum, while Table 5.2 lists the comparison of the true values and the negative/positive positions observed from difference spectra for GTP and Mg•GTP in solution (Wang, 1998b). The true frequencies of GTP bound to Ras are then obtained as an extrapolation by calculating the average position of the shift in the average of the minimum and maximum position in the water and Ras difference spectra and adding this to the known water position. This procedure has been shown to give good values for shifts even if the bandwidths are affected by binding. The actual positions are listed in Table 5.3. The position from ν_a measured here is in good agreement with the previous IR studies using caged GTP compounds and singly labeled P••O bonds which place an IR active mode at 1143 cm^{-1} for one of the γ-phosphate P••O stretch modes of bound GTP (Cepus, 1998) and at 1142 cm^{-1} (Du, 2000). The latter IR study, however,

assigned a band at 1158 cm^{-1} to a second antisymmetric mode suggested to arise from lifting the C_{3v} symmetry of the γ-PO_3^{2-} moiety for bound GTP. This observation may correspond to the weak mode located at about 1163 cm^{-1} in Figure 4b in our study. This band is almost certainly not a second antisymmetric mode, we believe, for the following reasons. (1) The band is quite small in intensity (the two bands should have quite similar intensities). (2) It appears as a weak shoulder in the GTP solution data (Figure 5.4a). (3) The bandwidth of the 1144 cm^{-1} mode is quite broad, indicating weak interactions at the active site with the γ-PO_3^{2-} moiety. (4) The band also seems to appear in the GDP data in Figure 5.3. It may correspond to one of the O-P-O bending modes. The bandwidth of the antisymmetric mode of the γ-phosphate for Mg•GTP in water comes from ref (Wang, 1998b). The bandwidth of the GTP-bound mode was estimated by fitting the difference spectrum to trial Gaussian functions of varying half-widths. The positions for ν_a in Ras•[γ-$^{16}O_3$]GTP have been previously measured (Wang, 1998a; Wang, 1998b).

5.4 Structural Information

Using the relationship between vibrational frequency and bond length (or bond order) having been developed for phosphate P••O and P-O bonds (Eq. 3.5 in Chapter III), we are able to calculate the bond lengths of P-O bridging bonds of GDP or GTP bound to Ras. We rewrite the equation here,

$$L_{PO} = 0.2835 \cdot \ln(224500/\nu) \tag{3.5}$$

Table 5.1 and 5.3 list the bond lengths and bond orders of the nonbridging P••O bonds and bridging P-O bond using equation 3.1 and 3.2 while holding the sum of the bond order about the phosphorus atom to 5.

The positions of the symmetric and antisymmetric modes of phosphate depend on the angle, θ, between the nonbridging O••P••O bonds of the PO_3^{2-} moiety and the ratio of the stretch force constant for the P••O bond to the P••O/ P••O stretch/stretch off-diagonal force constant, see Eq. 3.8. Using ab initio calculations (at the HF/3-21 g* level), it is estimated (Wang, 1998a) that θ ~ 115° for the terminal PO_3^{2-} group of triphosphate, agreeing well within the average angle of ATP molecules found in the Cambridge Structural Database, which is about 113.5° (an angle of 120° means a planar PO_3^{2-} moiety as would be found, for example, in metaphosphate; (Wang, 1998a)). The change in the angle of the PO_3^{2-} moiety as GTP binds to Ras can be estimated from changes in the two frequencies. Given that ν_s = 916 cm^{-1}, ν_a = 1138 cm^{-1} for Ras•[γ-$^{16}O_3$]GTP (Table 2), it is calculated that the θ of O••P••O bonds widens by about +2.1° (i.e., become substantially more planar) when the nucleotide binds (Wang, 1998a).

The width of antisymmetric stretch modes of dianionic monoesters in solution are quite broad (42 cm^{-1} for GTP in water), while those of symmetric stretch modes are relatively narrow (< 10 cm^{-1} for GTP). This is due to varying values of θ arising from the nucleotide and concomitant heterogeneous broadening of the antisymmetric mode. The symmetric mode frequency is not sensitive to varying values of θ for the particular structure of GTP. From the width of the antisymmetric stretch, it is estimated previously (Deng, 1998a; Wang, 1998a) that the angle (Δθ) of the O••P••O group of the PO_3^{2-} moiety ranges over about 2.7° (±0.5°) for GTP in aqueous solution. It is clear (Figure 5.4b) that the antisymmetric bandwidth is smaller for GTP bound to Ras than for GTP in water. We estimate that the width of the stretch mode is reduced to 26 cm^{-1}, and this reduces the excursion of the O••P••O angle to 1.8°. Similar calculations yield the variation in θ values for GDP in water and when bound to Ras from the data of Figure 5.3 are listed in Table 5.1.

5.5 Insights to Mechanisms of GTPase

The measurement of the antisymmetric modes of Ras bound GDP or GTP has been approached in two previous studies using time-resolved FTIR studies of "caged" GTP analogues. In agreement with these results, the terminal phosphate group of GDP is clearly highly immobilized when bound to Ras. This is seen most cogently in the >42 cm^{-1} collapse in the bandwidth of the β-phosphate antisymmetric mode that occurs as GDP moves from solution into the active site. The large solution bandwidth is a result, primarily, of the conformation flexibility of the PO_3^{2-} group in water with regard to the O••P••O angle. The antisymmetric mode stretch frequency is a sensitive function of this angle, and as the phosphate group accesses various conformations with regard to this coordinate, each conformation will result in a somewhat different antisymmetric P••O stretch frequency that gives rise to the heterogeneously broadened bandwidth of this mode. The estimated angle variation of the terminal phosphate group of GDP in the nonrigid, aqueous environment, based on the measured bandwidth, is about ±2° from equilibrium for a total of variation of 4°. This estimation is quite consistent with calculations on a model phosphate (methyl phosphate) using ab initio methods (b31yp/6-31g* basis set; (Wang, 1998a)). The calculations suggest that a change in the O••P••O angle from its equilibrium value by 2° costs only 0.4 kcal/mol. Thus, the variation of ±2° from equilibrium observed in solution is easily driven by thermal motion. On the other hand, the variation of the O••P••O angle of the terminal phosphate for GDP bound to Ras is restricted to less than 0.7°.

In addition to the restricted angular motion of the β-phosphate, the interactions between the phosphate and the binding pocket of Ras break the approximate C_{3v}

symmetry of the phosphate group. Two strong antisymmetric bands are observed in the IR difference spectrum. Using an ab initio quantum mechanical approach, it was found for the model phosphate that the degeneracy of the β-PO_3^{2-} group is lifted. Two antisymmetric-like modes were calculated, one shifted by –6 cm^{-1} and the other shifted by –54 cm^{-1} from the solution frequency. This is in semiquantitative agreement with the observed results (Table 5.1). Shifts of this magnitude result from significant polarization of the nonbridging P••O bonds are indicative of quite strong ionic interactions between the phosphate moiety and the protein. These calculations show what is clear from the experimental results, i.e., that the β-phosphate group of Ras-bound GDP is tightly bound and relatively rigid.

On the basis of the frequency changes of the GTP terminal P••O stretch modes upon binding to Ras (Table 5.3), it can be calculated that the average terminal P••O bond order is increased by 0.004 vu and that the average O••P••O angle is increased by ~2.1°. From this, the bond length of the terminal P-O bridging bond increases by at least 0.0005 Å upon binding (Table 5.3). This is a rather small change but is, however, larger than experimental error. Also the dispersion of the O••P••O angle of about 1.8° is comparable to what is seen for Mg2+•GTP in solution (i.e., 2.7°; Table 5.3). Thus, in contrast to the β-phosphate group of GDP, the active site has preserved the conformational flexibility of the γ-phosphate group of GTP bond angles close to that seen in solution, yet, it causes the γ-PO_3^{2-} moiety to become substantially more planar. This enzyme-driven lengthening of the terminal bridging P-O bond and the opening of the O••P••O bond angle represents a structural destabilization of the γ-PO_3^{2-} group toward to a more planar, or transition-state-like, structure. It is important to realize, however, that the energy cost of such changes is on the order of < 1 kcal/mol since, as indicated above, ab initio calculations yield energies of this size on model phosphate systems for destabilization of the P-O bridging bond or O••P••O angle changes that are observed. Such destabilization energy in the

ground state is very small compared to the solution-phase activation energy for GTP hydrolysis, ~ 25 kcal/mol (Di Sabato, 1961; Herschlag, 1986).

The current studies provide an intimate view of the bonding changes that occur when Mg2+GTP binds to Ras and suggest that substrate begins to acquire transition-state-like features in the enzyme-bound ground state: the γ-PO_3^{2-} group approaches a more planar geometry expected in the transition state, and the bridging P-O bond is slightly weakened. In the solution chemistry of phosphoryl transfer of dianionic phosphate monoesters, it has been shown by classical analyses of Brönsted plots for hydrolysis versus changes in the pKa of the RO^- leaving group that the structure of the transition state is primarily dissociative, i.e., $RO^-\cdots\cdots PO_3^{2-}\cdots\cdots$:NU, with NU being the attacking nucleophile. Stabilization of this type of transition state suggests that ground-state effects on the electronic makeup of the molecule would be small since the ground state is so unlike the transition state in structure. However, stabilization of the RO^- leaving group, as observed in the present studies of bound GDP and in Ras, is consistent with solution chemistry and would leave a small signature in the ground state by weakening the bridging P-O bond of GDP- PO_3^{2-} as is observed. To make these qualitative considerations more quantitative, we would like to apply the correlation of bond order and hydrolysis rate we derived in chapter IV to the hydrolysis of GTP bound to Ras. If the hydrolysis of GTP bound to Ras proceeds in the same way as in solution, the bond length change should predict the rate enhancement to the same order. A change in rate constant of a factor of 10 corresponds to a weakening of the P-O bridging bond of 0.0038 Å over a very wide range, more than 10 decades, in rates. Then the observed 0.005 Å decrease in the GTP PO-P bond order predicts a hydrolysis rate increased 40 fold over that in solution, which is more than 10-fold less than what is observed in Ras (Maegley, 1996). This disagreement seems to imply that the observed bonding changes may not lie on the reaction coordinate appropriate for a pure dissociative mechanism. However, we

noticed that the bond length change of the P-O bridging bond from GTP to GTP•Mg^{2+} also predicts a rate enhancement of 80 times while the actual rate change is within 2 times. So, we have to be careful with GTP•Mg^{2+} since its hydrolysis mechanism is unclear. Although a study of the hydrolysis of PNPP dianions in water and substituted pyridines shows that Mg^{2+} and Ca^{2+} catalyze the reaction but do not increase the associative character of the transition state due to the small value of β_{nuc} for PNPP or PNPP with metal ions (Herschlag, 1989), we still suspect that the Mg^{2+} could partially change the dissociative property of the transition state for GTP hydrolysis. This is based on the following observations: the difference between GTP and PNPP is that GTP has three phosphates, that might all interact with the metal ions. Ab initio calculations performed in our lab (Wang, 1999) show that the Mg^{2+} binds to α-, β-, and γ-phosphate in solution, which is totally different from the pattern of Mg^{2+} binding in PNPP. Therefore, the conclusion from PNPP may not apply to GTP. The calculation also shows that Mg^{2+} is only coordinated to β- and γ-phosphate in the Ras protein, which agrees with crystallography results. Hence, if we assume the Ras-catalyzed GTP hydrolysis adopts the similar mechanism as hydrolysis in solution, the appropriate way to test it is to compare the rates and bond length with those in solution without Mg^{2+}. The antisymmetric and symmetric frequencies of GTP in water at pH 7.5 are 1119 cm^{-1} and 927 cm^{-1} respectively. So the bond length of the bridging P-O bond is calculated to be 1.605 Å. The 0.011 Å increase in bond length predicts the rate enhancement of ~1000 times. So our results demonstrate that the magnitudes of the observed changes found in the solution chemistry are comparable to what is expected in the substrate ground state of a phosphate monoester dianion hydrolysis reaction in a classical dissociative reaction mechanism where the rate acceleration is on the order of what is provided by Ras. As proposed in Ref. (Maegley, 1996), if the enzymatic catalysis proceeds via a dissociative transition state, then there will be some common features in the reaction.

1) The nonbridging γ-phosphoryl oxygens will show a decrease in electron density.

2) The β-γ bridging oxygen will undergo the largest charge increase.
3) There will be modest charge development on the β-phosphoryl nonbridging oxygen atoms.

We have observed the bond order increase of the nonbridging bond in the γ-phosphate. From the reasoning in Chapter IV, for phosphorus-oxygen bonds, increasing bond order means decreasing bond length, decreasing bond length results from decreasing electronegativity of the oxygen. Hence, the increasing of nonbridging bond order can be an indicator of the decrease in electron density of the oxygens in the nonbridging γ-phosphoryl bonds. Similar inference to the β-γ bridging bond can be also made to draw the conclusion that the β-γ bridging oxygen undergoes charge increase (larger electronegativity) due to the decreasing of the bridging bond length. However, the increasing of bond order or bond length is rather small to make any strong statements. We don't have any information about the vibrational modes involving the β-phosphoryl nonbridging oxygen atoms, so the third condition is not tested. But we would like to emphasize that all these coincidences do not necessarily exclude the possible mechanisms other than the dissociative one. We will discuss this issue more in Chapter VI.

Table 5.1: Frequencies (in cm^{-1}) of the symmetric, ν_s, antisymmetric, ν_a, and 'fundamental', ν, stretch modes of the non-bonded P••O stretch modes of the β-phosphate of GDP in water and when bound to Ras, the bandwidth (in cm^{-1}) of the antisymmetric mode, Γ_{ν_a}, bond orders, S (in vu), and bond lengths, L (in Å), of non-bridging and bridging bonds, and the approximate root mean square of the variation in the angle of the non-bridging O••P••O bonds, Δθ, due to the heterogeneous broadening.

	Mg•[γ-$^{16}O_3$]GTP in water	Ras•Mg•[γ-$^{16}O_3$]GTP
ν_s	942	915
ν_a	1123	1138 1100
ν	1066	1056
$S_{\beta\text{-nonbridging P••O}}$	1.327	1.316
$S_{\text{bridging P-O}}$	1.020	1.052
L	1.613	1.601
Γ_{ν_a}	62	~10
Δθ of O••P••O bonds	4.0°(±0.6°)	<0.7°

Table 5.2: Deduction of antisymmetric frequency of Ras•Mg•GTP.

	Min	Max	Average (center)	Measured frequency
GTP	1080	1130	1105	1119
Mg^{2+}•GTP	1088	1140	1114	1128
Ras•Mg•GTP	1106	1142	1124	1138 (anticipated)

Table 5.3: The frequencies (in cm^{-1}) of the symmetric, ν_s, antisymmetric, ν_a, and 'fundamental', ν, stretch modes of the non-bonded P••O stretch modes of the γ-phosphate of GTP in water and when bound to Ras, the bandwidth (in cm^{-1}) of the antisymmetric mode, Γ_{ν_a}, bond orders, S (in vu), and bond lengths, L (in Å), of non-bridging and bridging bonds, and the approximate root mean square of the variation in the angle of the non-bridging O••P••O bonds, Δθ, due to the heterogeneous broadening, and the angle, θ, of the non-bridging O••P••O bonds.

	Mg•[γ-$^{16}O_3$]GTP in water	Ras•Mg•[γ-$^{16}O_3$]GTP
ν_s	926	916
ν_a	1128	1138
ν	1065	1069
$S_{\gamma\text{-nonbridging P••O}}$	1.326	1.330
$S_{\text{bridging P-O}}$	1.023	1.011
L	1.611	1.616
Γ_{ν_a}	42	26
Δθ of O••P••O bonds	2.7°(±0.5°)	~1.8°
θ of O••P••O bonds	115°	115°+2.1°

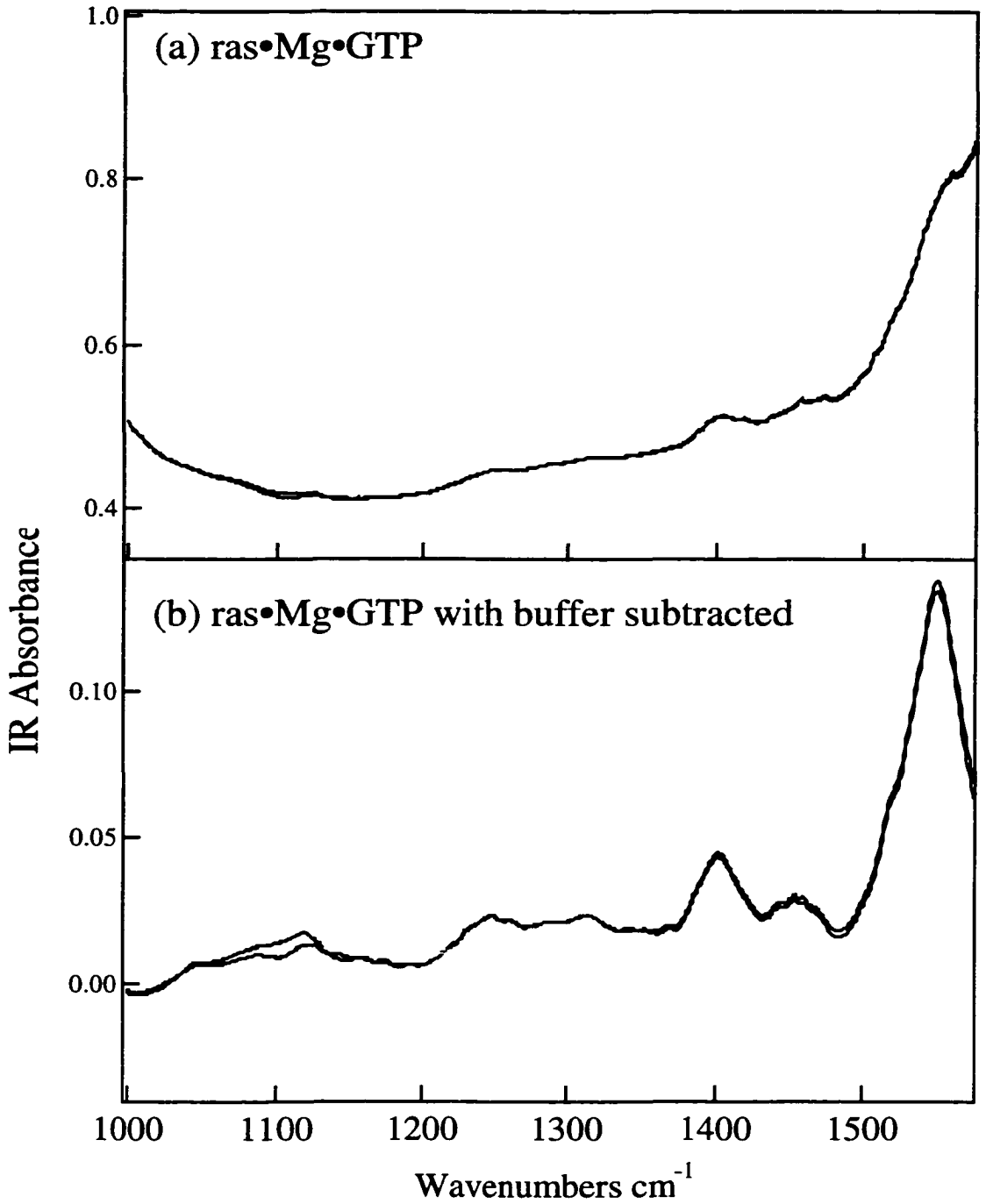

Figure 5.1: (a) IR spectra of 5 mM Ras•Mg•GTP and Ras•Mg•(γ-$^{18}O_3$)GTP in 20 mM Tris-HCl buffer, at pH 7.5 and at 4 °C. (b) spectra in with the spectrum of Tris buffer subtracted.

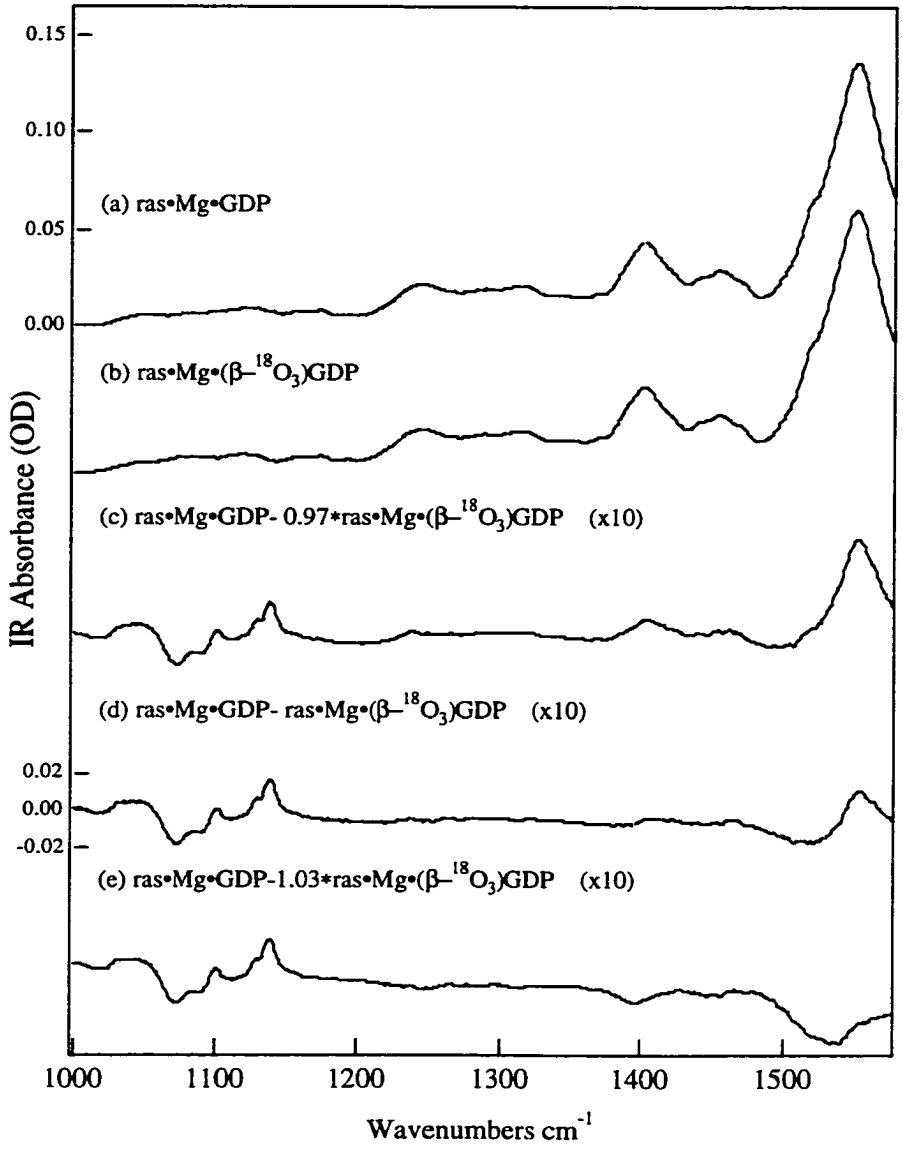

Figure 5.2: (a) IR spectrum of Ras•Mg•GDP, (b) IR spectrum of Ras•Mg•(γ-$^{18}O_3$)GDP, (c) difference spectrum between Ras•Mg•GDP and Ras•Mg•(γ-$^{18}O_3$)GDP, a factor of 0.97 was multiplied on the latter spectrum and the result multiplied by a factor of 10, (d) difference spectrum between Ras•Mg•GDP and Ras•Mg•(γ-$^{18}O_3$)GDP, and the result multiplied by a factor of 10, (e) difference spectrum between Ras•Mg•GDP and Ras•Mg•(γ-$^{18}O_3$)GDP, a factor of 1.03 was multiplied on the latter spectrum and the result multiplied by a factor of 10.

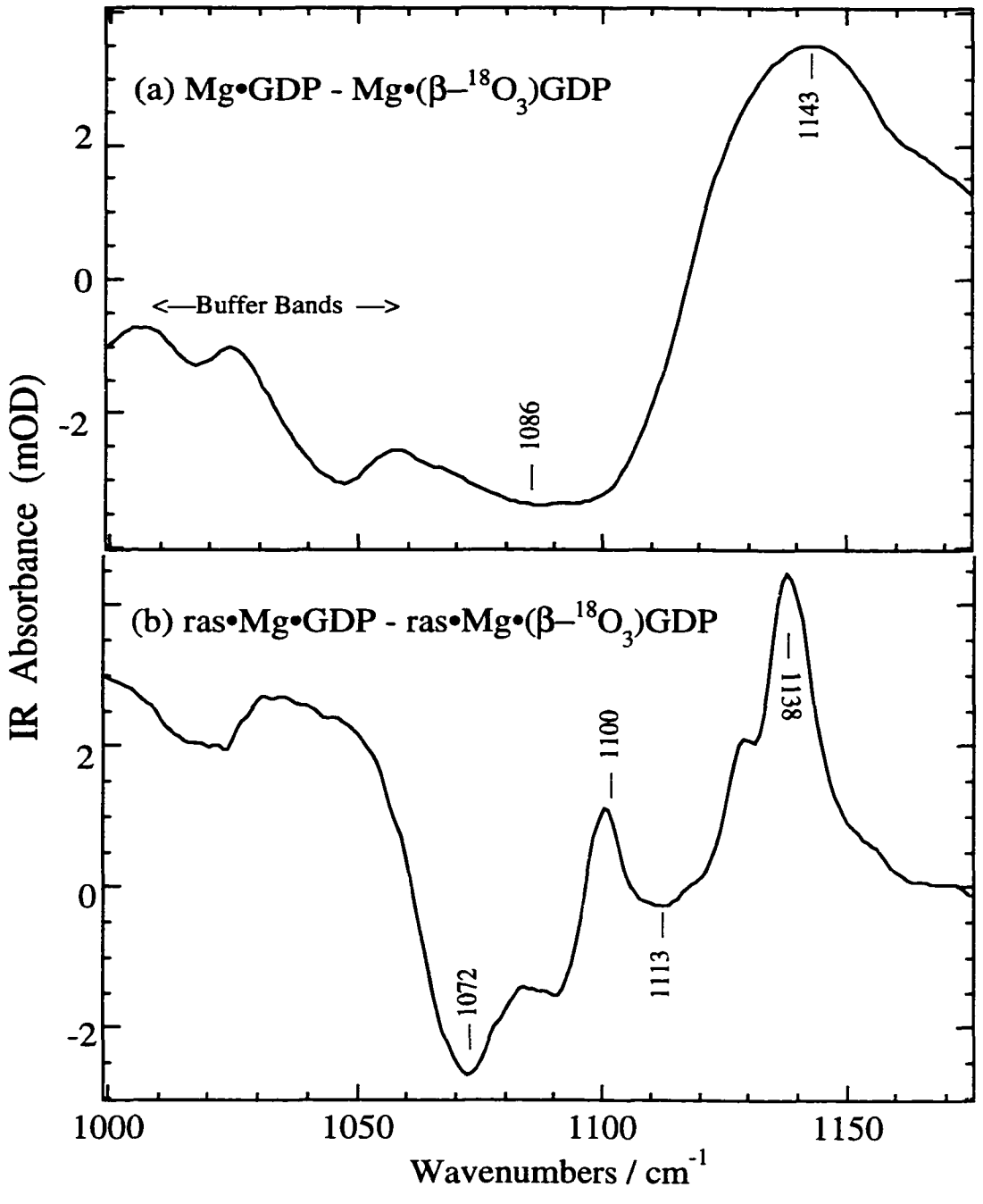

Figure 5.3: IR difference spectrum in aqueous solution at pH 7.5 and 4 °C. (a) Mg•GTP minus Mg•(γ-$^{18}O_3$)GTP, (b) Ras•Mg•GTP minus Ras•Mg•(γ-$^{18}O_3$)GTP

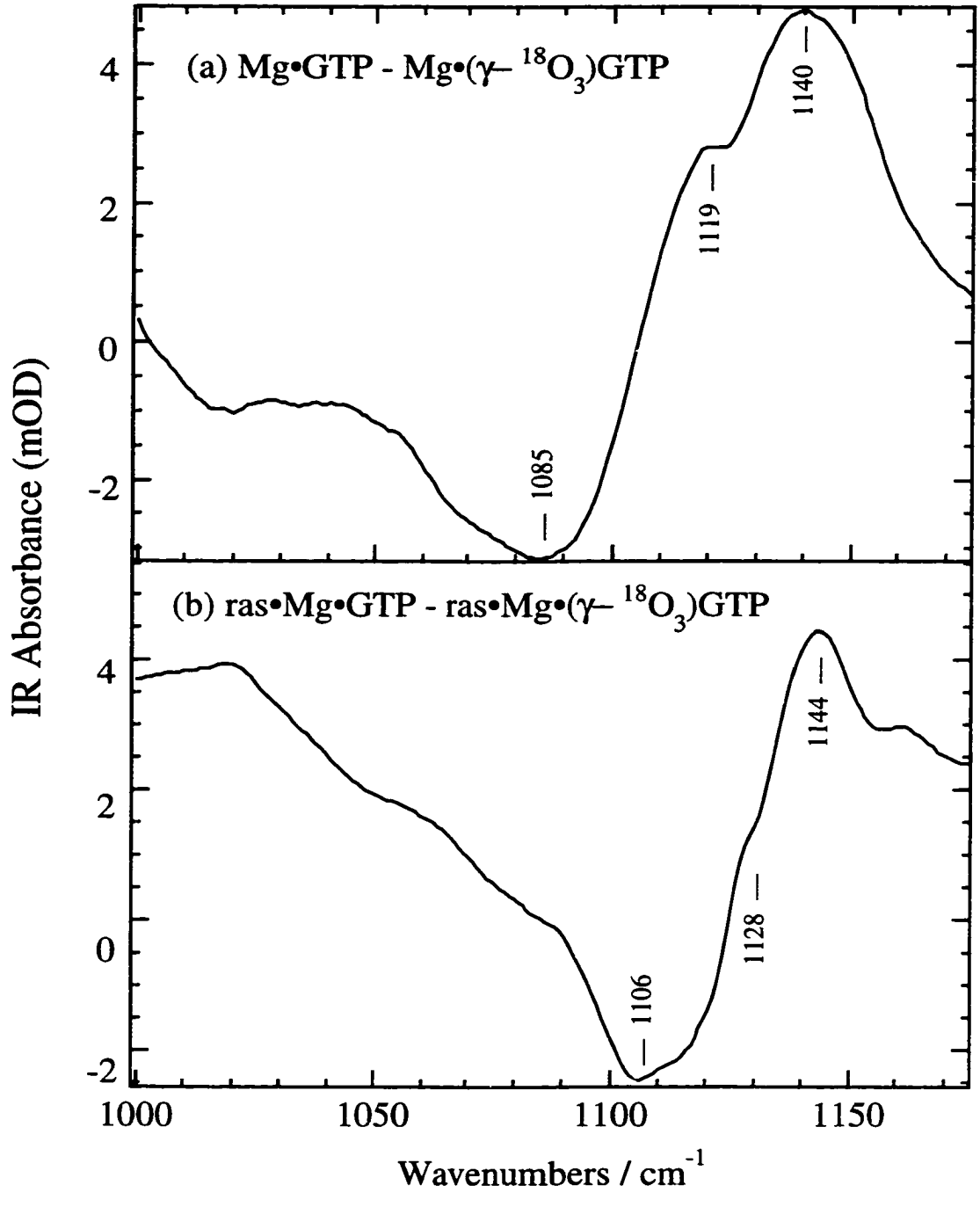

Figure 5.4: IR difference spectrum in aqueous solution at pH 7.5 and 4 °C. (a) Mg•GTP minus Mg•(γ-$^{18}O_3$)GTP, (b) Ras•Mg•GTP minus Ras•Mg•(γ-$^{18}O_3$)GTP

CHAPTER VI

RAS•GTP AND RAS•GDP AT LOW pH

6.1 Introduction

How Ras, and other G-proteins, bring about hydrolysis of GTP is poorly understood. In contrast to the mechanism that prefers a dissociative transition state, some proposals in favor of an associative transition state were also raised. One idea that has been advanced for Ras is that the attacking water molecule 'activated' by converting it to hydroxyl. However, this requires a general base. There are a number of groups at the Ras binding site, but a review of recent theoretical and experimental results using mutant proteins in binding and kinetic studies suggest that none of the active site protein residues can adequately serve as the base (Schweins, 1995). For example, the putative attacking water molecule is lined up between the γ-phosphorous of bound GTP and the side chain of Gln61. Although originally proposed as a possible base, there are several results that argue against this role for Gln61 (see (Schweins, 1995) and references therein). This has left GTP itself as the putative general base. A NMR titration study of Ras•Mg^{2+}•GTP concluded that the pK_a of the γ-phosphorous is 2.9 (solution value is 6.2), and this is close to the pK_a of the intrinsic hydrolysis rate of bound GTP (Schweins, 1995). Moreover, a Brönsted relationship of the GTPase reaction versus apparent pK_a of the terminal phosphate (varied by using mutant proteins) was found. This has prompted the suggestion of 'substrate assisted' catalysis that has the terminal phosphate abstracting a proton from wat-175. However, the NMR analysis is far from clear. The measurements in our group showed no evidence for a protonated γ-phosphate (Wang, 1998a) (although the measurements were carried out at pH 7.5 where a substantial amount of protonated

phosphate is not expected). All three GTP phosphorous atoms showed altered ^{31}P-NMR signals, suggesting the possibility of an altered conformation of the bound substrate rather than protonation. Since the titrations were performed from 2 to 7, it is very possible that the protein has unfolded at low pH. Although the shape and position of the NMR signals indicated a bound GTP, proteins can partially unfold as a function of pH; and a reversible partial unfolding whose structure involves a bound nucleotide is very plausible. Therefore, the measurement of the pK_a of the γ-phosphate of GTP bound to Ras should be carried out with different approaches as a comparison. To this end, we design our experiments in two ways. One is trying to derive the pK_a of γ-phosphate with IR spectroscopy. Another is to explore the effect of low pH to the pK_a measurements in both NMR and IR spectroscopy. Our results give some insight for the interpretation of the NMR data and the mechanism of GTPase as well.

6.2 Determination of pK_a from vibrational modes

Vibrational spectroscopy is very sensitive to the change of environment. Many bands vary in accordance with pH change of the solution. Particularly, if the hydrogen is involved in the molecular vibrations, then the spectrum of the protonated group will show big differences from that of unprotonated one. For example, a frequency change of 90 cm^{-1} is observed for the phosphate P••O non-bonded stretch modes, and the frequency positions are very distinctive (Deng, 1998a). In many cases, spectroscopy is a good method to measure pKa of the ligands in proteins by monitoring the bands only associated with the vibrational modes of the ligands other than protein. Raman spectroscopy has been successfully used to measure pKa of some small molecules bound to protein (Chen, 1994; Chen, 1997). In this study, we will use FTIR to investigate the ionization of the phosphate moieties in Ras by monitoring the antisymmetric bands.

Despite all the advantages mentioned above, things are a little complicated in GTP and GDP. One reason is that the IR bands from the terminal phosphate are tangled with those from the inner PO_2 (see Figure 3.3), and the shifts under pH change are not as big as those in single phosphate (Wang, 1998b). Another difficulty is that we can only use difference spectra of normal nucleotide and isotope edited one, leaving the interpretation more involved. Therefore, we make our first step by looking at the difference spectrum of GDP/GTP in solution. And it will be easier to go further to the difference spectrum of these compounds in the enzyme.

Figure 6.1 is the titration curve of GTP in solution in the presence of Mg^{2+}. The pK_a is determined to be 4.3 after fitting the data to Henderson-Hasselbalch equation. This value is about 2 units lower than that without Mg^{2+}. The magnesium cation is coordinated with two oxygen atoms from both β- and γ- phosphate group and brings down the pK_a.

To get a flavor of how the vibrational modes are affected by isotope editing as well as protonation, we want to see the original spectra of GTP and ^{18}O labeled GTP at pH 7.5 and pH 5.0. These spectra are shown in Figure 6.2. The vibrational modes were assigned earlier. The 1120 cm^{-1} band in (a) Panel A corresponds to the antisymmetric vibrational mode of GTP, this band shifts to 1085 cm^{-1} in the (γ-^{18}O) labeled GTP. The wavenumber difference from isotope labeling is 35 cm^{-1}, which is big enough for resolving the frequencies in the difference spectrum. At pH 5.1, the symmetry of the terminal phosphate is C_{2v}, hence, the spectrum looks totally different. Although the bands were assigned to many coupled vibrational modes, we are not bothered here since we are only interested in the profile of the difference spectrum. The isotope difference spectra at pH 7.5 and pH 5.1 are not alike here.

To test how well the difference spectrum can tell us the pK_a value and to aid assigning the Ras•GTP•Mg^{2+} difference spectra as well as provide comparisons between the active site and solution behavior of the γ-phosphate, the difference spectra for the γ-phosphate-protonated and -deprotonated forms of both GTP and GTP•Mg^{2+} in solution are obtained. Figure 6.3 shows the difference spectra of GTP and GTP•Mg^{2+} at different pH values. Here we focus on the region of 1000-1200 cm^{-1} because the symmetric vibrational mode of the terminal phosphate is not sensitive to pH change, we only monitor the change of antisymmetric vibrational modes which are within this range. From the profile change of the difference spectra, we see that the protonated and deprotonated spectra do not change a lot when the pH value is far from the pK_a value. The spectrum in the middle (where the pH value is close to the pK_a value) is somehow like the average of the spectra at highest and lowest pH. We may estimate the pK_a of γ-phosphate by comparing the spectrum to the average of the protonated and unprotonated difference spectra. The pK_a value is then around 6.4 for GTP and 4.5 for GTP•Mg^{2+}. These numbers are quite close to the pK_a values obtained from direct titration, which are 6.7 without Mg^{2+} and 4.3 in the presence of Mg^{2+}.

The pH dependence of the Ras•GTP•Mg^{2+} difference spectra is shown in Figure 6.4. If we compare the spectra with those for GTP and GTP•Mg^{2+} in solution, the spectra from pH 7.5 down to 3.3 are very similar to the unprotonated ones in solution phase. These similarities strongly support the notion that the γ-phosphate is dianionic in the active site. The spectrum begins to change at pH 3.3, indicating that the γ-phosphate remains largely unprotonated at this pH, in other words, the pK_a must be quite a little smaller than 3.3. Thus, the active site of Ras has decreased the pK_a of the γ-phosphate by at least 1.1 units compared with solution. As the pH decreases below 3.3, the difference spectrum becomes distinctly different, indicating a considerable change in the electronic structure of the γ-phosphate. However, the spectrum does not resemble that for the

protonated GTP•Mg^{2+} in solution. Therefore, the spectral change below pH 3.3 cannot be explained simply on the basis of a protonation of the γ-phosphate. Whether or not γ-phosphate protonation occurs, there must be a substantial change at the active site to yield the very unusual observed bands.

We can also try to find the pK_a value in some quantitative ways. For the spectra of GTP•Mg^{2+}, for instance, it is noticed that the spectra at pH values above 5.0 are very similar. This is also true for the spectra at pH values below 3.4. Hence, the spectra do show close correlation with the degree of protonation of the γ-phosphate. If we choose the variables properly, we may determine the pK_a from the Henderson Hasselbalch fitting. We find that at certain wavenumbers, the intensity of IR signal is pretty sensitive to pH change in the vicinity of pK_a. Therefore, these bands are good indicator of protonation and deprotonation. The approach we used for Ras•GTP•Mg^{2+} is like the following: all the differences are scaled according to the intensity of the amide II bands (the advantage over GTP•Mg^{2+} is we have a reference band here). Two wavenumbers, which correspond to the maximum and minimum in the difference spectrum at pH 7.5, are chosen to calculate the intensity difference. Then the data are fit to the Henderson-Hasselbalch equation. The procedure is shown in Figure 6.5 and the apparent pK_a of the γ-phosphate we obtained is 2.95.

6.3 Instability of Ras under extreme pH

Many factors can affect protein's activities. For instance, a protein can be denatured in non-biological environments such as extremes of pH, heat, oxidation, mechanical forces, etc. (Volkin, 1989). Many proteins unfold at pH values less than 5 or greater than 10. This is because the change of ionic environment may expose the buried non-ionized

groups in the folded form and make them ionize. Therefore, it is important to examine the effect of low pH on the conformation change of Ras protein in our pK_a measurement. It is well established that the IR absorbance of Amide I is associated with secondary structure. Protein amide I spectra (~1600-1700 cm^{-1}) arise from the C=O stretch of the polypeptide backbone. The position of a C=O band within the amide I region is determined primarily by its hydrogen bonding and transition dipole coupling to other C=O groups, which is distance- and orientation-dependent. The unique geometric and bonding characteristics of the different secondary structures result in structure-specific amide I absorbance bands. Previous correlations between band position and secondary structure (Prestrelski, 1991a) (Prestrelski, 1991b) have revealed that normally, the absorbance centered at 1650 -1655 cm^{-1} is attributed to the α-helix and absorbance at 1635 cm^{-1} and 1675 cm- to the low (intense) and high (weak) frequency components of the β-sheet structure; peaks at 1668, 1675 and 1686 cm^{-1} are indicative of turns, and the 1645 cm^{-1} region is associated with a disordered polypeptide. Despite ongoing efforts, accurate quantitative determination of the secondary structural composition from amide I spectra is not yet generally feasible (Surewicz, 1993). However, changes in an amide I spectrum are frequently used as a sensitive indicator of secondary structural change (Fraser, 1991; Kennedy, 1990; Muga, 1991; Trewhella, 1989).

In our experiments of monitoring the pD*-induced change (pD* is the apparent pH meter reading) amide I band of Ras•GDP•Mg^{2+}, the protein was originally in the aqueous Tris buffer. Then deuterated Tris buffer was used to exchange out the water. After that, same amount of the deuterated Tris buffer was prepared, and acid was added to both the protein solution and the buffer to lower the pD. The pD of the buffer was adjusted to be identical to that of protein. After the pD was stable, IR spectra were taken for both protein and buffer. Then difference spectra were obtained by subtracting the two. Figure 6.6 shows the spectra of amide I of Ras•GDP•Mg^{2+} under various pD*. We clearly see

that the overall spectrum shifts to the high frequency end with decreasing pD*. To better see the relative small change, Fourier self-deconvolution method is applied to the spectra (Kauppinen, 1981; Wi, 1998). The enhancement factor is set to 1.5 and the intrinsic bandwidth 17 cm^{-1}. Comparing the spectra at pD* 7.7 and pD* 2.4, the peak of 1638 cm^{-1} at high pD* is shifted to 1641 cm^{-1} upon protonation. Since this peak corresponds to the β-sheet structure in the protein, the departure from its typical frequency suggests that destruction of this secondary structure takes place to some extent. The other peak of 1653 cm^{-1}, which is an indicator of the α-helix structure, is also shifted to 1658 cm^{-1}, strongly indicating α-helices also experience the structure change under the low pD*. Therefore, we observe both secondary structure changes upon big pD* decrease.

These results are understandable in the sense of unfolding of the protein due to the electrostatic interactions (Anderson, 1990; Matthew, 1986). If the pH is extremely low, the protein could denature completely. But to what extent can the protein still be good? In other words, is there a pH range in which the unfolding-folding transition is reversible? To this end, we used Ras•GDP•Mg^{2+} to do the experiment since it is stable in the period of titration which is quite long. Base was added to the low pH complex with the similar procedure as for the titration with acids in the above. The two spectra with same pD* but at different stage of titration are shown in Figure 6.6. Comparing the two pairs of spectra of pH 3.1 and pD* 7.7, we find that they look very similar. To get better resolution, FSD with the same parameter was performed. The FSD spectra show that these spectra of amide I band at same pD* are essentially identical. Hence, the unfolding process of Ras•GDP•Mg^{2+} is reversible in the pD* range of 2.4-7.7. Although this result is for Ras•GDP•Mg^{2+}, we expect it holds for Ras•GTP•Mg^{2+} as well since it is about the global conformation change of the protein and is solely induced by ionic interactions.

Figure 6.7 Panel B shows the spectra of amide I of Ras•GTP•Mg^{2+}, Here we observe the similar trends as for Ras•GTP•Mg^{2+}. From the FSD spectra, we see that 1635 cm^{-1} and 1651 cm^{-1} are replaced by 1640 cm^{-1} and 1657 cm^{-1} respectively. As in the case of Ras•GDP•Mg^{2+}, the frequency shifts also give evidences of the change of secondary structure with pD*. The study of Ras•GDP•Mg^{2+} has shown that the change is reversible for pD*>2.4, here we want to explore the behavior of protein under even lower pD* conditions. The long-short-long dashed line in Figure 6.7 represents the amide I spectrum of Ras•GTP•Mg^{2+} at pD* 1.7, the corresponding FSD spectrum is also shown. The distinction of this spectrum from those above pD* 2.6 indicates disruption of much more secondary structure under this low pD*. Therefore, two transitions exist in the titration of Ras•GTP•Mg^{2+} complex: the first, between pD* 5.4 and 2.6, is well behaved and reversible. The second, between pD* 2.6 and 1.7, is not well behaved. The results were not reproducible at pD* values below 2.6. We suspect that this is due to a tendency for Ras to aggregate at this low pD* value, a common finding for acid-unfolded protein.

To better understand the pD* dependence of the first (reversible) transition for both GTP and GDP bound Ras, titration curves of the amide I changes were constructed. In this case, we want to monitor the change of the amide I bands with pD*. However, these changes are concomitant in both intensity and frequency. The biggest change in intensity, according to the spectra, takes place at the frequency pair of (1635, 1640) for GDP complex and (1638, 1641) for GTP complex. It is possible to choose these pair frequencies, calculating their intensity differences for every pD* value. To get rid of the errors in concentration between each measurement, we divided the results by the corresponding amide I intensities. The outcome gives very small numbers. We may rescale them to the interval of [0. 1]. The data points then are fit to the Henderson-Hasselbalch equation. Here we assume the reversible folding-unfolding process is driven by the addition of acid. For simplicity, a two-state model is adopted (Zwanzig, 1997),

namely, the protein molecule will change between two conformation states, the folded and unfolded without any intermediate states. We can write the reaction equation as

$$F + n \cdot H^+ \leftrightarrow U, \tag{6.1}$$

where F stands for the normal folded state of a protein molecule and U stands for the unfolded state induced by acid (it does not necessarily need to be the fully unfolded state which has no secondary structure at all). Here we put n before the proton, considering there might be more than one proton involved in the transition. At certain pH, the reaction reaches equilibrium, then we have

$$K = \frac{[U]}{[F][H^+]^n}. \tag{6.2}$$

The above equation can be rewritten in the following form

$$pK = \log\frac{[U]}{[F]} + n \cdot pH. \tag{6.3}$$

Taking into account that $[F]+[U] = [F]_0$, where $[F]_0$ is the initial concentration of folded protein, we get

$$n \cdot pH - pK = \log\left(\frac{[F]_0}{[U]} - 1\right). \tag{6.4}$$

Then we have the unfolded fraction in terms of pH and pK,

$$\frac{[U]}{[F]_0} = \frac{1}{1 + 10^{n \cdot pH - pK}}. \tag{6.5}$$

As we have seen from Figure 6.7, the transition from folded state to unfolded one only cause minor changes in spectra. Despite that they share a large portion in IR spectra, we believe that the difference of the spectra will still reflect their structural changes. If we focus on the component corresponding to the β-sheet structure, it is appropriate to assume that the intensity is a linear function of the unfolding extent, at both frequencies of the pair (1635, 1640) or (1638, 1641), i.e.

$$I^A = {I_0}^A + \frac{[U]}{[F]_0} \cdot \Delta^A \tag{6.6}$$

at position A, and

$$I^B = {I_0}^B - \frac{[U]}{[F]_0} \cdot \Delta^B \tag{6.7}$$

at position B, where A and B represent the frequency positions in the spectra (A is smaller than B) and I^A and I^B are the corresponding IR intensities. $\Delta^{A,B}$ denotes the total change in intensity for the transition. Since the folded and unfolded states have a large portion of structure in common, this is reflected in the constant term ${I_0}^{A,B}$. Subtracting the above two equations, we obtain

$$I^A - I^B = {I_0}^A - {I_0}^B + \frac{[U]}{[F]_0} \cdot \left(\Delta^A + \Delta^B\right), \tag{6.8}$$

or

$$\frac{I^A - I^B - \left({I_0}^A - {I_0}^B\right)}{\Delta^A + \Delta^B} = \frac{[U]}{[F]_0}. \tag{6.9}$$

Recalling equation (6.5) we derived earlier, we finally have the following relationship:

$$\frac{I^A - I^B - \left(I_0{}^A - I_0{}^B\right)}{\Delta^A + \Delta^B} = \frac{1}{1+10^{n\cdot pH - pK}}. \qquad (6.10)$$

The left-hand-side of the above equation gives the procedure of rescaling of intensity difference to the interval of [0, 1].

Figure 6.8 shows the fitting of the titration of both Ras•GDP•Mg^{2+} and Ras•GTP•Mg^{2+}. The Ras•GDP•Mg^{2+} titration is fit well by a model in which the observed changes are due to the addition of a single proton, with a pK_a of 4.8. However, the single-proton scheme does not describe the Ras•GTP•Mg^{2+} titration well; a two-proton uptake model provides an excellent fit. The apparent pK_a predicted by the fit was 3.7. Since the experiments were carried out in D_2O instead of water. There is a 0.4 unit of pK_a difference in the two solvents, i.e., pH = pD*+0.4. So the pK_a of Ras•GDP•Mg^{2+} and Ras•GTP•Mg^{2+} in water will be 4.1 and 5.2 respectively. The 1.1 pK_a difference in the midpoints of the denaturation curves for the GDP and GTP complex indicates that the γ-phosphate•Ras contacts stabilize the protein toward acid-driven unfolding. The structure of the protein is altered by these contacts such that the unfolding appears to be simultaneous with the addition of approximately two protons, instead of one.

Ligand-induced stabilization of the folded state of proteins is well documented (Shortle, 1993; Shortle, 1996; Yutani, 1992). In the urea-induced equilibrium unfolding studies of Ras•GDP•Mg^{2+} (Zhang, 1998a; Zhang, 1998b), Zhang et al has shown that the ligand of GDP and Mg^{2+} play an important role in the stabilization of the protein. Removal of Mg^{2+} will loosen the aromatic side chain packing but only induce minor change of the secondary structure; removal of both GDP and Mg^{2+} completely release the side chain packing but the secondary structure is intact in large. From the titration spectra of the γ-phosphate of Ras•GDP•Mg^{2+}, the similarity between pH 7.5 and pH 3.3 suggests

that GTP is still bound to the folded or partially unfolded protein. We believe it is also true for Ras•GDP•Mg^{2+} at low pH. Hence, in our pH-induced unfolding, the side chain packing is probably intact. And this side chain packing could be the factor which resists the unfolding process. GTP, which has one more phosphate than GDP, will have more bonds with the amino acids around the active site, and as a result, have more ability to prevent the secondary structure from changing due to the ionic environment change. X-ray crystallography study also shows that two regions: residues 30 to 38 and residues 60-76 are quite different in conformation for GTP complex and GDP complex (Milburn, 1990). This could explain why the apparent pK_a of Ras•GTP•Mg^{2+} is 1.1 units lower than that of Ras•GDP•Mg^{2+} in the unfolding transition. The two-proton mechanism for Ras•GTP•Mg^{2+} also indicates that GTP is more resistant to the pH change.

6.4 Discussion

Our experiments show that the apparent pK_a of the γ-phosphate of GTP bound to Ras is definitely less than 3.3. However, due to the irreversible unfolding of the protein at lower pH, the accurate number is not available by this method. An empirical curve fitting of the data to Henderson-Hasselbalch equation gives the pK_a value of 2.95, which agrees well with the NMR result. The reversible unfolding process for pH values greater than 2.6 will not affect our measurement because of the following reasons: first, the pK_a measurement is monitoring the change of the antisymmetric bands solely from the γ-phosphate of GTP in Ras. Secondly, the apparent pK_a of unfolding is 3.7 for Ras•GTP•Mg^{2+} in D_2O, the value will then be 4.1 in aqueous solution, which is considerably large than the pK_a value of the γ-phosphate. Therefore, it is unlikely that the two processes will entangle.

The current study affirms several of the interpretations made in previous work (Schweins, 1995). The α-, β-, and γ-phosphate ^{31}P NMR resonances of Ras•GTP•Mg^{2+} were shown to shift concomitantly with a midpoint of 2.9, which is interpreted to be the pK_a of the γ-phosphate. It is not possible, based solely on this correlation, to unambiguously assign the physical basis of the chemical shift to protonation. For example, the shift could be caused by a pH-dependent migration of the Mg^{2+} ion on the tripolyphosphate chain or by protein structural change in the near environment of the γ-phosphate. In support of the previous interpretation, our experiments provide direct, site-specific conformation of the facts that the γ-phosphate is not protonated at pH > 3.3 in the Ras•GTP•Mg^{2+} complex and that its pK_a is brought down to ~2.9 from solution value of 4.5 by the active site environment.

Consistent with our unfolding studies, the pH dependence of the ^{1}H-NMR spectrum of Ras•GTP•Mg^{2+} shows that the complex partially unfolds between pH 6.8 and 3.3. In the pH range 3.3-2.2, which includes the 2.9 midpoint, the ^{1}H-NMR changes are slight, suggesting that no major structural changes occur in the complex; however, our amide I data clearly show that the secondary structure of the complex changes in this pH range. A pH-dependent change in the structure of the Ras•GTP•Mg^{2+} complex can explain the observed pH dependence of the ^{31}P chemical shift as well as the simultaneous shift in the α-, β-, and γ-phosphate ^{31}P NMR resonances. Structural change could also be the basis for the pH rate inactivation profiles used to construct the free energy plot ($\Delta G^{\ddagger}$ versus pK_a) we mentioned before. The slope of the free energy plot (*i.e.*, 2.1) (Schweins, 1995) has been interpreted in several ways, including a protein isomerization that precedes hydrolysis. This isomerization could possibly be the unfolding of the protein. The pH-dependent unfolding of the Ras•GTP•Mg^{2+} provides a fully consistent, alternative interpretation of the experimental support for the γ-phosphate general base hypothesis

and thus raises the issue of whether this mechanism is operative in GTPase-catalyzed reactions.

In Chapter V, we have shown that our results favor a transition state with dissociative character in the hydrolysis of GTP bound to Ras. Now the titration and unfolding studies of Ras•GTP•Mg^{2+} suggest the γ-phosphate may serve as the general base in an associative pathway. In any case, the information we obtained is insufficient to completely exclude other possibilities. For instance, the pK_a of the γ-phosphate is still 2.9 due to the interaction between the phosphates and the side chains in the active site but without facilitating the abstraction of a proton from the nearby water. With the features from both associative and dissociative mechanisms, it is very plausible that a concerted transition state is adopted for the GTPase reaction. This means the bond to the γ-phosphate breaks down simultaneously with the formation of the bond to the nucleophile. There is not an intermediate state in the pathway. The concerted mechanism can explain most of our observations, for example, the pK_a of the γ-phosphate, the bridging bond lengthening in the ground state. The time-resolved FTIR studies of this problem also suggest that the mechanism is probably concerted with the transition state having a considerable amount of dissociative character.

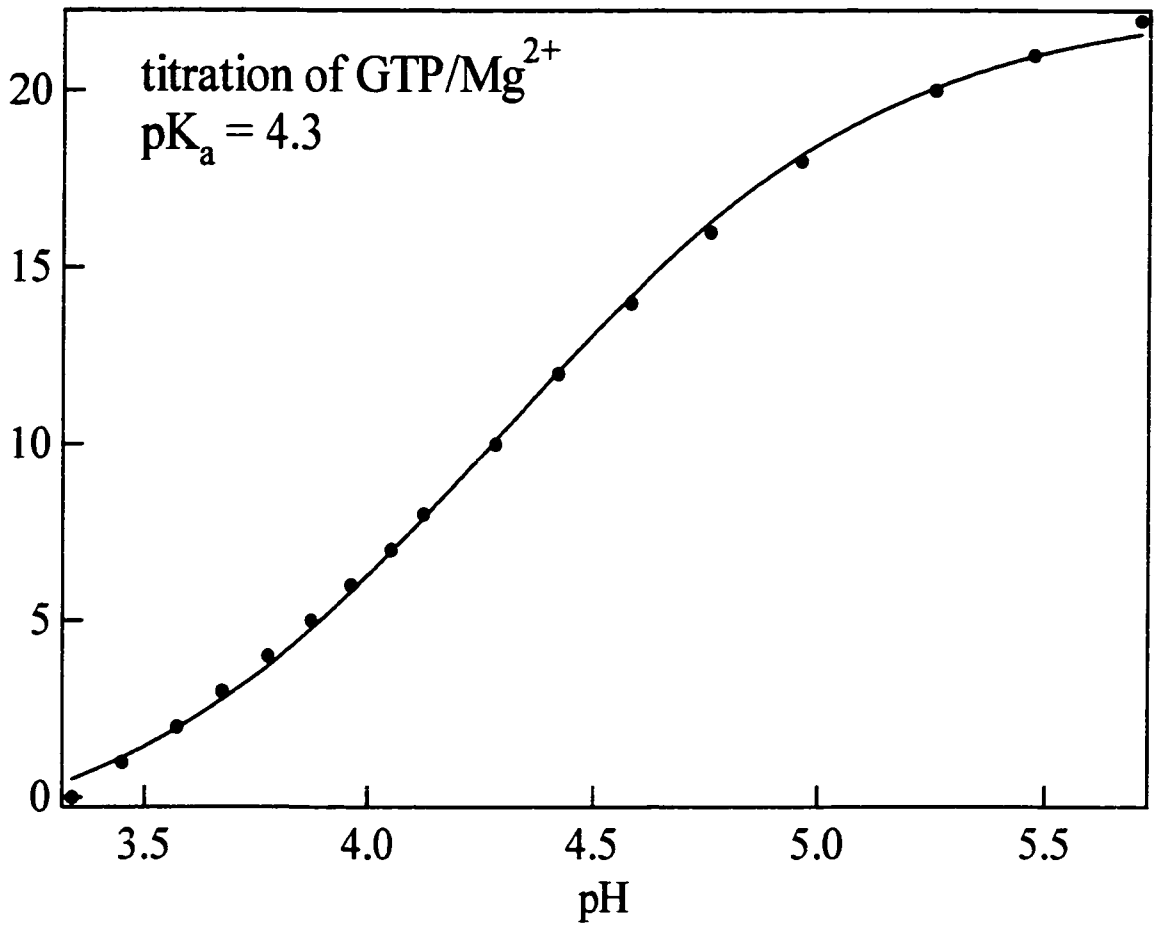

Figure 6.1: Titration curve of Ras•GTP•Mg^{2+} in solution. Concentration of GTP is 5 mM; concentration of Mg^{2+} is 10 mM. The pK_a is determined to be 4.3 by fitting the data to Henderson-Hasselbalch equation.

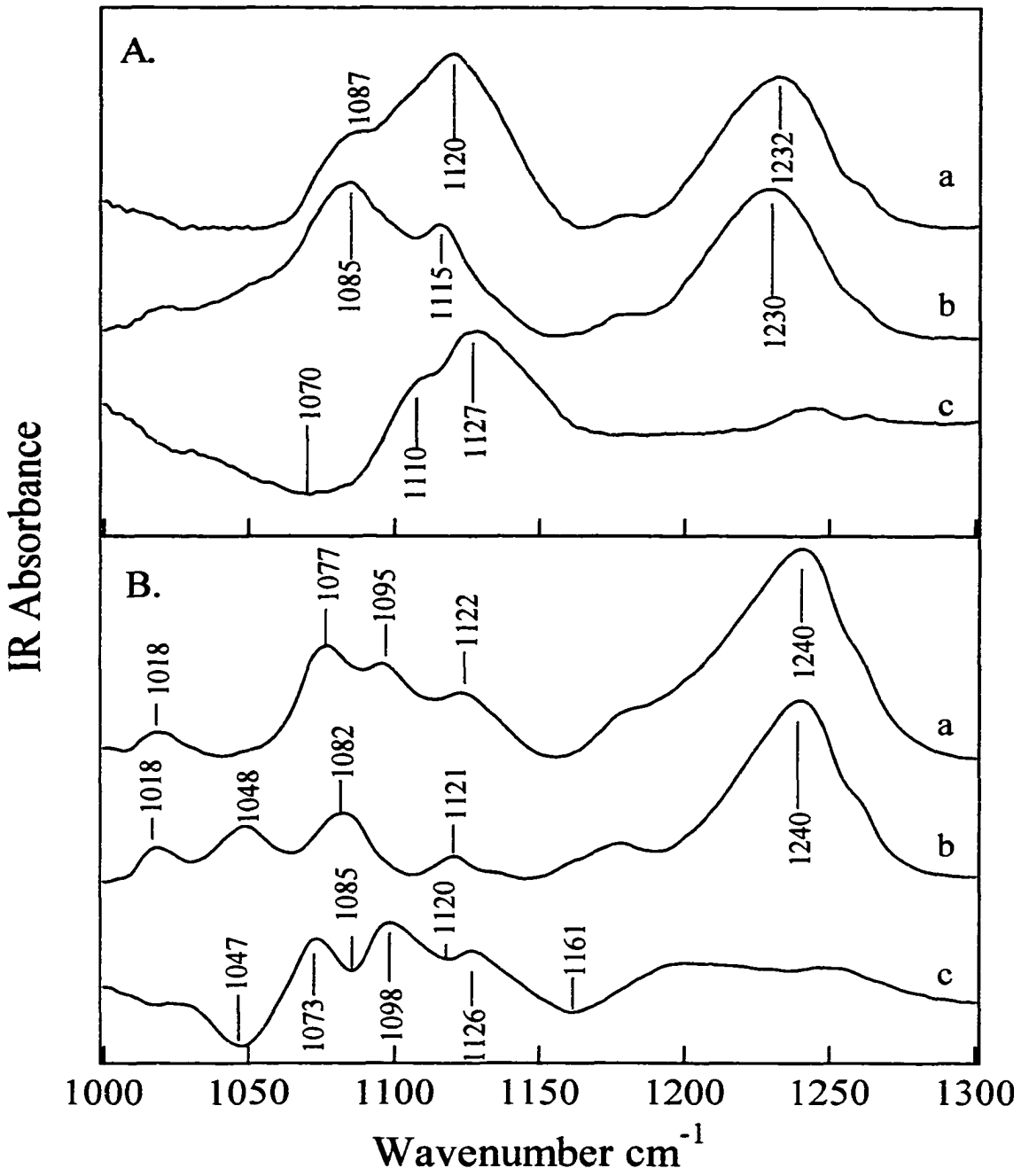

Figure 6.2: Spectra of GTP (a) and (γ-^{18}O) GTP (b) and their difference spectra (c) at pH 7.5 (Panel A) and pH 5.1 (Panel B) in aqueous solutions.

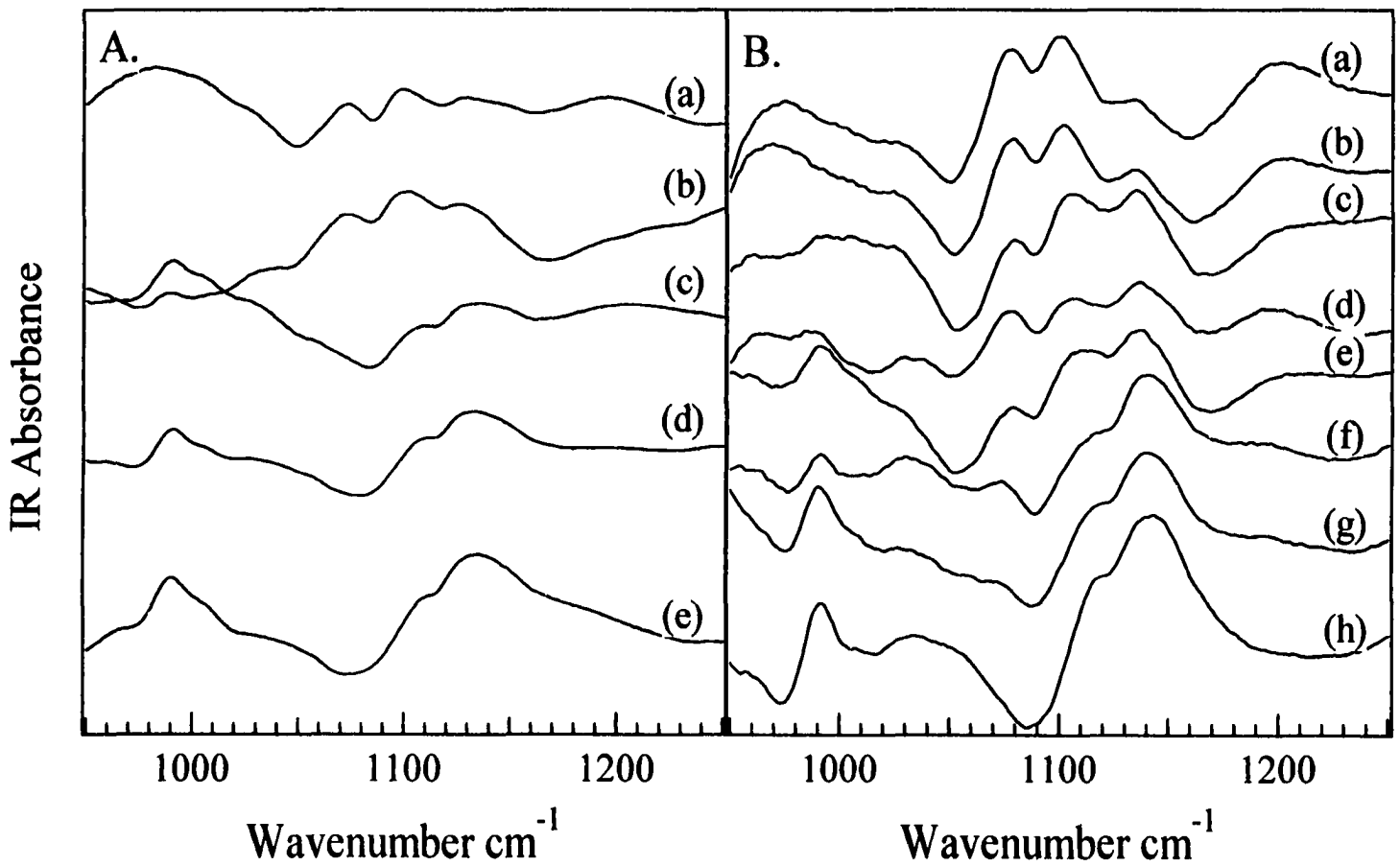

Figure 6.3: Isotope difference spectrum of GTP and GTP•Mg^{2+} at different pH values. The pH values in Panel A are: (a) 4.4; (b) 6.5; (c) 7.1; (d) 7.5; (e) 8.4. The pH values in Panel B are: (a) 2.8; (b) 3.4; (c) 4.3; (d) 4.5; (e) 4.8; (f) 5.0; (g) 5.4; (h) 5.9.

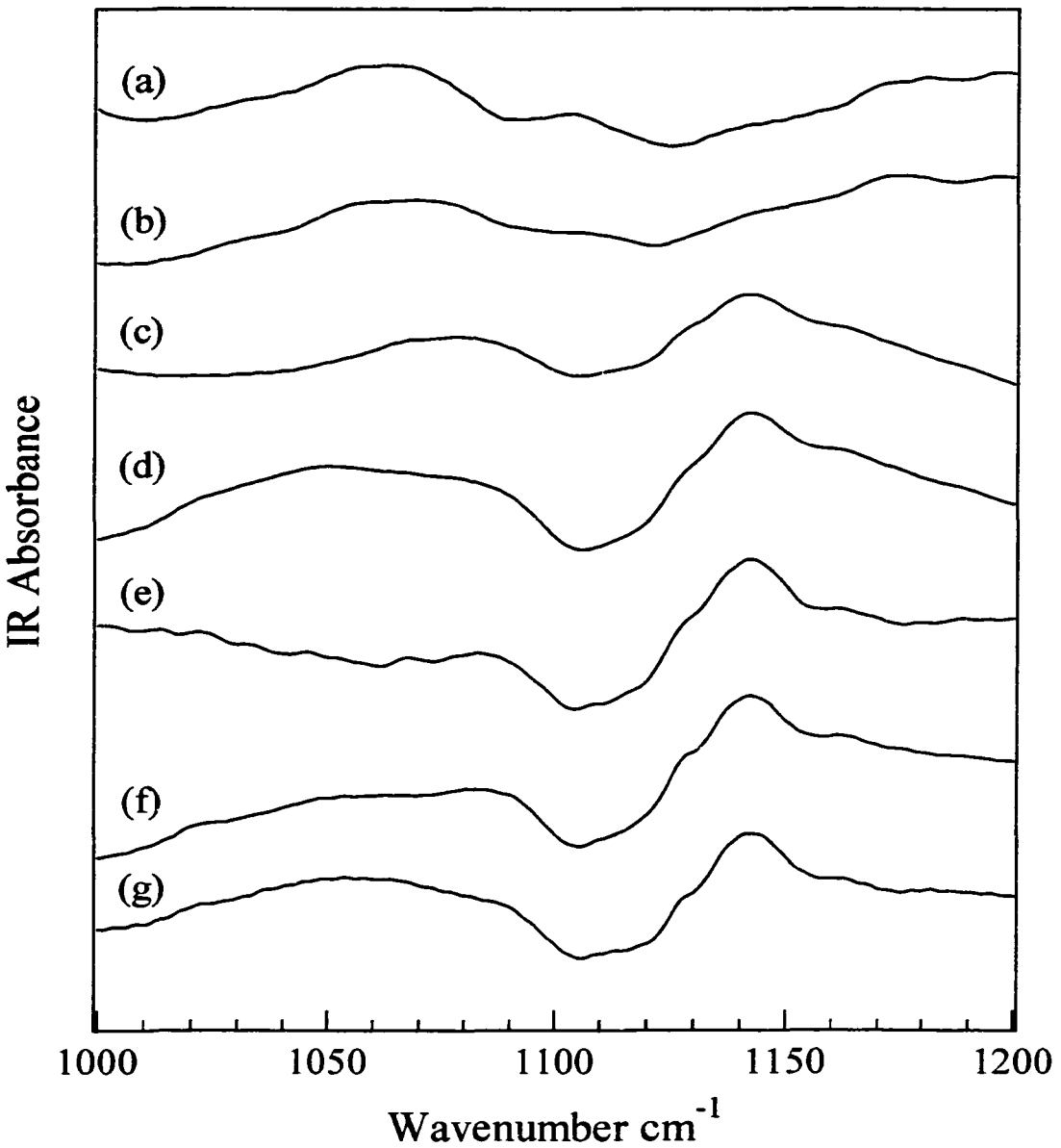

Figure 6.4: Difference spectrum of Ras•GTP•Mg^{2+} at different pH values: (a) 2.0; (b) 2.8; (c) 3.3; (d) 3.7; (e) 4.0; (f) 4.3; (g) 7.5.

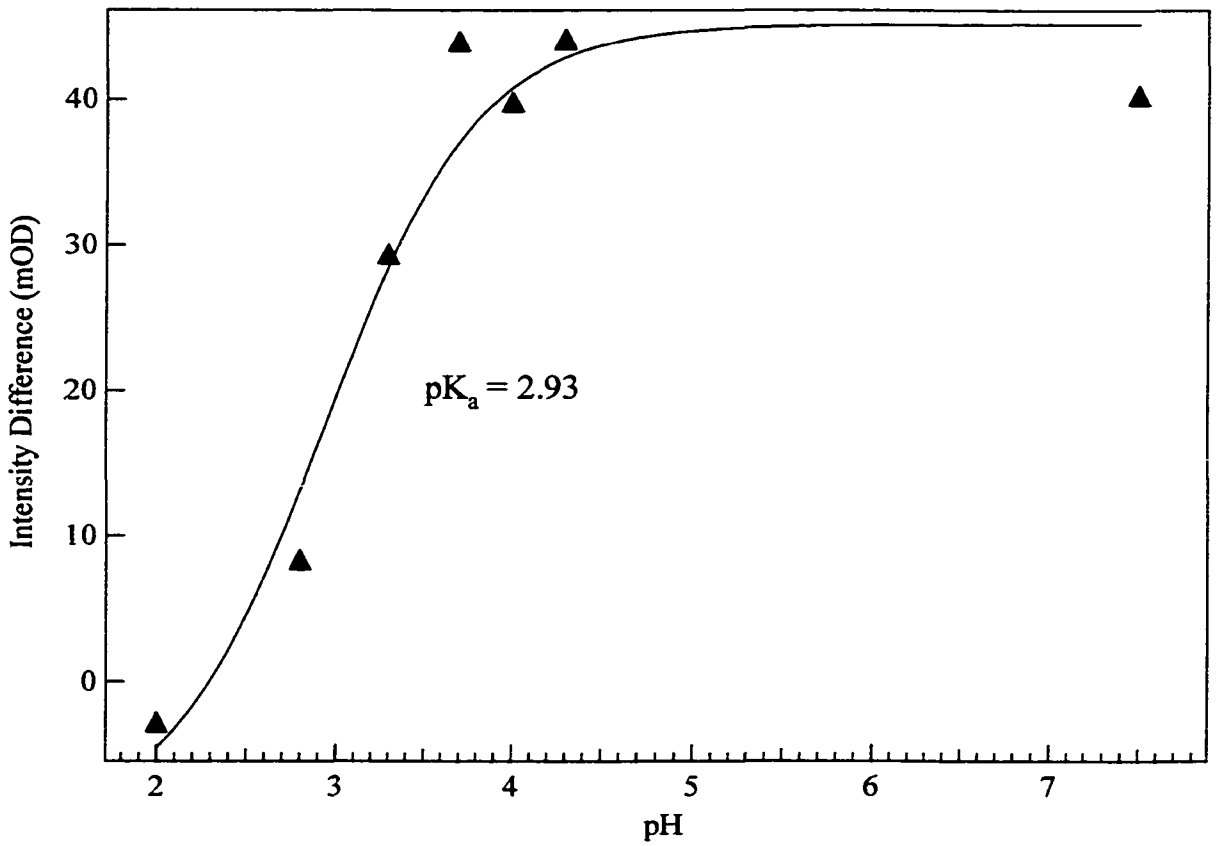

Figure 6.5: Curve fitting of Ras•GTP•Mg^{2+} to get the pK_a of the γ-phosphate of bound GTP. From the difference spectra in Figure 6.4, we choose two wave numbers that correspond to the maximal and minimal intensities in the difference spectrum at pH 7.5, and then calculate the intensity differences at these two wavenumbers for the difference spectrum of each pH value. The values are scaled according to the intensity of the amide II band. Then the data is fitted to the Henderson-Hasselbalch equation. The pK_a obtained is 2.93.

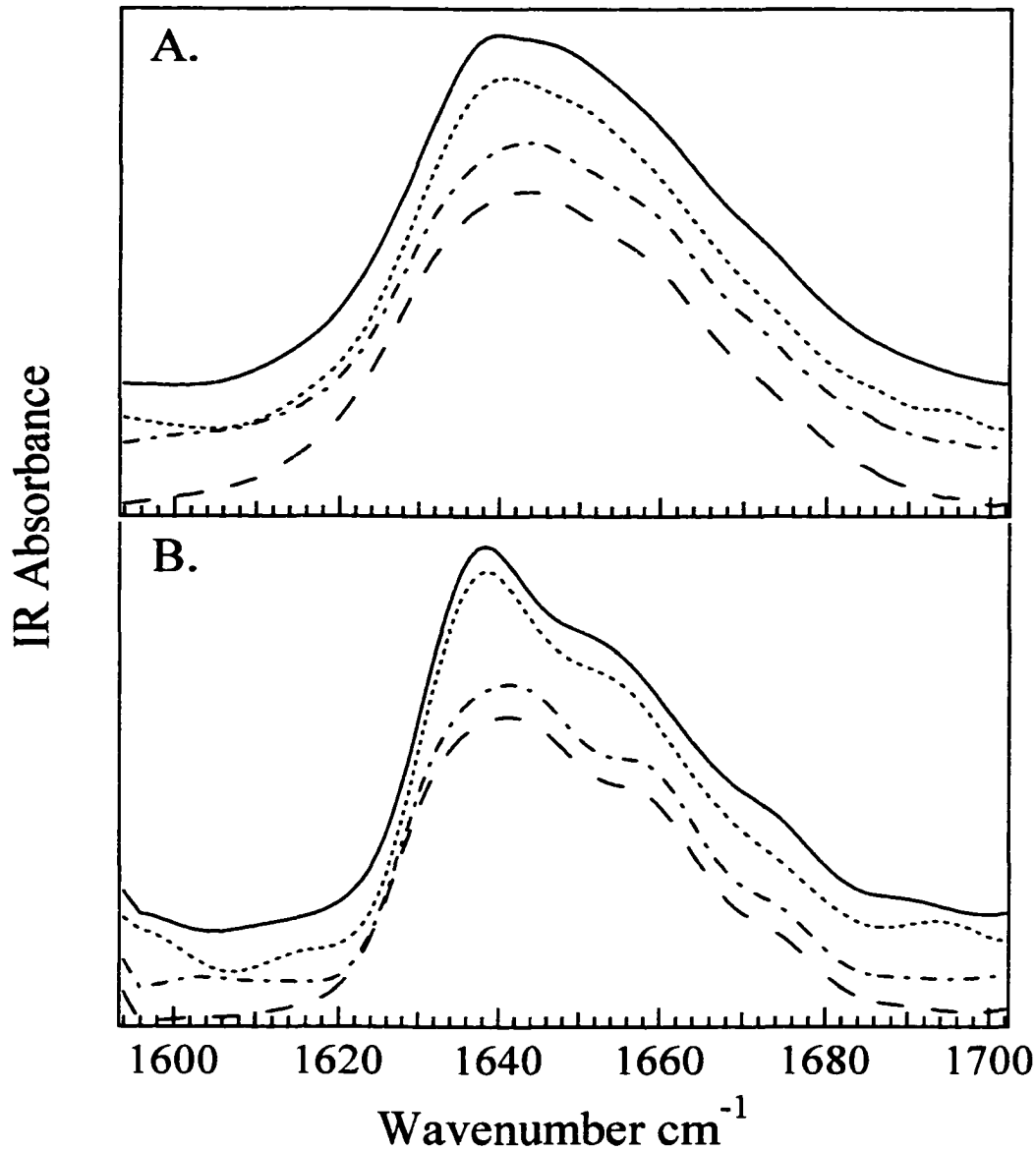

Figure 6.6: Spectra of Ras•GDP•Mg^{2+} at different pD* values (Panel A), and their FSD spectra (Panel B). Solid line and dotted line are the data at pD* 7.7 during the titration and reverse titration respectively. The dash-dotted and the dashed line are the data at pD* 3.3 during the titration and reverse titration respectively.

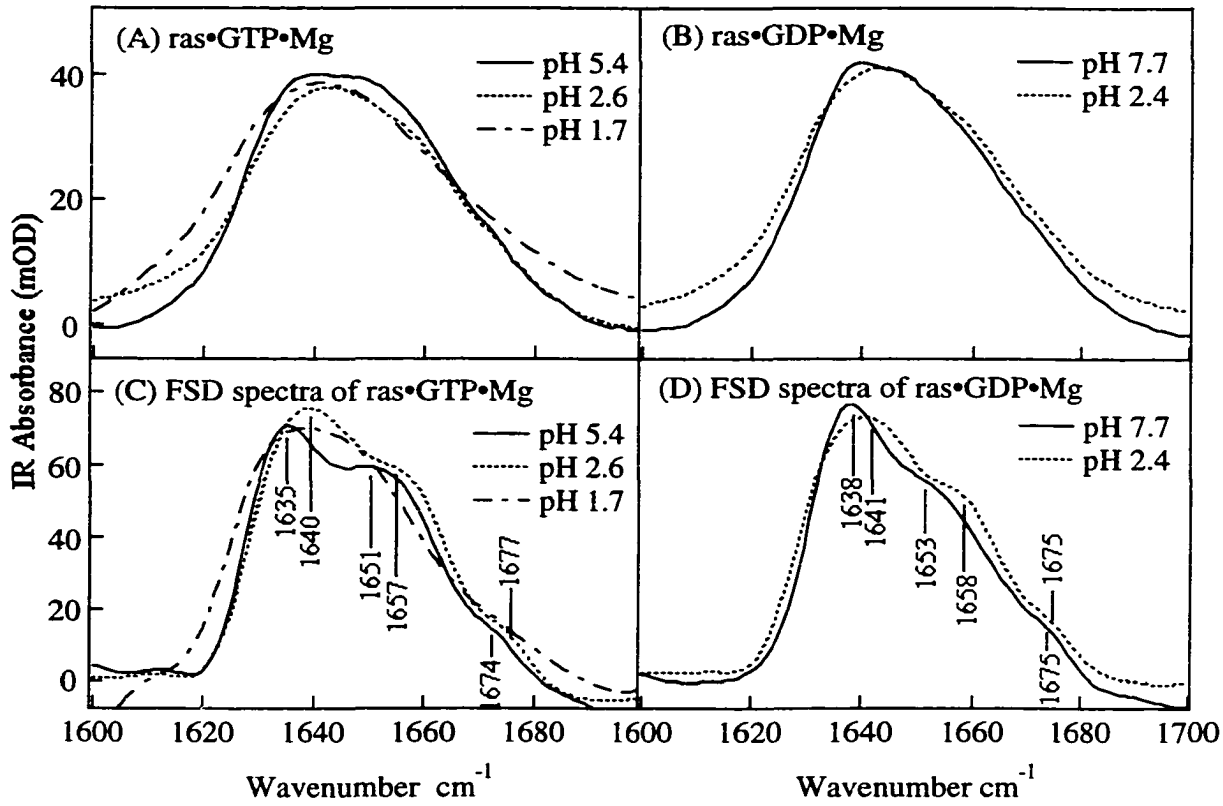

Figure 6.7: The pH dependence of the amide I spectra of Ras•GDP•Mg^{2+} and Ras•GTP•Mg^{2+}. Fourier Self- Deconvolution (FSD) was performed to resolve the intrinsic bands. Enhancement factor is 1.5 and intrinsic bandwidth is taken to be 17 cm^{-1}.

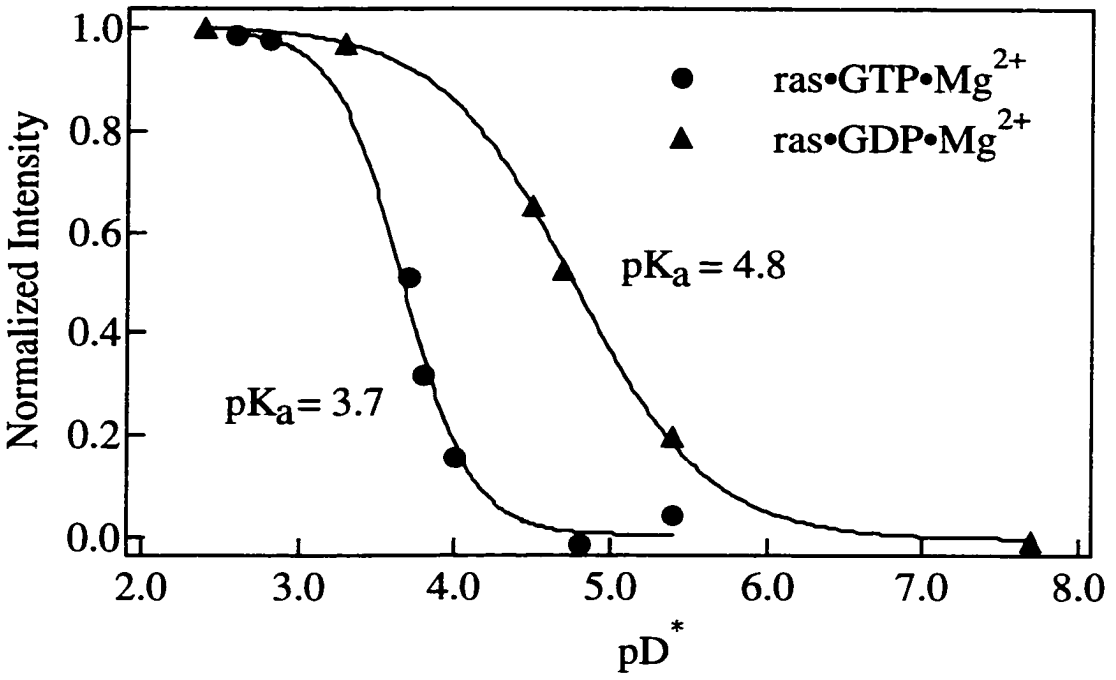

Figure 6.8: The pD* dependent unfolding of Ras•GDP•Mg^{2+} and Ras•GTP•Mg^{2+}. A second non-reversible transition occurs for Ras•GTP•Mg^{2+} below pD* 2.6 is not shown. The apparent pK_a values are obtained by fitting the data using Henderson-Hasselbalch equation for one (▲) or two (•) protons.

References:

Abell, K.W.Y., & Kirby, A. J. (1986) *J. Tetrahedron Lett.*, **27**, 1085-1088.

Adari, H., Lowy, D. R., Der, C. J., & McCormick, F. (1988) *Science*, **240**, 518-521.

Admiraal, S.J., & Herschlag, D. (1995) *Chem. & Biol.*, **2**, 729-939.

Albery, W.J. (1980) *Annu. Rev. Phys. Chem.*, **31**, 227-263.

Allen, F.H.K., A. J. (1984) *J. Am. Chem. Soc.*, **106**, 6197-6200.

Anderson, D.E., Becktel, W. J., & Dahlquist, F. W. (1990) *Biochemistry*, **29**, 2403-2408.

Badger, R.M., & Bauer, S. H. (1937) *J. Chem. Phys.*, **5**, 839-855.

Barbacid, M. (1987) *Annu. Rev. Biochem*, **56**, 779-827.

Benkovic, S.J., & Schray, K. J. (1978) *The mechanism of phosphoryl transfer, In Transition States of Biochemical Processes,* Plenum, New York.

Bollag, G., & McCormick, F. (1991) *Nature*, **351**, 576-579.

Bourne, H.R. (1997) *Science*, **278**, 1898-1899.

Bourne, N.W., A. (1984) *J. Org. Chem.*, **49**, 1200-1204.

Briggs, A.J., Glenn, R., Jones, P. G., Kirby, A. J. & Ramaswamy, P. (1983) *J. Am. Chem. Soc.*, **106**, 6200-6206.

Brown, I.D., & Shannon, R. D. (1973) *Acta Crystallogr. A29*, 1957-1959.

Brown, I.D. (1992) *Act. Crystallogr*, **B48**, 553-572.

Brown, I.D.W., K. K. (1976) *Acta Cryst.*, **B32**, 1957-1959.

Buncel, E., Um, I. H., & Hoz, S. (1989) *K. Am. Chem. Soc.*, **111**, 971-975.

Cales, C., Hancock, J. F., Marshall, C. J. & Hall, A. (1988) *Nature*, **332**, 548-551.

Callender, R., & Deng, H. (1994) *Annu. Rev. Biophys. Biomol. Struc.*, **23**, 215-245.

Catrina, I.E., & Hengge, A. C. (1999) *J. Am. Chem. Soc.*, **121**, 2156-2163.

Cepus, V., Scheidig, A. J., Goody, R. S. & Gerwert, K. (1998) *Biochemistry*, **37**, 10263-10271.

Chen, Y.-Q., Kraut, J., Blakley, R. L., & Callender, R. H. (1994) *Biochemistry*, **33**, 7021-7026.

Chen, Y.-Q., Kraut, J., & Callender, R. H. (1997) *Biophys. J.*, **72**, 936-941.

Cleland, W.W., & Hengge, A. C. (1995) *FASEB J.*, **9**, 1585-1594.

Colthup, N.B., Daly, L. H., & Wiberley, S. E. (1990) *Introduction to Infrared and Raman Spectroscopy*, Academic Press, San Diego, 1990.

Deng, H., Manor, D., Weng, G., Chen, C.-X., Balogh-Nair, V., & Callender, R. H. (1993) *Proceedings of International Society for Optical Engineering*. International Society for Optical Engineering, Los Angeles, pp. 114-122.

Deng, H., Wang, J., Callender, R., & Ray, W. J. (1998a) *J. Phys. Chem. B*, **102**, 3617-3623.

Deng, H., Wang, J.,Callender, R. H., Grammer, J. C. & Yount, R. G. (1998b) *Biochemistry*, **37**, 10972-10979.

deVos, A.M., Tong, L., Milburn, M. V., Matias, P. M., Jancarik, J., Noguchi, S., Nishimura, S., Miura, K., Ohtsuka, E., & Kim, S.-H. (1988) *Science*, **239**, 888-893.

Di Sabato, G., & Jencks, W. P. (1961) *L. Am. Chem. Soc.*, **83**, 4400-4405.

Du, X., Frei, Heinz, & Kim, Sung-Hou. (2000) *J. Biol. Chem.*, **275**, 8492-8500.

Fasano, O., Aldrich, T., Tamanoi, F., Taparowsky, E., Furth, M. & Wigler, M. (1984) *Proc. Natl. Acad. Soc.*, **82**, 4008-4012.

Fraser, P.E., Nguyen, J. T., Surewicz, W. K., & Kirschmer, D. A. (1991) *Biophys. J.*, **60**, 1190-1201.

Gibbs, J.B., Sigal, I. S., Poe, M., & Scolnick, E. M. (1984) *Proc. Natl. Acad. Sci.*, **81**, 5704-5708.

Gilman, A.G.A. (1987) *Rev. Biochem.*, **56**, 615-649.

Gordy, W. (1946) *J. Chem. Phys.*, **14**, 305-320.

Grand, R.J.A., & Owen, D. (1991) *Biochem. J.*, **279**, 609-631.

Griffiths, P.R., & de Haseth, J. A. (1986) *Fourier Transform Infrared Spectrometry*, John Wiley & Sons, New York.

Hall, A.D.W., A. (1986) *Biochemistry*, **25**, 4784-4790.

Hardcastle, F.D.W., I. E. (1991) *J. Phys. Chem.*, **95**, 5031-5041.

Hardcastle, F.W., I. E. (1990) *J. Raman Spectrosc.*, **21**, 683-691.

Hengge, A.C., Sowa, G. A., Wu, L. & Zhang, Z.-Y. (1996) *Biochemistry*, **34**, 13982-13987.

Herschlag, D., & Jencks, W. (1986) *J. Am. Chem. Soc.*, **108**, 7938-7946.

Herschlag, D.J., W. P. (1989) *J. Am. Chem. Soc.*, **111**, 7579-7586.

Hoff, R.H., & Hengge, A. C. (1998) *J. Org. Chem.*, **63**, 6680-6688.

Hollfelder, F., & Herschlag, D. (1995) *Biochemistry*, **34**, 12255-12264.

Jencks, W.P. (1987) *Catalysis in Chemistry and Enzymology*. Dover, New York.

John, J., Sohmen, R., Feurstein, J., Linke, R., Wittinghofer, A. & Goody, R. S. (1990) *Biochemistry*, **29**, 6058-6065.

John, J., Rensland, H., Schlichting, I., Vetter, I., Borasio, G. D., Goody, R. S. & Wittinghofer, A. (1993) *J. Biol. Chem.*, **268**, 923-929.

Jones, P.G.K., A. J. (1984a) *J. Am. Chem. Soc.*, **106**, 6207-6212.

Jones, P.G.S., G. M. (1984b) *Acta Cryst.*, **C40**, 550-552.

Kauppinen, J.K., Moffatt, D. J., Mansh, H. H., & Cameron, D. G. (1981) *Appl. Spectrosc.*, **35**, 271-276.

Kaziro, Y. (1978) *Biochim. Biophys. Acta*, **505**, 95-127.

Kennedy, D.F., Slotboom, A. J., de Haas, G. H., & Chapman, D. (1990) *Biochim. Biophys. Acta.*, **1040**, 317-326.

Kirby, A.J., & Varvoglis, A. G. (1967) *J. Am. Chem. Soc.*, **89**, 415-423.

Kirby, A.J., & Varvoglis, A. G. (1968) *J. Chem. Soc.*, **B**, 135-141.

Kirby, A.J.J., W. P. (1965) *J. Am. Chem. Soc.*, **87**, 3209-3216.

Krengel, U., Schlichting, I., Scherer, A., Schumann, R., Frech, M., John, J., Kabsch, W., Pai, E. F. & Wittinghofer, A. (1990) *Cell*, **62**, 539-548.

Maegley, K.A., Admiraal, S., J., & Herschlag. D. (1996) *Proc. Natl. Acad. Sci. USA*, Vol. 93, pp. 8160-8166.

Manor, D., Weng, G., Deng, H., Cosloy, S., Chen, C.-X., Balogh-Nair, V., Delaria, K., Jurnak, F., & Callender, R. (1991) *Biochemistry*, **30**, 10914-10920.

Marcus, R.A. (1964) *Annu. Rev. Phys, Chem.*, **15**, 155-196.

Matthew, J.B., & Gurd, F. R. N. (1986) *Methods Enzymol.*, **130**, 413-453.

McCormick, F. (1989) *Cell*, **56**, 5-8.

Milburn, M.V., Tong, L., deVos, A. M., Brunger, A., Yamaizumi, Z., Nishimura, S., & Kim, S.-H. (1990) *Science*, **247**, 939-945.

Muga, A., Mantsch, H. H., & Surewicz, W. K. (1991) *Biochemistry*, **30**, 7219-7224.

Neal, S.E., Eccleston, J. F., Hall, A. & Webb, M. R. (1988) *J. Biol. Chem.*, **263**, 19718-19722.

Pai, E.F., Kabsch, W., Krengel, U., Holmes, K. C., John, J. & Wittinghofer, A. (1989) *Nature*, **341**, 209-214.

Pai, E.F., Krengel, U., Petsko, G. A., Goody, R. S., Kabsch, W., & Wittinghofer, A. (1990) *The EMBO J.*, **9**, 2351-2359.

Pouchert, C.J. (1985) *The Aldrich Library of FTIR Spectra*. Edition I, **Volume 2**.

Prestrelski, S.J., Byler, D. M., & Liebman, M. N. (1991a) *Biochemistry*, **30**, 133-143.

Prestrelski, S.J., Byler, D. M., & Thompson, M. P. (1991b) *Int. J. Pept. Protein Res.*, **37**, 508-512.

Ritchie, C.D. (1990) *Physical Organic Chemistry, The Fundamental Concepts*. Marcel Dekker, Inc., New York.

Rucker, V.C.B., L. D. (2000) *J. Am. Chem. Soc.*, **122**, 8365-8369.

Scheffzek, K., Ahmadian, M. R., Kabsch, W., Wiesmuller, L., Lautwein, A., Schmitz, F., & Wittinghofer, A. (1997) *Science*, **277**, 333-338.

Schlichting, I., Almo, S. C., Rapp, G., Wilson, K., Petratos, K., Lentfer, A., Wittinghofer, A., Kabsch, W., Pai, E. F., Petsko, G. A. & Goody, R. S. (1990) *Nature*, **345**, 309-315.

Schweins, T., Langen, R. & Warshel, A. (1994) *Nature Strut. Biol.*, **1**, 476-484.

Schweins, T., Geyer, M., Scheffzek, K., Warshel, A., Kalbitzer, H. R., & Wittinghofer, A. (1995) *Nature Struct. Biol.*, **2**, 36-44.

Schweins, T., & Warshel, A. (1996) *Biochemistry*, **35**, 14232-14243.

Shortle, D., & Abeyguanawardana, C. (1993) *Structure*, **1**, 121-134.

Shortle, D. (1996) *FASEB J.*, **10**, 27-34.

Sprang, S.R. (1997) *Annu. Rev. Biochem.*, **66**, 639-678.

Spiro, T. G. (1987) Biological Applications of Raman Spectroscopy, Wiley & Sons, New York.

Surewicz, W.K., Mantsch, H. H., & Chapman, D. (1993) *Biochemistry*, **32**, 389-394.

Thatcher, G.R.J., & Kluger, R. (1989) *Adv. Phys. Org. Chem.*, **25**, 99-265.

Trahey, M., & McCormick, F. (1987) *Science*, **238**, 542-545.

Trewhella, J., Liddle, W. K., Heidorn, D. B., & Strynadka, N. (1989) *Biochemistry*, **28**, 1294-1301.

Volkin, D.B., & Klibanov, A. M. (1989) In Creighton (ed.) *Protein Functions*. IRL Press, Oxford, pp. 1-24.

Wang, J., Xiao, D., Deng, H, Webb, M. R., & Callender, R. (1998a) *Biochemistry*, **37**, 11106-11116.

Wang, J., Xiao, D., Deng, H, Callender, R. & Webb, M. R. (1998b) *Biospectroscoy*, **4**, 219-227.

Wang, J. (1999) *CUNY, Ph. D. Thesis.*

Wi, S., Pancoska, P., & Keiderling, T. A. (1998) *Biospectroscopy*, **4**, 93-106.

Williams, A. (1992) *Adv. Phys. Org. Chem.*, **27**, 1-55.

Wittinghofer, F., Krengel, U., John, J., Kabsch, W. & Pai, E. F. (1991) *Environmental Health Perspectives*, **93**, 11-15.

Yutani, K., Ogasahara, K., & Kuwajima, K. (1992) *J. Mol. Biol.*, **228**, 347-350.

Zhang, J., & Matthews, C. R. (1998a) *Biochemistry*, **37**, 14891-14899.

Zhang, J., & Matthews, C. R. (1998b) *Biochemistry*, **37**, 14881-14890.

Zhang, X.F., Settleman, J., Kyriakis, J., Takeuchi-Suzuki, E., Elledre, S. J., Marshall, M. S., Brudeer, J. T., Rapp, U. R. & Avruch, J. (1993) *Nature*, **364**, 308-313.

Zwanzig, R. (1997) *Proc. Natl. Acad. Sci. USA*, **94**, 148-150.